2010-03-18

Syngas Fermentation: Quantification of Assay Techniques, Reaction Kinetics, and Pressure Dependencies of the Clostridial P11 Hydrogenase

Bradley E. Skidmore
Brigham Young University - Provo

Syngas Fermentation: Quantification of Assay Techniques, Reaction Kinetics, and Pressure Dependencies of the Clostridial P11 Hydrogenase

Bradley Skidmore

A thesis submitted to the faculty of
Brigham Young University
in partial fulfillment of the requirements for the degree of

Master of Science

Randy S. Lewis, Chair
Steven R. Herron
Thomas A. Knotts

Department of Chemical Engineering

Brigham Young University

April 2010

ABSTRACT

Syngas Fermentation: Quantification of Assay Techniques, Reaction Kinetics, and Pressure Dependencies of the Clostridial P11 Hydrogenase

Bradley Skidmore

Department of Chemical Engineering

Master of Science

Ethanol usage as a transportation fuel is rapidly increasing in the United States. Production of ethanol from cellulose feedstocks via gasification followed by syngas fermentation offers an environmentally friendly approach that mitigates many of the adverse effects associated with production from corn. In the syngas fermentation process, the hydrogenase enzyme of the fermentation bacterium, Clostridium P11 for this work, supplies electrons to the metabolic pathway, facilitating ethanol production.

In this thesis, an assay for P11 hydrogenase activity was developed. It was determined that 1) less than 4 minutes of sparging with 50 sccm H_2 is needed to reduce O_2 levels to below 1 ppm in a 3 mL aqueous solution, while less than 1 minute of purging at the same rate is needed to fill an air-filled 3.5 mL cuvette to 99.9999% H_2, 2) 12.5 mM DTT included in the reaction mixture at pH 6 helps scavenge O_2, 3) H_2 diffusion is slow compared to enzymatic reaction rates, 4) CO_2 lowers media pH, 5) 0.084 atm CO causes 90% inhibition of P11 hydrogenase, 6) prolonged Triton X-100 exposure diminishes hydrogenase activity, and 7) variations in H_2 pressure and electron acceptor identity and concentration affect measured hydrogenase activities.

The assay developed for P11 hydrogenase activity was used to perform kinetic studies. The Okura rapid-equilibrium rate law best described this activity. A constant that regulates the effect of H_2 pressure on hydrogenase activity, K_{H2}, was determined to be independent of electron acceptor and to have a value of 0.31 atm, implying that H_2 must be supplied to the syngas fermentation at ~3 atm to maximize hydrogenase activity. K_{BV} and K_{MV}, constants that regulate the effect of benzyl viologen and methyl viologen on hydrogenase activity, were determined to be 1.7-2.4 mM and 10.6 mM, respectively. Additionally, hydrogenase activity was temporally correlated with ethanol production in batch cultures of P11 and strongly dependent on pH. The intracellular pH of P11 was determined to be approximately 5.5.

Keywords: ethanol, hydrogenase, syngas, fermentation, Clostridium, P11, assay

ACKNOWLEDGMENTS

I am most indebted to my advisor, Randy Lewis, and to the four undergraduate students with whom I worked to perform this research: Doug Tree, Jason Bray, Dila Banjade, and Ryan Baker. Their insights, hard work, and encouragement have been invaluable. I am grateful for the other professors and graduate students who have contributed their wisdom, time, ideas, and facilities to the furtherance of this work. Additionally, I am grateful to the staffs of both Brigham Young University and Los Alamos National Laboratory who have made it possible to carry this work through to completion. Finally, I am grateful to my wife, Jessica, and to my parents, Cary and Wendy, whose love and support has strengthened me at each step along the journey.

TABLE OF CONTENTS

LIST OF TABLES

LIST OF FIGURES

1 INTRODUCTION

1.1 Current and Projected Production of Fuel Ethanol

Volatile fuel prices, diminishing world oil supply, and concern over increasing anthropogenic carbon dioxide emissions have created a desire to find alternatives to traditional oil-derived transportation fuels. Biofuels, or fuels derived from plant matter, are among the most sought after alternatives. The most prevalent bio-derived fuel currently being used as a replacement for gasoline is ethanol. Total ethanol production in the United States in 2008 was 9.2 billion gallons, or 6.7 % of the fully refined motor gasoline supplied to the United States in that year (EIA, 2009). Ethanol, which is typically mixed with gasoline, is expected to make an increasing contribution to the U.S. fuel supply (USDOE, 2007).

Virtually all of the commercial fuel-ethanol produced in the United States comes from corn, while sugar cane is used heavily in Brazil and sugar beets are a popular feedstock in Europe. Each of these plants is used as a source of simple sugars that are fermented to make ethanol. This production method leaves large portions of the plant (cellulose, hemicellulose, and lignin) unused, but additional processing (required to break the bonds of these more complex molecules) makes it possible to turn this extra biomass, as well as biomass from non-food sources, into fermentable compounds as well. Ethanol produced by these “next generation” processes is known as “cellulosic ethanol” (USDOE, 2007).

1.2 Methods of Ethanol Production

The most prevalent methods of producing cellulosic ethanol begin with either hydrolysis or gasification. In the first method, cellulose and hemicellulose are converted to simple sugars by acid or enzyme hydrolysis. These sugars are then fermented while the lignin, a molecule that provides strength to the cell walls of plants, can be burned as a combustion fuel (USDOE, 2007). In the second method, the feedstock is partially combusted (gasified) to form synthesis gas (syngas), an energetic mixture of gases primarily composed of carbon monoxide (CO), hydrogen (H_2), and carbon dioxide (CO_2). The syngas is then converted to ethanol either by chemical catalysis or by microbial fermentation (See Figure 1-1).

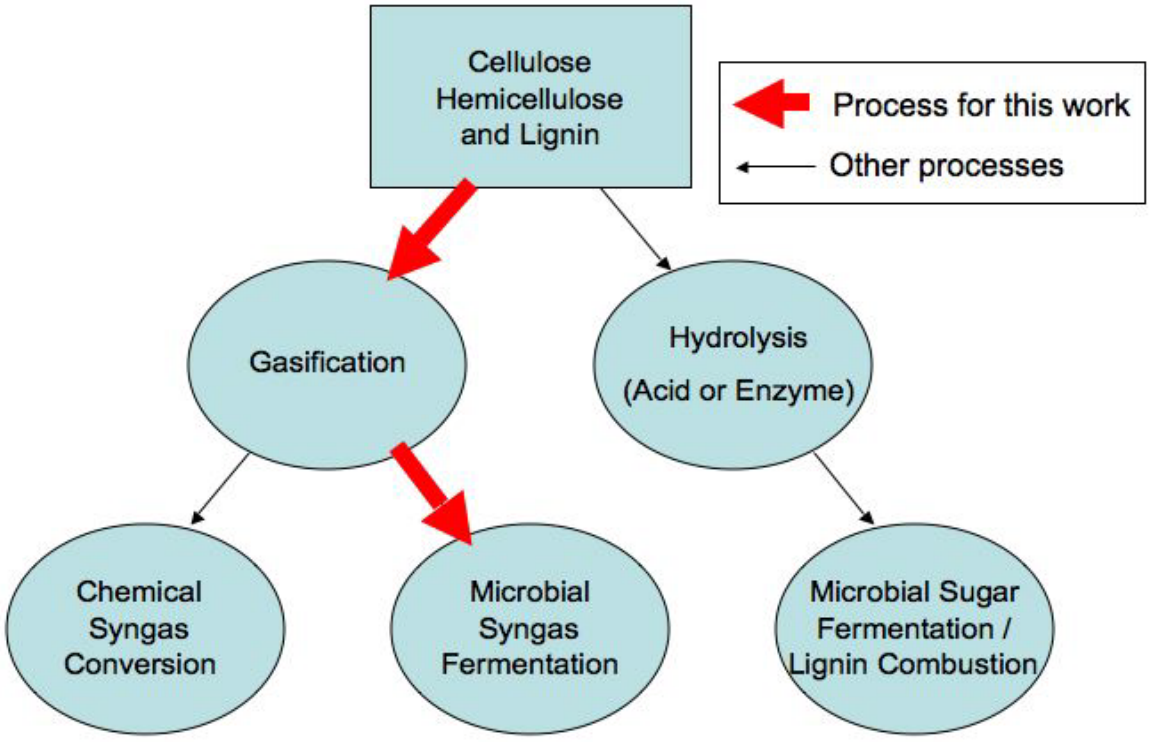

Figure 1-1: Cellulosic ethanol production methods

Gasification has several significant advantages over the hydrolysis process. First, gasification frees virtually all of the carbon from biomass, making it available for product formation. In contrast, the hydrolysis process cannot directly utilize the lignin component, which is approximately 10 – 30 % of the biomass (USDOE, 2004). Second, the enzymes required for enzymatic hydrolysis are expensive, and the acid hydrolysis process creates harmful waste streams (Sun, 2002).

There are also several distinct advantages of microbial syngas fermentation (using bacteria to make the ethanol) over chemical syngas conversion (using metal catalysts). The advantages are that microbes are less sensitive to impurities than chemical catalysts, that microbial processes operate at lower pressures and temperatures, and that microbial processes have greater product specificity. Disadvantages are that microbial fermentation processes occur more slowly than the chemical conversion process (Klasson, 1992) and that the microbes used for fermentation require anaerobic conditions. The gasification pathway, followed by microbial syngas fermentation, is the process relevant to this study.

1.3 Metabolic Pathway of Acetogenic Syngas Fermentation

The current study employs the bacterium Clostridium P11, which was recently isolated from an agricultural settling lagoon (Board of Regents, 2008), and which is believed to follow the acetyl-CoA pathway shown in Figure 1-2. This figure shows that P11 produces cell mass, ethanol, and acetic acid from syngas via a series of enzymatic reactions, many of which are oxidation-reduction reactions (denoted by $2e^-$).

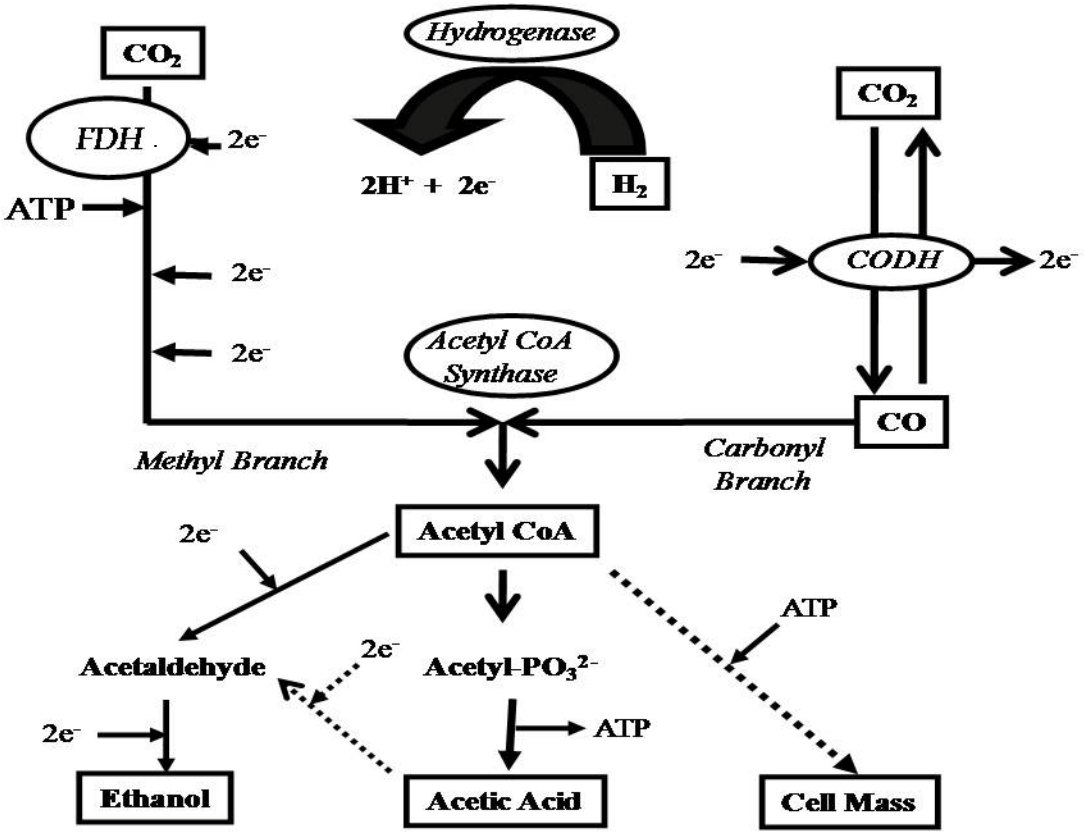

Figure 1-2: Simplified acetyl-CoA pathway

Specifically, the carbon needed to form the acetyl group of acetyl-CoA (Figure 1-3) is brought into the metabolic pathway in two ways. First, CO_2 from the syngas is converted through a series of reactions to the methyl portion of the acetyl unit. Second, CO_2 is reduced to CO, which is integrated into acetyl-CoA as the carbonyl group of the acetyl unit. However, CO can also be utilized directly in the carbonyl branch. The electrons needed for the metabolic process are obtained by either the oxidation of H_2 via hydrogenase (White, 2000) or the oxidation of CO. For industrial processes, it is preferred to obtain electrons from H_2, as this leaves the CO available for incorporation into the desired organic chemicals. Processes that depend on CO oxidation to supply electrons greatly reduce their carbon-to-product yield. Acetyl-CoA is the

crucial intermediate formed from the syngas, as it can then be converted into any of the three desirable products, ethanol, acetic acid, and/or cell mass.

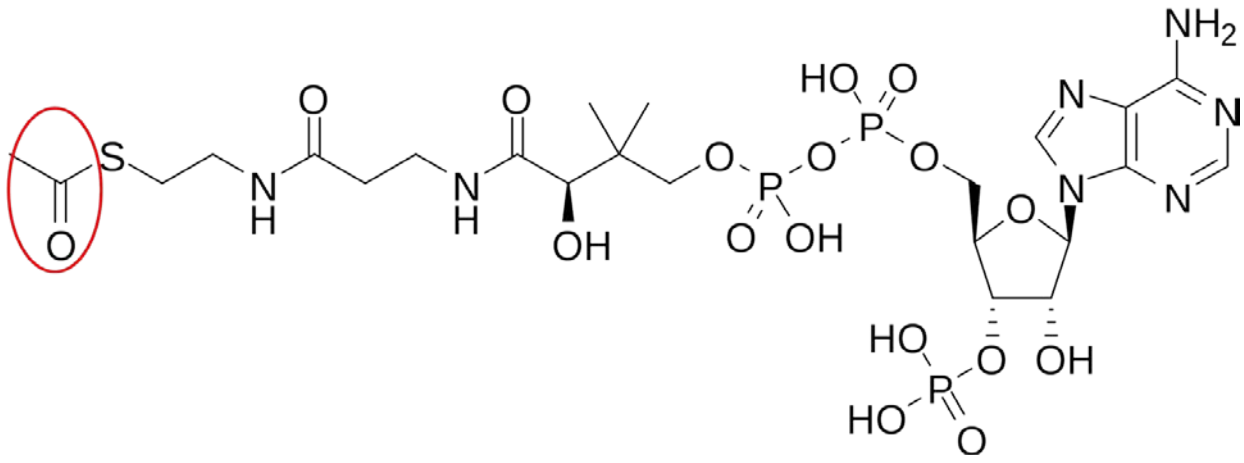

Figure 1-3: Acetyl-CoA molecule, with acetyl group circled

1.4 Pressure Dependence of Enzymatic Reaction Rates

The rate at which ethanol can be produced by P11 is a function of both the number of enzymes present in the cell and the efficiency with which the enzymes perform their metabolic functions. It is important that hydrogenase operates efficiently so that the CO will not need to be oxidized to generate electrons, limiting product yield. Genetic engineering may eventually be used to over-express the enzymes in the cell (See von Abendroth, 2008), but changing the number of enzymes present does not improve the efficiency at which each enzyme operates. Three of the enzymes, hydrogenase, formate dehydrogenase (FDH), and carbon monoxide dehydrogenase (CODH), use the gases of the syngas feed stream as their substrates and can have their efficiencies affected by the partial pressures to which the enzymes are exposed. This means

that ethanol production efficiency might be improved by optimizing concentration (pressure) ranges of the components of the syngas feedstream. However, knowledge of the kinetic parameters is critical for assessing optimal concentration ranges.

Since kinetic parameters for P11's hydrogenase were previously unavailable, published kinetic parameters from *Clostridium pasteurianum* (Adams and Mortenson, 1984) were used to conduct a preliminary analysis to reveal the possible magnitude of H_2 partial pressure effects on enzyme efficiency. In this analysis, a published Michaelis constant (Adams and Mortenson, 1984), K_M, of 0.4 mM (0.51 atm after conversion to pressure units with a Henry's Law constant of 0.783 mM/atm (derived from Perry, 1997)) was used in the Michaelis-Menten rate equation to obtain a velocity versus H_2 pressure curve (Figure 1-4). The equation is:

$$\frac{V_0}{V_{\max}} = \frac{P_H}{K_M + P_H} \quad , \tag{1.1}$$

where V_0 is the predicted velocity of the reaction, V_{max} is the theoretical maximum reaction velocity, and P_H is the H_2 partial pressure.

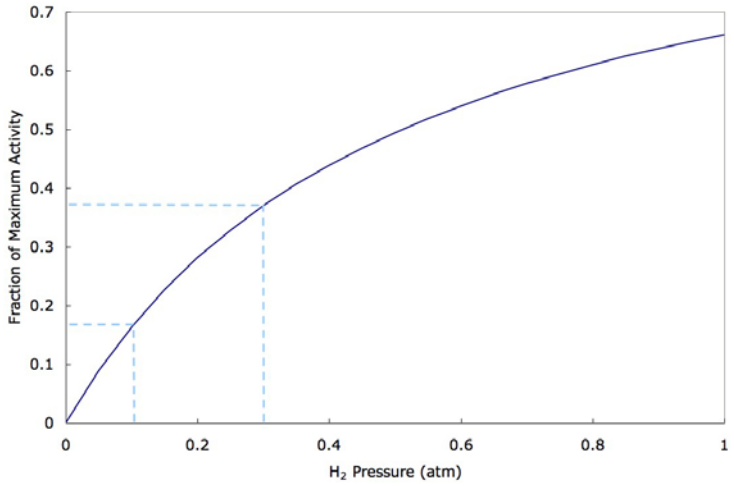

Figure 1-4: Hydrogenase activity has the potential to more than double with an increase in H_2 pressure of only 0.2 atm. Equation 1.1 was used to generate the figure.

The curve obtained using these parameters applies only to the specific assay conditions used, but the results do give a rough estimate of the effects of H_2 on the hydrogenase reaction rate. Tests that give more broadly applicable results are discussed in Chapter 4 of this work. Nevertheless, when a pressure of 0.1 atm H_2 is used in Equation 1.1, it is revealed that hydrogenase is only functioning at 16.4% of its maximum capacity. When a pressure of 0.3 atm H_2 is used, hydrogenase is found to function at 37.0% of its maximum capacity. This indicates that an increase of only 0.20 atm H_2 partial pressure could increase hydrogenase activity by more than two-fold. Both of the pressures used in this analysis are reasonable pressures for H_2 obtained from a biomass gasifier, demonstrating that increasing H_2 partial pressure in a syngas fermentation reactor may be critical for maximizing the efficiency of the hydrogenase enzyme. It is important that hydrogenase operates efficiently so that the CO will not need to be oxidized to generate electrons, limiting product yield.

Unfortunately, reactor pressure cannot be increased indiscriminately to improve enzyme activity because CO, which is a substrate for the CODH enzyme, is a known inhibitor of hydrogenase (Tibelius and Knowles, 1984). Thus, increasing CO partial pressure would likely improve CODH efficiency, but it would also decrease hydrogenase efficiency. Other inhibition effects might also occur if certain partial pressures of the syngas components are too high. Additionally, gas partial pressures change as the substrate gases are consumed by the enzymatic reactions. Determining the optimal balance of these effects, or in other words, determining a range of syngas partial pressure operating conditions that will promote both gas utilization and enzyme efficiency will require accurate kinetic models of hydrogenase, FDH, and CODH activity as functions of H_2, CO, and CO_2 partial pressures.

1.5 Research Objectives

The goal of this research has been to accurately model the effects of H_2 partial pressure on hydrogenase activity in the ethanol producing bacterium Clostridium P11 and to recommend an operating pressure for H_2 during syngas fermentation processes that employ this bacterial strain. Three objectives have lead to the accomplishment of this goal and are summarized as follows.

1.5.1 Objective 1- Assay Development

Development of an accurate assay for hydrogenase activity is crucial to obtaining accurate kinetic data. Assay procedures found in literature, though plentiful, are extremely varied and the results obtained from them, such as the K_m, often appear conflicted (Table 1-1). Many researchers have expressed frustration over this non-standardization. In this objective, a reliable assay for measuring H_2 oxidation via Clostridium P11's hydrogenase is developed. This includes quantification of many of the sources of variability: oxygen scavenging systems, cell permeabilization systems, pressure/solubility effects, competing reactions, and enzyme inhibition. The improved assay made it possible to have consistent and reliable kinetic measurements.

Table 1-1: Published apparent Michaelis constants (K_m). MB is methylene blue, MV is methyl viologen and BV is benzyl viologen.

Organism	Method	Indicator	K_m (mM)	Source
Clostridium pasteurianum	Purified (I)	MB	0.18	(Adams and Mortensen, 1984)
	Purified (I)	MV	5	(Adams and Mortensen, 1984)
	Purified (II)	MB	0.4	(Adams and Mortensen, 1984)
	Purified (II)	MV	5.7	(Adams and Mortensen, 1984)
Megasphaera elsdenii	Purified	BV	5.7	(Van Dijk, 1980)
	Purified	MV	171	(Van Dijk, 1980)
Sporomusa sphaeroides	Purified	BV	0.341	(Dobrindt and Blaut, 1996)

1.5.2 Objective 2- Kinetic Modeling

A multitude of kinetic models have been proposed for hydrogenase and mechanistic understanding is still growing. This process is complicated by the fact that multiple kinds of hydrogenase exist. In Objective 2 an appropriate kinetic model for P11's hydrogenase is selected from the published literature. The experiments which lead to the selection of the model are presented. The kinetic model is used to calculate the value of a kinetic constant associated with hydrogenase's dependence on H_2 partial pressure. From this information, a recommendation of the H_2 operating pressure needed for optimizing the hydrogenase activity during syngas fermentation is provided.

1.5.3 Objective 3- Physiological Insights

It is well known that hydrogenase activities are strongly affected by pH. However, since P11 is a novel bacterium, this pH dependence has not previously been documented. In Objective 3, experiments are presented which demonstrate the effect of pH on P11's hydrogenase activity. This includes measurements of both intracellular and extracellular pH, and a discussion on the effect of the pH gradient across the cell membrane. Additionally, it is well understood that hydrogenase's primary role in syngas fermentation is to supply reducing power (needed for ethanol production), and Objective 3 contains data from P11 that contributes to this understanding. Specifically, a possible link between the time of greatest hydrogenase activity and the time of greatest ethanol productivity is discussed in light of P11 data and data from the literature.

2 LITERATURE REVIEW

The purpose of the research presented in this thesis is to accurately model the effects of H_2 partial pressure on hydrogenase activity in the ethanol producing bacterium Clostridium P11. This modeling will enable recommendation of an operating pressure for H_2 during syngas fermentation processes that employ this bacterial strain. In order to reach this objective, accurate and consistent assays of hydrogenase activity need to be performed. Chapter 2 reviews published assay procedures and demonstrates some of the published difficulties encountered when performing these assays. This sets the appropriate context for the development of P11's assay discussed in Chapter 3. Chapter 2 also reviews published reaction mechanisms and kinetic rate laws for hydrogenase, to enable selection of the appropriate rate law for P11's hydrogenase (presented in Chapter 4). Finally, Chapter 2 reviews the current understanding of hydrogenase's physiological role in syngas fermentation. This sets the context for discussion of the physiological role of P11's hydrogenase, found in Chapter 5.

2.1 Hydrogenase Assay Procedures

The hydrogenase enzyme catalyzes the reversible conversion of H_2 to its component protons and electrons:

$$H_2 \xleftrightarrow{hydrogenase} 2H^+ + 2e^- \tag{2.1}$$

In systems without an external electron acceptor, this reaction results in either an ortho/para conversion of the H_2 molecule or in a deuterium or tritium exchange reaction with water (Cammack, 2001). In physiological systems, the electrons are exchanged with an electron carrier such as NADPH/$NADP^+$ (de Luca, 1998) or ferredoxin (Chen and Blanchard, 1979), but these are often substituted for color-changing dyes such as methylene blue (Maness and Weaver, 2001) and benzyl or methyl viologen (Van Dijk, 1979) during experimentation. Alternatively, researchers have assessed hydrogenase activity by measuring changes in H_2 pressure with a manometer (Gest, 1954). Finally, researchers can also use electrochemical techniques to investigate reaction kinetics (De Lacey, 2000). As H_2 oxidation via hydrogenase is critical for the best conversion efficiency of carbon in syngas to carbon in ethanol, the following review focuses on assay procedures previously used to assess H_2 oxidation activity via hydrogenase. Activity (U) in this thesis is defined to be:

$$Activity = \frac{\mu mol_{H_2}}{\min} = U \tag{2.2}$$

Specific activity in this work is the activity normalized by either the purified enzyme mass or the whole cell dry mass used for the assay:

$$SpecificActivity = \frac{Activity}{mass} = \frac{U}{mg} \tag{2.3}$$

When specific activity is used, the normalization species will be expressed explicitly.

2.1.1 Manometric Assay

One of the first assays of hydrogenase used a manometer to measure H_2 consumption over a solution of hydrogenase containing bacteria and oxidized electron acceptor (Gest, 1954). In this instance the volume of H_2 removed from the system by oxidation was normalized by the

amount of bacteria present to obtain an estimate of hydrogenase activity. Manometric assays have largely been replaced by more sophisticated techniques.

2.1.2 Ferredoxin Assay

The physiological electron partner for hydrogenase in many Clostridia is ferredoxin (Adams, 1981) though flavodoxin is known as a physiological partner as well (Demuez, 2007). Chen and Blanchard (Chen and Blanchard, 1979) describe an assay procedure for reduction of ferredoxin by hydrogenase that is still utilized today (Demuez, 2007). In this procedure ferredoxin is reduced by hydrogenase in the presence of H_2. The reduced ferredoxin reduces metronidazole, which experiences a loss in absorption at 320 nm during reduction. The direct reduction of metronidazole (w/o ferredoxin) by hydrogenase is minimal so this allows the rate of reduction of ferredoxin by hydrogenase to be monitored spectrophotometrically. The rate of reduction can be associated with the hydrogenase activity.

2.1.3 Artificial Dye Assays

Instead of using a double reduction reaction scheme as was presented for the ferredoxin assay, many researchers eliminate a step by substituting an artificial redox dye, such as methyl viologen, for the physiological electron acceptor. In one form of this assay, anaerobic cuvettes filled with H_2 in the headspace and oxidized methyl viologen and buffer in the liquid phase are injected with purified hydrogenase. A color change associated with methyl viologen reduction is monitored spectrophotometrically to quantify the hydrogenase activity (Serebryakova, 1996). In a variation on this approach, viable cells are permeabilized with a detergent to facilitate

interaction of the dye with hydrogenase, while leaving the hydrogenase more nearly in its physiological setting (Shenkman, 2003). Assays using artificial redox dyes are the most prevalent in the literature and are the historical work-horse of hydrogenase kinetic studies. A modified version of this assay is employed in the current study.

2.1.4 Electrochemical Assays

A more recent hydrogenase assay is one that immobilizes purified hydrogenase on an electrode and measures its activity (both oxidation and reduction of H_2) as the electric potential of the electrode is varied. The major advantage to this technique is that the H_2 half-reaction interacts directly with the electrode and can be decoupled from the accompanying oxidation/reduction of the physiological or artificial electron partner. This decoupling allows for extremely rapid turnover rates and very high-resolution kinetic measurements (Pershad, 1999). (This is the method employed by researchers to determine the molecular mechanism of the hydrogenase reaction.) The major weakness of this technique for syngas fermentation is that in syngas fermentation the hydrogenase reaction occurs *in vivo* and hydrogenase donates its electrons to a redox partner. Thus, though these assays yield the most precise kinetic information for hydrogenase independent of a redox partner, the assays neglect many true phenomena associated with the syngas fermentation system of interest to this study.

2.2 Complications with Performing Hydrogenase Assays

Performing a hydrogenase assay to obtain useful kinetic information can be a very difficult undertaking. The literature is ripe with examples of the difficulties that can be

encountered: maintaining anaerobic conditions (Fisher, 1954), limited gas solubility and slow gas diffusion rates (Leroux, 2008), enzyme inhibition (Tibelius and Knowles, 1984), decisions about whether to purify the enzyme or test permeablized cells (Cammack, 2001) (Shenkman, 2003), and rate discrepancies with different electron acceptors (Serebryakova and Sheremetieva, 2006). A brief review of these challenges follows, accompanied by brief statements of how these phenomena relate to the current study of P11.

2.2.1 Anaerobic Conditions

One of the major difficulties in assaying hydrogenase is its extreme sensitivity to oxygen. Living P11 cells cannot be exposed to oxygen as P11 is a strict anaerobe and purified hydrogenase is inactivated by oxygen (Fisher, 1954). Though various anoxic procedures exist, such as gas sparging and utilization of an anaerobic chamber, at least one researcher has found that utilization of an anaerobic chamber yields more precise confidence intervals than extensive gas sparging (Shenkman, 2003).

Another frequently applied approach is the addition of an oxygen-scavenging reducing agent to the reaction mixture. Three commonly used agents are glucose/glucose oxidaze, 2-mercaptoethanol/vitamin-B12 derivative, and dithiothreitol (DTT). Unfortunately, all of these systems can result in false activity being observed. Typical control experiments to eliminate this effect include subtracting the blank activity or verifying that it is small compared to the true reaction rate (Van Dijk, 1979) (Shenkman, 2003). Anaerobic chambers, gas sparging, and addition of a reducing agent are all used in the assay of P11 and Chapter 3 explains how these techniques can be effectively used together during this assay.

2.2.2 Gas Solubility and Diffusion

An additional difficulty with performing hydrogenase assays and with syngas fermentation in general is the biphasic nature of the reacting system. The primary substrate, the syngas, is all in the gas phase, while the enzyme is in the liquid phase. A useful tool for studying biphasic systems incorporates Henry's Law,

$$P_i = x_i H_i \tag{2.4}$$

which relates the partial pressure of a gas in the headspace above a liquid, P_i, to the mole fraction of that species in the liquid, x_i, by means of a species-specific proportionality constant, H_i, known as the Henry's Law coefficient. Perry's Chemical Engineering Handbook reports a Henry's Law coefficient of 74200 atm for H_2 at 35°C (Perry, 1997), which corresponds to a liquid mole fraction of only 1.35×10^{-5} for an aqueous solution under 1 atm H_2. The scarcity of H_2 molecules in solution limits its interaction with hydrogenase and can cause observed activities to be lower than the true activity.

To additionally complicate the situation, once the H_2 is dissolved in the assaying medium, it (and its corresponding electron acceptor) must diffuse to the enzyme. Two studies give particular insight into this process. Tatsumi et al. (Tatsumi, 2000) modeled mass transfer of H_2 to a viable *Desulfovibrio vulgaris* cell surface and through the cell membrane and compared it to the actual rate of the catalytic H_2 oxidation. They concluded that the slowest step was the H_2 diffusing through the liquid toward the cell. Additionally, they observed that the catalytic reaction occurred at near mass-transfer limited rates. The other study involved an in depth look at diffusion of H_2 through a tunnel on the hydrogenase enzyme leading to the active site (Leroux, 2008). From these articles it is apparent that the hydrogenase reaction is far more complicated

than it appears at first glance. In Chapter 3 calculations are presented which allow comparison of P11 hydrogenase reaction rates to the diffusion capabilities of the assaying system.

2.2.3 Enzyme Inhibition

Most enzymatic reactions have inhibitors and it is important to know the species that inhibit the necessary enzymatic reactions in a process. Often, the product of a reaction inhibits further reaction of that enzyme. In syngas fermentation, CO, which is one of the three primary substrates of the entire process, inhibits hydrogenase activity. The magnitude of this inhibition has been quantified for many bacterial hydrogenases, and in Chapter 3 it is quantified for P11's hydrogenase. Implications of this inhibition for syngas fermentation are also discussed.

2.2.4 Whole Cell vs Purified Enzymes

A second difficulty in assaying hydrogenase is specificity. Cellular networks are highly complicated and many potential electron acceptors exist in the cellular environment. For example, even if the electrons generated by the hydrogenase reactions are transferred to ferredoxin, they could very rapidly be transferred to NAD^+ and from the resulting NADH to any number of cellular molecules. The most commonly employed method of eliminating this complication is to purify hydrogenase. However, different purification techniques have been shown to dramatically affect measured activities (Demuez, 2007). Often this is due to the different activation states of purified hydrogenase. Another approach to avoiding unmonitored side reactions is to supply an electron acceptor, such as methyl viologen, that short-circuits the physiological pathways (Demuez, 2007). When whole cells are used with an artificial redox dye,

as in the assay of P11's hydrogenase, the problems with activation are avoided and the enzyme is able to stay in its physiological environment for longer. However, the detergent used to permeabilize the cell membrane is believed to degrade hydrogenase over time. This effect is quantified in Chapter 3 to give researchers a more exact understanding of the effect of Trition X-100, a common detergent, on P11's hydrogenase. As an alternative to detergents, ultrasound (Guzmán, 2001) or electroporation (Tekle, 1994) may be able to be used to disrupt the cell membrane.

2.2.5 Rate Discrepancies with Electron Acceptors

Performing hydrogenase assays with different electron acceptors results in different rates of reaction. Serebryakova and Sheremetieva (Serebryakova and Sheremetieva, 2006) performed an experiment where they measured hydrogenase activity using NAD^+/NADH, $NADP^+$/NADPH, methyl viologen, and benzyl viologen. They concluded that the rates of reaction with the physiological molecules were significantly slower than the rates of the reactions using the viologen dyes. This implies that the rate of H_2 oxidation is inherently coupled to which molecule accepts the electrons and may make measuring and modeling the physiological reaction more difficult. The kinetic rate laws for hydrogenase discussed in this chapter and again in Chapter 4, show mathematically how different electron acceptors affect the rate of P11's hydrogenase. In Chapter 4, a kinetic constant associated with H_2 partial pressure is determined that is independent of the electron acceptor used in the reaction. It is the determination of this constant that makes possible the recommendation of a H_2 partial pressure to be used for syngas fermentation.

2.3 Kinetic Modeling of Hydrogenase

The intricacies of the hydrogenase reaction system and the abundance of the aforementioned assaying complications lead to difficulties in measuring and understanding true hydrogenase kinetics. The classical approach is to use the single substrate Michaelis-Menten equation:

$$V_0 = \frac{V_{\max}[S]}{K_S + [S]} \tag{2.5}$$

where V_0 is the measured reaction rate, V_{max} is the theoretical maximum reaction rate, [S] is the concentration of the reacting substrate (e.g. H_2), and K_S is the Michaelis constant. The Michaelis constant is defined as

$$K_S = \frac{k_2 + k_{-1}}{k_1} \tag{2.6}$$

where the *k* values represent the reaction rate constants for the individual reaction steps shown in the following simple reaction mechanism:

$$E + S \underset{k_{-1}}{\overset{k_1}{\rightleftarrows}} ES \xrightarrow{k_2} E + P \ . \tag{2.7}$$

In Equation 2.7, *E* represents hydrogenase, *P* represents the reaction product (protons), and S is the same as defined above.

The Michaelis-Menten equation has received such widespread usage because of its simplicity and because it accurately describes many reactions, even many reactions that do not meet the assumptions imposed in the derivation of the equation. Finally, this model can also be easily expanded to include various forms of inhibition, making it extremely versatile (Nelson, 2005).

In recent years however, researchers have begun exploring the reaction kinetics of hydrogenase much more thoroughly. This has been a result of better understanding of reaction mechanisms and has resulted in significantly improved kinetic models. Tatsumi et al. used an equation similar to the Michaelis-Menten equation, but it was improved in that it accounts for both substrates (H_2 and the electron acceptor) at the same time instead of separately (Tatsumi, 2000):

$$V_0 = \frac{V_{\max}}{1 + \frac{K_S}{[S]} + \frac{K_M}{[M_{ox}]}} \tag{2.8}$$

Here V_0, V_{max}, and [S] are all defined the same as in the Michaelis-Menten equation, $[M_{ox}]$ is the concentration of the oxidized form of the electron acceptor, and K_S and K_M are constants associated with the H_2 and electron substrates, respectively. How this equation was derived and the reaction model associated with it were described by Ikeda et al. (Ikeda, 1996). They assumed the following reaction model:

$$E_{ox} + S \underset{k_{-1}}{\overset{k_1}{\rightleftarrows}} ES \xrightarrow{k_2} E_{red} + P \tag{2.9}$$

$$E_{red} + M_{ox} \underset{k_{-3}}{\overset{k_3}{\rightleftarrows}} EM \xrightarrow{k_4} E_{ox} + M_{red} \tag{2.10}$$

where the variables are all the same as defined above with the addition of P representing the product (in this case protons) into which S is converted and E represents the hydrogenase enzyme in either its oxidized, E_{ox}, or reduced, E_{red}, state. The k values represent kinetic rate constants of the individual reaction steps.

Using these assumptions the specific definitions of K_S and K_M were determined to be:

$$K_S = \frac{k_4}{k_2 + k_4} \frac{k_{-1} + k_2}{k_1} \tag{2.11}$$

$$K_M = \frac{k_2}{k_2 + k_4} \frac{k_{-3} + k_4}{k_3} \tag{2.12}$$

which shows that K_S for this model is clearly different from the K_S shown in Equation 2.6.

It is interesting to observe from the above definitions that K_S depends on k_4, which is the rate of release of the electron acceptor from the enzyme and that similarly, K_M depends on k_2, the rate of release of the protons from the enzyme. This implies that K_S and K_M are not only functions of the identity of the chemical species with which they are associated, but depend inherently on the other species as well, giving a truly coupled system. Greater discussion of this idea is presented in Chapter 4 of this work.

The most accurate and applicable rate laws are those that account for the physiological mechanism. The true mechanism of hydrogenase action is currently under intense study and consensus has not been reached on all aspects of this process. However, it is generally accepted that iron-iron hydrogenases have two stable oxidation states, denoted simply E_{ox} and E_{red}, and that nickel-iron hydrogenases have three stable oxidation states, denoted Ni-R, Ni-C, and Ni-SI (De Lacey, 2007). The way electrons are transferred between these states can be expressed in a few simple models and their corresponding rates laws.

2.3.1 Nickel-Iron Hydrogenase

The nickel in the active site of an activated nickel-iron hydrogenase has three redox states: Ni-S, Ni-C, and Ni-SR (this source uses slightly different names from the previous source). Kinetic theories on this subject can be condensed into two primary models: the triangular kinetic model and the double cycle model. In the triangular model, molecular H_2 binds to hydrogenase in the S state and causes a shift to the C state. One proton and one electron

are given up as the enzyme switches from the C state to the SR state. Finally, another proton and electron are given up as the SR state converts back to the S state, and the cycle begins again. In the double-cycle model H_2 can bind to either the S state or the C state, converting hydrogenase to the C state or SR state, respectively. Protons and electrons are given up as the SR state reverts back to the C state or the C state reverts back to the S state. The triangular model and double cycle model are shown in Figures 2-1 and 2-2, respectively. An autocatalytic addition to the triangular model was also considered in which the occurrence of Ni-C encourages more rapid conversion of Ni-S to Ni-C (Osz, 2005).

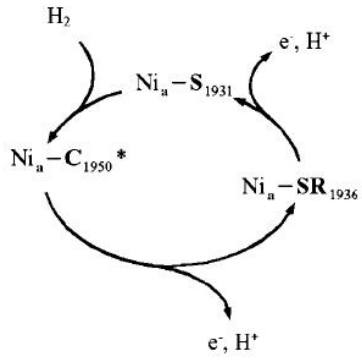

Figure 2-1: Triangular reaction mechanism for Ni-Fe hydrogenases (Osz, 2005)

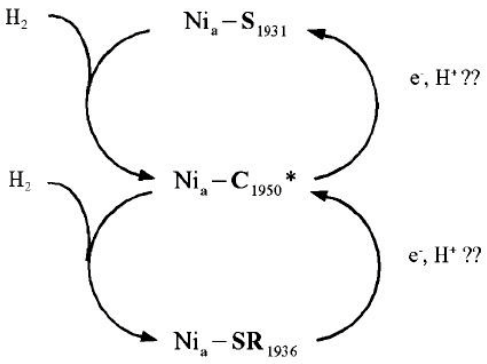

Figure 2-2: Double cycle reaction mechanism for Ni-Fe hydrogenases (Osz, 2005)

Osz et al. (Osz, 2005) converted the traditional triangular model into the following rate law:

$$V_0 = \frac{2bcd[H_2][M_{ox}]^2}{cd[H_2][M_{ox}]^2 + bd[H_2][M_{ox}]^2 + bc}[E_t] \tag{2.13}$$

where *b*, *c*, and *d* represent kinetic constants for the conversion of the S state to the C state, the C state to the SR state, and the SR state back to the S state, respectively. E_t is the total active enzyme concentration and the other variables are as defined above. The rate law for the autocatalytic triangular model was shown to be:

$$V_0 = \frac{2cd[H_2][BV]^2}{d[H_2][BV]^2 + c}\left([E_t] - \frac{c}{b}\right) \tag{2.14}$$

where the variables are the same as above.

When electrochemical methods are used to measure activities of Ni-Fe hydrogenases (as described in section 2.1.4), a current is produced at the electrode that is a function of the enzyme activity and the number of enzymes on the electrode. Because current is included in the resulting rate law instead of an electron acceptor, rate laws derived from electrochemical methods appear different from traditional rate laws. The details of these rate laws can be found in the literature (Leger, 2002) (De Lacey, 2000) but are unnecessary to the current discussion, as this work employs a viologen assay.

2.3.2 Iron-Iron Hydrogenase

The kinetic model for the iron-iron hydrogenase is significantly simpler than the kinetic model for the nickel-iron hydrogenase. It is similar to the rate law and kinetic mechanism described in Equations 2.8-2.10, except that the Fe-Fe hydrogenase model accounts for specific

and discrete electron and proton transfer steps instead of lumping all the steps into one "black-box" substrate-to-product conversion step. The iron-iron hydrogenase model describes two active site oxidation states: E_{ox} and E_{red}. The E_{ox} state is the state that binds molecular H_2 and the E_{red} state is the state capable of reducing protons in the reverse reaction. Two electrons are transferred for each H_2 molecule that is oxidized, but there is only one electron difference between the two states. It has been concluded that the extra electron is given to a neighboring iron-sulfur complex during the reaction. One possible mechanism is detailed in Figure 2-3 (De Lacey, 2007). The rate laws that can be derived from mechanisms like these (with varying orders of proton and electron transfer) are discussed further in Chapter 4, as a rate law derived from this type of mechanism was found to most accurately fit P11's hydrogenase.

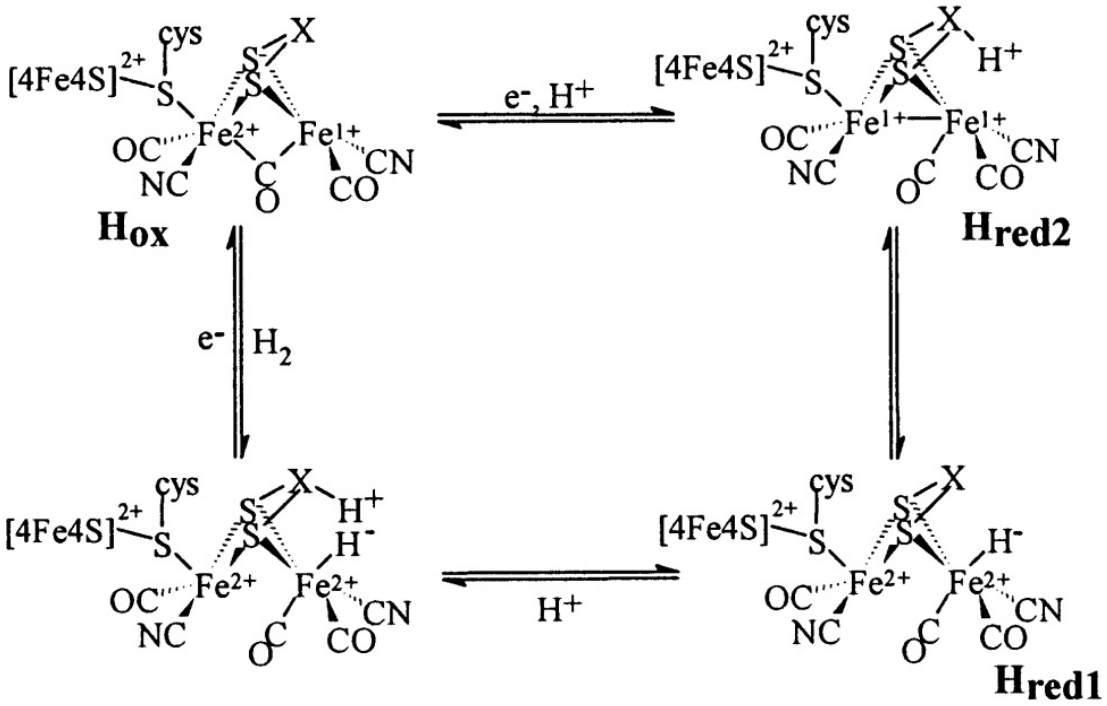

Figure 2-3: Possible reaction mechanism for Fe-Fe hydrogenase (De Lacey, 2007)

2.4 Physiological Role of Hydrogenase

The end goal of the research presented in this thesis is to determine the partial pressure of H_2 needed to optimize hydrogenase activity in P11 during syngas fermentation. Improving hydrogenase activity should allow P11 to produce more ethanol. However, metabolic systems are highly complex and no inference should go untested. In this section the physiological role of hydrogenase in various bacteria is explored. Specifically, hydrogenase's role in regulating redox potential is discussed, followed by a discussion how the extracellular environment affects hydrogenase. Next, a link between hydrogenase activity and ethanol production is explored, and a discussion of how hydrogenase activity is affected by intracellular and extracellular pH concludes the chapter. These discussions establish the context for interpreting the results of several experiments of physiological consequence with P11 presented in Chapter 5.

2.4.1 Regulation of Redox Potential

The reaction hydrogenase catalyzes is a direct player in the oxidation/reduction (redox) environment of a cell because the hydrogenase enzyme either contributes electrons by oxidizing H_2 or removes electrons by forming H_2:

$$H_2 \xleftrightarrow{hydrogenase} 2H^+ + 2e^- \tag{2.15}$$

A review on hydrogenase by Adams et al. (Adams, 1981) explains that H_2 supplies organisms with reducing power which can be used to produce energy. Alternatively, if an organism is overly reduced it can produce H_2 to restore the desired equilibrium. Since electrons do not exist free of chemical compounds in biological systems, the electrons are typically transferred to or from common redox agents such as NAD^+ or NADH, the relative ratio of which is the major

determinant of a cell's redox state (Lee, 2008a). Reduced ferredoxin is known to be the physiological electron donor in *Clostridium acetobutylicum* (Demuez, 2007). Adams (Adams, 1981) discusses that when H_2 is produced, the cell is typically trying to recycle the electron carriers that become reduced during fermentation. When H_2 is consumed for energy, ATP is produced by the electron transport chain instead of by phosphorylation from other metabolic species. It is also noted that when hydrogenase is associated with an electron transport chain, it has the potential to create a transmembrane electromotive gradient. Hydrogenase is thus believed to play an important role in maintaining an appropriate redox level in many bacterial cells.

2.4.2 Hydrogenase Activity as a Function of Extracellular Environment

An experiment was performed by Kellum and Drake (Kellum, 1984) that showed that the expression/activity of hydrogenase in the cell is affected by its external environment. In this experiment, the authors cultivated *Clostridium thermoaceticum* under 5 different gas headspaces (CO_2, CO, N_2, H_2, and 80%H_2/20% CO_2). Dissolved glucose was the primary energy source for each study. The authors measured hydrogenase specific activity, cell growth, and the production/consumption of H_2 and CO_2. When grown under pure CO headspace, both the liquid phase and the gas phase were composed of high energy molecules. As a result, this extra reducing potential was disposed of as H_2. More H_2 was produced and measured hydrogenase activity was higher than for any of the other headspaces. Conversely, for the H_2-CO_2 headspace, H_2 was consumed as an energy source, despite the presence of glucose in the media. CO_2 was also consumed for this headspace, while it was produced for all the others. This consumption of CO_2 and H_2 is the subject most related to the current study.

2.4.3 Hydrogenase Activity Linked to Ethanol Production

Since it is known that ethanol is produced during the solventogenic phase of bacterial growth and that H_2 can supply reducing power to a cellular system, it is interesting to consider a link between ethanol production and hydrogenase activity. Lee (Lee, 2008b) reports the findings of Mitchell et al. (Mitchell, 1998) that a reducing environment is needed for *Clostridia* to make butanol and ethanol and more reducing environments cause more solvent production. These statements are confirmed in an interesting experiment conducted by Younesi et al. (Younesi, 2005).

In this experiment, the researchers measured CO, CO_2, and H_2 usage and acetic acid and ethanol production with time for different syngas (CO, CO_2, and H_2) pressures. Although CO and CO_2 were purported to be the only carbon source, fructose was present in the media, so this may have confounded the results. Nevertheless, the findings seem to agree with theory. First, CO was the initial gas phase molecule to be consumed. This was accompanied by an increase in CO_2 pressure. Both ethanol and acetic acid were produced during this time. The increase in CO_2 pressure seems to indicate that either CO was being oxidized to CO_2 to provide electrons to the metabolic pathway, or CO_2 was being produced by the oxidation of the fructose. H_2 pressures remained constant during this time, giving credence to the idea that the CO consumption was a result of its oxidation to supply reducing power. Another complementary reason that H_2 composition remained unchanged during this time is that CO is a known inhibitor of hydrogenase (Kim, 1984). This idea was confirmed after the CO is exhausted in the two highest pressure tests. Immediately, once the inhibitor was gone, the H_2 began to be utilized. This was accompanied by utilization of CO_2. Ethanol was produced both as the CO was being utilized and after it was exhausted. This seems to indicate that ethanol can be produced using both CO and

H_2 as a source of reductant, but that CO is used preferentially, either because it is a more favorable electron donor or because its presence inhibits hydrogenase function. A similar experiment performed by Heiskanen, et al. (Heiskanen, 2007) offered similar results and conclusions when it was noted that the CO in the experiments had been almost completely used before the H_2 started disappearing. Ethanol was apparently produced during both H_2 and CO utilization in this experiment as well.

2.4.4 Hydrogenase Activity as a Function of Internal and External pH

A very important parameter in nearly every biological system is the pH of the system. This is particularly true for hydrogenase because its reactant/product is hydrogen ions, the direct determiner of pH. Just like the electrons of the hydrogenase reaction (Eqn 2.15) affect redox potentials, the protons of the hydrogenase reaction affect pH:

$$pH = -\log\left[H^+\right] \tag{2.16}$$

That pH is an important parameter in fermentation is confirmed by Lee et al (Lee, 2008b). It was shown that the formation of acetic and butyric acid during acetogenesis causes a decrease in pH, but that when the pH reaches a certain threshold, solventogenesis begins and the acids are converted into the desired solvents. Lee cites Kim et al. (Kim, 1984) as being responsible for some of this information. It is interesting to consider how low pH (high H^+ concentration) affects hydrogenase activity.

The studies of Victor Fernandez (Fernandez, 1983) indicated that the optimal pH for hydrogenase activity (evolution of H_2) was around 5 when methyl viologen (which is used to reduce the protons) was reduced electrochemically, but that the optimal pH was around 7 when dithionite was used to reduce the methyl viologen. He explains the discrepancy by saying that at

low pH the relative ratio of dithionite to bisulfate becomes inefficient at reducing methyl viologen. It seems that for H_2 production a low pH leads to higher hydrogenase activity. This makes conceptual sense as a high concentration of reactant (H^+ ions) typically causes higher reaction rates.

Conversely, for H_2 consuming reactions it would make sense that the optimal pH would be basic, immediately consuming any hydrogen ions that are produced and compelling the reaction forward. This idea was confirmed by the findings of Tsygankov et al. (Tsygankov, 2007). They found that the hydrogenase uptake activity was maximal around pH of 8.5 for *D. baculatum* and around 9.5 for *T. roseopersicina* when these enzymes were in solution. They conclude from this and other work that though a changing proton concentration does affect enzyme conformation and the protonation of some components of the active site, another significant reason that hydrogenase activities change with changing pH is that the reaction free energy changes.

One very interesting physiological idea is that the pH of the growth media or the assaying media may not be the same as the intracellular pH. Thus, researchers may learn the activity of hydrogenase at one pH, but this may not actually represent the true pH at which the enzyme is operating. Two recent papers discuss this idea in some detail.

Valli et al. (Valli, 2005) discuss a method of determining the intracellular pH in yeast cells (*Saccharomyces cerevisiae*). They use a fluorescent probe known as SNARF-4F which emits differently depending on the pH that it encounters. They discuss how the yeast cells are able to maintain a relatively constant internal pH even in a dramatically changing external environment. They learned that cells in the stationary phase (solvent producing phase) are more

resilient to changes in external pH than are cells in the growth phase. Another option for evaluating pH gradients across membranes is to used radiolabeled compounds (Harrigan, 1992).

An experiment performed by Huang et al. (Huang, 1985) used radiolabled probes to explore the chemical and electrical components of the proton motive force in *Clostridium acetobutylicum*. They found that the cells maintained a relatively constant internal pH despite a decreasing external pH and concluded that *C. acetobutylicum* is able to deacidify itself by converting its acids into solvents. It seems that a proton gradient (which may affect the activity of the hydrogenase enzyme) results in production of solvents, such as ethanol. The interplay between internal and external pH and their link to hydrogenase activity is explored further in Chapter 5 using data from P11.

2.5 Chapter Summary

This chapter began by surveying the wide variety of assays used to access hydrogenase activity. Many of the complications of performing these assays were then discussed in order to establish a context for the work presented in Chapter 3, where many of the assay difficulties discussed in this chapter will be quantified with data obtained during P11's hydrogenase assay development and the reliable working assay for P11's hydrogenase will be presented.

Next, the kinetic mechanisms and associated rate laws for hydrogenase available in the published literature were summarized. This compilation sets the context for the work reported in Chapter 4, where an appropriate rate law for P11's hydrogenase is selected. Selection of this rate law and the accompanying calculation of a kinetic constant associated solely with the H_2 partial pressure allows the recommendation of an operating H_2 partial pressure for syngas fermentation, which is the focus of this work.

Finally, the physiological role of hydrogenase in various bacteria was explored. Specifically, hydrogenase's role in redox regulation, the effect of the extracellular environment, a possible link between ethanol production and hydrogenase activity, and the effect of intracellular and extracellular pH on hydrogenase activity were all explored, establishing the context for experimental observations made about P11's hydrogenase in Chapter 5.

3 OPTIMIZING P11'S HYDROGENASE ASSAY

P11 is a new bacterial strain and its hydrogenase enzyme is not fully characterized. Consequently, its exact structure is unknown and it is uncertain whether assay procedures established for hydrogenases from other bacteria will work for assaying P11 hydrogenase. The non-standardization of the various published assaying techniques has resulted in contradictory kinetic measurements (van Haaster, 2005) (Osz, 2005). Specifically, the use of different electron acceptors (Serebryakova and Sheremetieva, 2006) and different purification procedures (Demuez, 2007) result in different observed activities. Multiple types of hydrogenase (Fe-Fe, Ni-Fe, or Fe-S) exist (De Lacey, 2007) and can function concurrently in the same bacteria (Demuez, 2007). For these reasons, it was necessary to develop an optimized assay for P11 hydrogenase.

The initial starting point for this work involved Shenkman's procedure (Shenkman, 2003) for assaying the hydrogenase of Clostridial strain P7. Many difficulties were encountered in early attempts to use Shenkman's procedure for assaying P11 hydrogenase. In an effort to understand the difficulties associated with assaying hydrogenase, an engineering analysis of many aspects of the assay procedure was conducted. Extremely valuable insights into the intricacies of the hydrogenase assay have been obtained and are presented in this chapter. The optimized assay procedure is presented first, followed by the studies that lead to the optimization.

3.1 Current Hydrogenase Assay and Data Analysis

The optimized hydrogenase assay was developed following the analysis of six aspects of the assay procedure. The six aspects are: 1) the means necessary to ensure anaerobic conditions (including gas purging and use of an O_2-scavenging agent), 2) H_2 solubility and diffusion, 3) hydrogenase inhibition, 4) relative value of whole-cell vs purified enzyme studies, 5) effects of different electron acceptors, and 6) effects of variations in H_2 pressure. Each of these aspects will be discussed following the presentation of the optimized assay.

3.1.1 Optimized Hydrogenase Assay

P11 cell broth is prepared according the recipes shown in Tables 3-1 through 3-6. All of the ingredients listed in Table 3-1, except the cysteine sulfide solution, are mixed in a large flask and the pH of the mixture is adjusted to 6.0 using a 5N potassium hydroxide solution. Approximately 30 mL of media is then poured into each of three 250 mL passage bottles and ~100 mL of media is poured into a fourth 250 mL bottle (Wheaton). The media in each bottle is boiled for ~4 minutes while N_2 is purged through the liquid. This serves to remove any O_2 from the media. Next, the bottle are sealed with a #1 rubber stopper and metal cap (Wheaton) and are subjected to 3 repetitions of vacuuming of the headspace followed by pressurization with N_2 to ~1.4 atm gauge pressure, all occurring through a 22-gauge needle inserted through the stopper. This process in concluded by venting of the excess N_2 pressure. Next, 0.3 mL of the cysteine sulfide solution (Table 3-5) is injected into each passage bottle and 1 mL is injected into the bottle containing 100 mL of media. The bottles are then autoclaved at 121°C for 15 minutes.

After the bottles have cooled to near room temperature, the first passage bottle is inoculated with a 10% inoculum of P11 (3 mL of 0.6 optical density (OD) solution) and placed in a shaking incubator at 37°C. P11 was obtained originally from Dr. Ralph Tanner of the University of Oklahoma. The other bottles are placed in a refrigerator until needed. When the cells in the 1st passage bottle are in the exponential growth phase (usually 1-2 days after inoculation) the second passage bottle is warmed in the shaking incubator and given a 10% inoculation from the first passage bottle. This process is repeated again for the 3rd passage bottle and subsequently for the final experimental bottle. This final experimental bottle provides the cell broth used in performing hydrogenase assays.

Table 3-1: P11 media composition (~per liter)

Component	Amount
Mineral Solution (Table 3-2)	25 mL
Calcium Solution (Table 3-3)	10 mL
Metals Solution (Table 3-4)	10 mL
Vitamin Solution (Table 3-5)	10 mL
Cysteine Sulfide Solution (Table 3-6)	10 mL
MES Buffer	10 gm
Deionized Water	945 mL
Resazurin	10 drops
Yeast Extract	0.5 gm

Table 3-2: Mineral solution

Component	Product #	Company	gm/L
Magnesium Sulfate Heptahydrate	M-1880	Sigma	20
Potassium Chloride	P-5405	Sigma	10
Potassium Phosphate Monobasic	P-5655	Sigma	10

Table 3-3: Calcium solution

Component	Product #	Company	gm/L
Calcium Chloride Dihydrate	C-3881	Sigma	10

Table 3-4: Metals solution

Component	Product #	Company	gm/L
Nitrilotriacetic Acid (adjust pH to 6.0 using KOH)	N-9877	Sigma	2
Manganese (II) Sulfate monohydrate	221287	Sigma	1
Cobalt(II) Chloride Hexahydrate	202185	Sigma	0.2
Nickel(II) Chloride Hexahydrate	223387	Sigma	0.2
Sodium Selenate, Anhydrous	S-8295	Sigma	0.1
Ammonium Iron(II) Sulfate Hexahydrate	F-3754	Sigma	0.8
Zinc Sulfate Heptahydrate 99%	221376	Sigma	1
Sodium Molybdate Dihydrate	331058	Sigma	0.02
Sodium Tungstate Dihydrate	223336	Sigma	0.2

Table 3-5: Cysteine sulfide solution

Component	Product #	Company	gm/L
Sodium sulfide nonahydrate	S2006	Sigma	40
L-cysteine	C7352	Sigma	40

Table 3-6: Vitamin solution

Component	Product #	Company	gm/L
p-(4)-Aminobenzoic Acid	A-9878	Sigma	0.005
d-Biotin	B-4639	Sigma	0.002
D-Pantothenic Acid hemicalcium salt	P-5155	Sigma	0.005
Folic Acid	F-8758	Sigma	0.002
MESNA (Sodium 2-mercapto-ethanesulfonate)	M-1511	Sigma	0.01
Nicotinic Acid	N-0761	Sigma	0.005
Pyridoxine hydrochloride	P-9755	Sigma	0.01
Riboflavin	R-9881	Sigma	0.005
Thiamine hydrochloride	T-4625	Sigma	0.005
Thioctic Acid (Lipoic Acid)	T-1395	Sigma	0.005
Vitamin B-12	V-2876	Sigma	0.005

Two mixtures, a cell mixture and an electron acceptor mixture, are prepared for each assay in separate 13 mL Hungate test tubes. The electron acceptor mixture is prepared in the anaerobic glovebox (nominally 90% N_2, 5% H_2, 5% CO_2). It is composed of 2.3 mL de-ionized water, 0.3 mL potassium phosphate buffer (1M, adjusted to $pH = 6$ by mixing 1M monobasic potassium phosphate, KH_2PO_4, and 1M dibasic potassium phosphate, K_2HPO_4), and 0.4 mL benzyl viologen dichloride (BV) stock solution (0.04 M). BV is in the oxidized form (BV^{2+}). Also in the anaerobic glove box, the cell mixture is created by mixing 1.8 mL de-ionized water, 0.3 mL potassium phosphate buffer (1M, adjusted to $pH = 6$ by mixing 1M KH_2PO_4 and 1M K_2HPO_4), 0.3 mL DTT (0.5M, prepared daily), and 0.3 mL P11 cell broth. All chemicals were obtained from Sigma-Aldrich.

Both the electron acceptor and cell mixtures are sealed with septum/cap assemblies. Also in the glovebox, 1 mL syringe/needle assemblies are filled with Triton X-100 (diluted 10-fold) for later use. Both of the sealed mixtures and the Triton X-100 filled syringes are then removed from the glovebox. Each mixture is then sparged with the needed gases (typically 100% H_2, but sometimes with an H_2-N_2 mixture) for 5 minutes. This is accomplished by inserting a long 20-gauge needle (with the gas flowing through it at 50 sccm) through the septum and into the solution to sparge the liquid. A short 22-gauge needle is inserted through the septum to provide a vent for the purging gas. The smaller gauge outlet needle helps maintain a positive gas pressure in the tube. A 3-mL syringe with the plunger removed is attached to the electron acceptor solution vent needle and a 1-mL syringe with the plunger removed is attached to the cell solution vent needle. One minute before the end of purging the cell mixture, 0.3 mL of the Triton X-100 solution is injected from the Triton filled syringe through a new hole in the septum into the Hungate tube of the cell mixture. This causes intense bubbling.

At the end of the 5 minutes, the plungers are reinserted into the syringes (stopping the vent flow) and approximately 0.3 atm gauge pressure is allowed to build up in each tube. Both mixtures are removed from the gas supply (with needles, syringes, and plungers all intact) to a water bath and warmed to 37°C. (If only one sparging station is available, the electron acceptor tube should be sparged first, followed by the cell tube. The electron acceptor tube can wait in the water bath while the cell tube is sparged).

While the Hungate tubes are warming, a 3.5 mL septum-sealed optical cuvette (Starna Cells, Inc.) is purged for 2-3 minutes using the same gas mixture as that with which the Hungate tubes were sparged. This is accomplished with two short 22-gauge needles as no liquid is present. At the conclusion of the purge time the vent needle is removed, 0.3 atm gauge pressure is allowed to build up, and the cuvette is removed from the gas supply and placed in the heated (37°C) receptacle of a spectrophotometer.

At this point, 2 mL of the warmed electron acceptor solution is removed from the Hungate tube and injected into the cuvette. This is followed by injecting 0.67 mL of the cell mixture into the same cuvette. The cuvette now has a significant excess of pressure, which is relieved by venting with another short 22-gauge needle joined to a 0.02 atm gauge pressure check valve. After hearing a brief pop (the gas leaves, and the cuvette then has approximately 0.02 atm gauge pressure or 0.86 atm absolute pressure, since ambient pressure in Provo, UT is 0.84 atm), the needle is removed and the cuvette is shaken vigorously several times before being replaced in the spectrophotometer. Figure 3-1 shows a typical output from an assay. The downward sloped region at the beginning is a result of the mixing occurring as the assay is initiated. The data of interest begins as the slope turns upward.

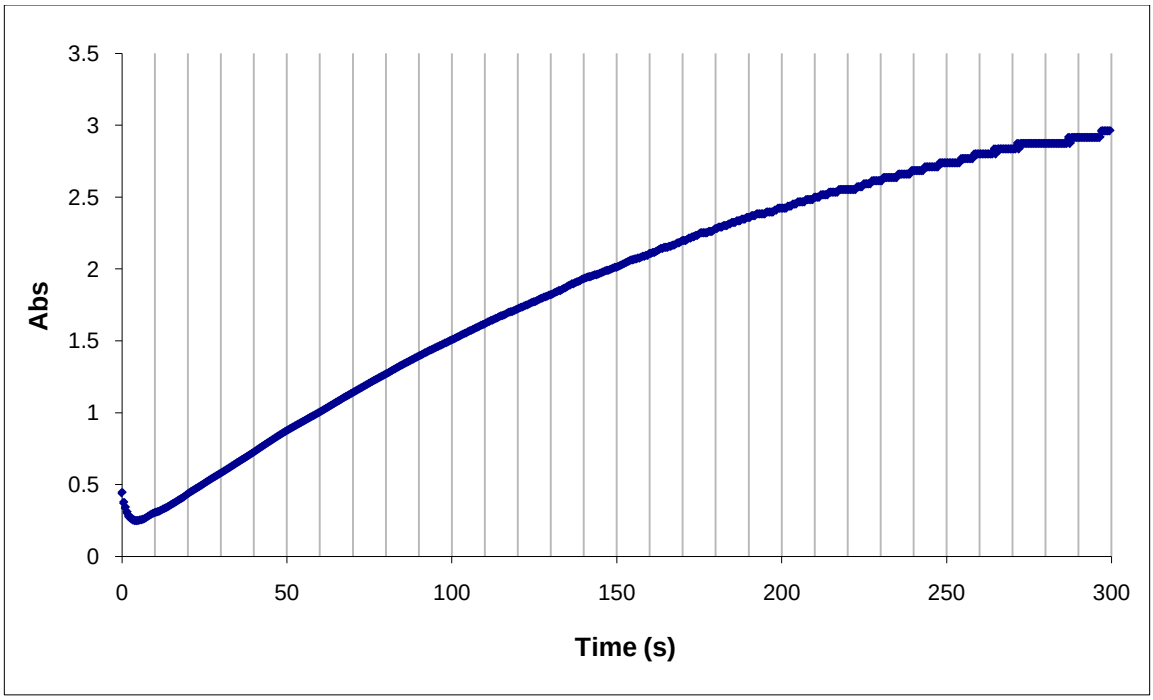

Figure 3-1: Typical absorbance vs time curve for a hydrogenase assay

3.1.2 Assay Data Analysis

The procedure just described gives initial reaction conditions of a saturated H_2 solution with a known oxidized BV concentration (BV^{2+}). As the H_2 and BV^{2+} react, their concentrations begin to decrease according to the following equation:

$$H_2 + 2BV^{2+} \Leftrightarrow 2H^+ + 2BV^+ . \qquad (3.1)$$

BV^{2+} is clear and does not absorb at 546 nm while the reduced form, BV^+, is violet colored and absorbs strongly. The spectrophotometer measures absorbance at 546 nm every 0.5 seconds for 5 minutes, generating an absorbance versus time curve such as the one shown in Figure 3-1, with the increasing BV^+ concentration responsible for the increasing absorbance. In order to avoid

complications in determining the activity with changing concentrations, only the initial slope of the data is used for analysis. Data reduction occurs as follows.

The Lambert-Beer Law governs the operation of spectrophotometers. It expresses a proportional relationship between the absorbance of a sample, *A*, and the concentration of the absorbing species, *c*, within that sample:

$$A = \varepsilon c l \tag{3.2}$$

where ε is the molar extinction coefficient of the absorbing species [7.55 $mM^{-1}cm^{-1}$ for BV, (Shenkman, 2003)], and *l* is the pathlength of the light through the sample (1 cm for this work). The concentration of BV^{+}, C_{BV^+}, represents *c* for this work. Since ε and *l* are fixed, the derivative of the Lambert-Beer Law is

$$\frac{dA}{dt} = \varepsilon l \frac{dC_{BV^+}}{dt} \ . \tag{3.3}$$

When $\frac{dA}{dt}$ is evaluated at the initial slope

$$\frac{dC_{BV^+}}{dt} = \frac{1}{\varepsilon l}(IntSlope) . \tag{3.4}$$

Multiplying both sides by the total volume of liquid in the cuvette, V_c, gives

$$\frac{dn_{BV^+}}{dt} = \frac{V_c}{\varepsilon l}(IntSlope) \tag{3.5}$$

From the stoichiometry of the reaction (Eqn 3.1) it is clear that

$$\frac{dn_{BV^+}}{dt} = -2\frac{dn_{H_2}}{dt} \tag{3.6}$$

which gives

$$\frac{dn_{H_2}}{dt} = -\frac{V_c}{2\varepsilon l}(IntSlope) \tag{3.7}$$

which is the total activity of the system. The final step in determining specific activity is to divide by the mass of cells present in the cuvette during the reaction. The following correlation was adapted from Shenkman (2003) for P7 that relates the mass of cells in a sample of cell broth to an optical density (*OD*) measurement of those cells

$$m_{cells} = V_{cb}\left(515 * OD - 26\right) \tag{3.8}$$

where V_{cb} is the volume of cell broth present in the cuvette and both constants have units of mg/L. This gives

$$SpAct = \frac{1}{m_{cells}}\frac{dn_{H_2}}{dt} = -\frac{1}{m_{cells}}\frac{V_c}{2\varepsilon l}(IntSlope). \tag{3.9}$$

The specific activity in this work is reported as U/(mg_{cells}) where 1 U represents 1 μmol of H_2 consumed per minute.

3.2 Anaerobic Conditions

One of the major difficulties of performing a hydrogenase assay is the extreme sensitivity of the system to oxygen (O_2). O_2 is toxic to the strictly anaerobic Clostridium P11. It is also a potent inhibitor of hydrogenase (Fisher, 1954). Anaerobic preparation chambers, gas purging, and O_2-scavenging agents are frequently used to maintain anaerobic conditions during hydrogenase assays. Shenkman (Shenkman, 2003) applies all of these techniques in his assay of P7 hydrogenase. He effectively defends and quantifies the merit of using an anaerobic chamber for assay preparation, but the gas purging and use of an oxygen-scavenging agent merit further investigation. Calculations justifying the choice of purge times presented in Section 3.1 are presented in the next section, followed by experiments justifying the use of DTT as an O_2-scavenging agent.

3.2.1 Gas Purging

Gas purging is often used to remove undesired gases from a system as well as to saturate systems with desired gases. In this section, a mole balance is used to estimate the amount of time necessary to purge a system. Specifically, the length of time needed to reduce the O_2 levels to below 1 ppm is calculated for both a Hungate tube filled with 3mL of liquid (used for assay preparation) and for an air-filled 3.5 mL cuvette (the reaction vessel).

Hungate Tube

Analysis begins with a system containing both liquid and gas. Mass transfer in this arrangement will be dominated by the liquid phase. Pure H_2 is sparged into a system containing O_2-saturated liquid. The O_2 mole balance in the liquid is:

$$V_R \frac{dC_{O_2}}{dt} = -(k_L a)_{O_2} C_{O_2} \tag{3.10}$$

where V_R is the liquid volume, $k_L a$ is the mass transfer coefficient for O_2, and C_{O2} is the dissolved O_2 concentration in the liquid. The balance assumes a well-mixed solution (likely valid with sparging the liquid) and no O_2 in the gas phase (likely valid with a fast gas flow rate-typically 50 sccm for this work). Integration of Equation 3.10 to determine the time to remove 99.9999% of the initial O_2 ($C_{O2,i}$) gives:

$$t = -\frac{V_R}{(k_L a)_{O_2}} \ln(0.000001) = \frac{13.8 V_R}{(k_L a)_{O_2}} \tag{3.11}$$

For O_2 mass transfer in shake flasks, $k_L a$ was estimated to range from 11-45 mL/min for shake flasks of 10-100 mL containing 10% liquid and shaking at 400 rpm (Wang, 1979). Since the application reported here involves gas sparging of the liquid, it is expected that mass transfer

coefficients should be higher. Choosing the lowest k_La value of 11 mL/min should give a very conservative estimate for the time. Therefore, for the Hungate tube containing 3 mL of solution, the estimated time to remove O_2 is 3.8 min. With a more realistic mass transfer coefficient, the time should even be much shorter.

Reaction Cuvette

The reaction cuvette contains only air before it is purged with H_2 and so the analysis proceeds differently. A mass balance is constructed to describe the accumulation of H_2 in the cuvette

$$n_{in}x_{H_2,in} - n_{out}x_{H_2,out} = \frac{d}{dt}\left(n_{tot}x_{H_2}\right) \tag{3.12}$$

where x_{H_2} represents the mole fraction of H_2 in each location. Since n_{in} is the same as $n_{out.}$, these values are replaced by n_{flow}. Also, since the system is perfectly mixed $x_{H_2,out} = x_{H_2}$ and because pure H_2 is used as the purge gas, the equation becomes:

$$n_{flow}\left(1 - x_{H_2}\right) = n_{tot}\frac{d}{dt}x_{H_2}\,. \tag{3.13}$$

After rearranging, the following equivalent integrals are obtained:

$$\frac{n_{flow}}{n_{tot}}\int_0^t dt = \int_0^{0.999999}\frac{1}{1-x_{H_2}}dx_{H_2} \tag{3.14}$$

with the boundaries of integration coming from the previously mentioned facts that no H_2 is present at time zero and that the desired information is the time, *t*, required for the mole fraction of H_2 in the system to reach 0.999999. Evaluation of the integrals yields

$$t = -\frac{n_{tot}}{n_{flow}}\ln\left|0.000001\right| = 13.8\frac{n_{tot}}{n_{flow}}. \tag{3.15}$$

n_{flow} is set using a mass flow controller but a typical value is 50 sccm (2 mmol/min when the standard conditions are those used to calibrate the controller). n_{tot} is calculated using the ideal gas law and ambient conditions in Provo, UT (0.84 atm, 20°C):

$$n_{tot} = \frac{PV}{RT} = \frac{(0.84 atm)(3.5 cm^3)}{[0.08206 L \cdot atm/(mol \cdot K)](293.15 K)} = 1.2 \times 10^{-4} mol \qquad (3.16)$$

When n_{flow} and n_{tot} are used in Eqn 3.15, the following value is obtained:

$$t = 51 \text{sec} \ . \qquad (3.17)$$

If the system is perfectly mixed, it is clear that one minute of purging should be sufficient for filling a 3.5 mL cuvette with H_2. The greater directionality of flow present in the real system would likely make this value even smaller.

The calculations described in this section justify the choice of purge times (5 minutes for Hungate tubes and 3 minutes for cuvettes) presented in Section 3.1. Though mass transfer calculations such as these are standard engineering problems, it was necessary to apply them to the specific experimental procedure used for this work. These purge times effectively remove O_2 from the system, especially when used in connection with the O_2-scavenging system described in the next section.

3.2.2 Use of O_2-scavenging Agent

An O_2-scavenging agent is often added to assay mixtures to react with residual O_2 in solution and effectively remove the O_2 from the system. It also serves to lessen the effects of O_2 seepage into the mixtures. Commonly used O_2-scavenging agents are glucose/glucose oxidaze, 2-mercaptoethanol/vitamin-B12 derivative, and dithiothreitol (DTT). DTT was the O_2-scavenger used by Shenkman (Shenkman, 2003). Unfortunately, DTT (like the other reducing agents) is

non-specific and thus can reduce other species in the solution. This is especially problematic when DTT reduces the electron acceptor, such as benzyl viologen, used to detect hydrogenase activity.

Early experiments with P11 showed a large "false-positive" from this direct reduction of benzyl viologen by DTT at pH 7.7 and 8.3 (data not shown). When the pH of the assay solution was reduced to 6 (more in agreement with the intended industrial specification) no false positive was evident (data not shown). It was later also shown that this pH value is near the internal pH of P11 cells (See Chapter 5) and performing assays at this pH would leave hydrogenase in a pH environment similar to it physiological environment. Thus, it was decided that the assay should be performed at pH 6. In the development of an assay for P11 hydrogenase, it was necessary to use a concentration of DTT that would effectively scavenge O_2, without false activity being observed (since increasing the DTT concentration could potentially cause a false positive). To this end, three experiments were performed to shed light on the usefulness of DTT for scavenging O_2 during assays.

In the first experiment, four assays were performed as explained in Section 3.1, with the exception that the check value was not yet used during venting. Two of the assays contained DTT (12.5 mM final concentration) and two did not, containing water instead. Shenkman (2003) used a final DTT concentration of 2 mM, but 12.5 mM was used in these studies for more aggressive O_2 removal. Both sets of assays (with 12.5 mM DTT and without DTT) were prepared anaerobically and sparged with H_2 gas before testing. The results can be seen in Figure 3-2 and Table 3-7. Since the hydrogenase activity is associated with the initial slope of a plot of absorbance versus time, it is apparent from the virtually identical initial slopes that at pH 6, 12.5 mM DTT does not result in an appreciable false positive.

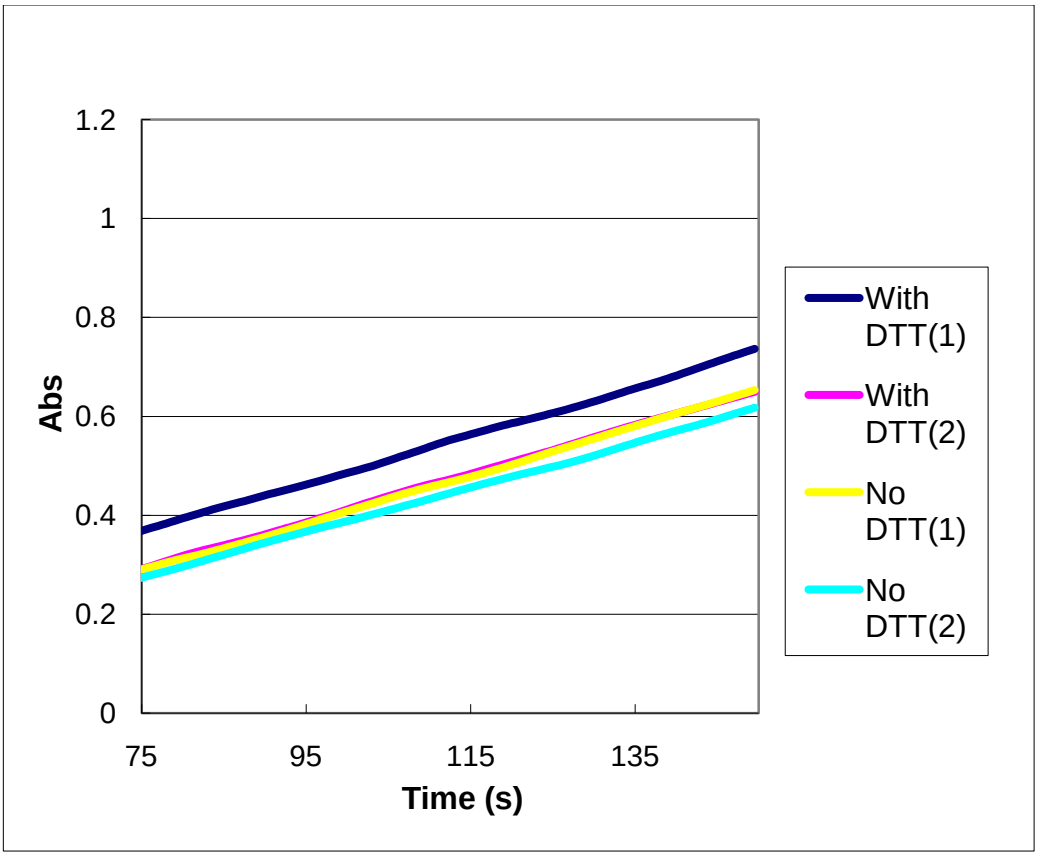

Figure 3-2: Hydrogenase assay with and without 12.5 mM DTT at pH 6

Table 3-7: Initial slopes from DTT false positive experiment with and without 12.5mM DTT at pH 6

Experiment	Slope (Abs/sec)
DTT(1)	4.90E-03
DTT(2)	4.84E-03
NoDTT(1)	4.86E-03
NoDTT(2)	4.61E-03
St. Dev.	1.32E-04

Knowing that DTT does not give a false positive at assay conditions is valuable, but it is also necessary to know that DTT is an effective O_2 scavenger at these same conditions. This was

demonstrated by a second experiment. In this experiment six cell mixtures and six electron acceptor mixtures were prepared: two of the cell mixtures containing 12.5 mM DTT, and four of the cell mixtures containing no DTT. All of the mixtures were sealed and stored in a water bath at 37°C for three hours. At the conclusion of the three hours, two of the cell mixture tubes that did not have any DTT were given a sufficient amount of DTT stock solution to result in a final concentration of 12.5 mM. (All other species concentrations were identical for all six assays.) Each set of tubes was then sparged with H_2 and the hydrogenase assay was performed. The large disparity in slope between the two samples stored with DTT and the four samples stored without DTT (even if DTT was added just before) demonstrate the effectiveness of DTT as an O_2 scavenger at the same conditions at which it was previously shown that no significant false positive exists. These results can be seen in Figure 3-3. It is also apparent that DTT needs to be added to the initial cell mixture preparation if it is to be effective at reducing the effects of O_2 seepage.

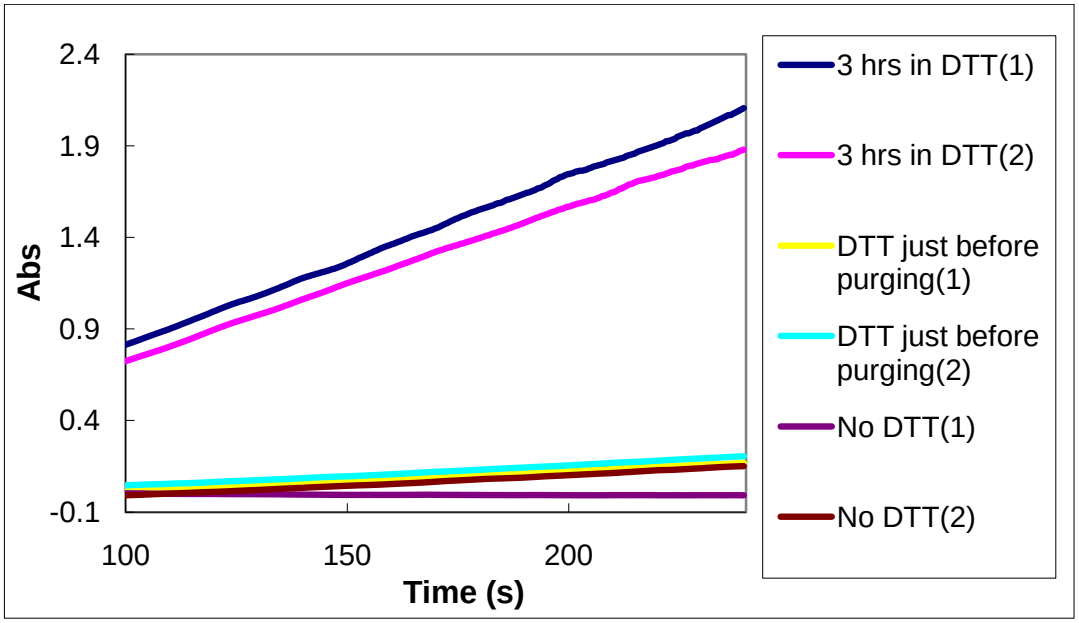

Figure 3-3: Hydrogenase assay in the presence and absence of DTT

The final piece of information needed to characterize the performance of DTT in hydrogenase assays is a comparison between assays (w/ DTT) prepared and run immediately and assays (w/DTT) that are stored for several hours before performing the assay. This information is important for planning large-scale experiments that take place over many hours, as are presented in Chapter 4. To test the effectiveness of DTT over time, six cell mixture and electron mixture tubes were prepared essentially as described in Section 3.1 (all containing DTT). Three cell mixture tubes and three electron mixture tubes were sparged with H_2 and then the assay was run immediately. The other three tubes of each mixture were stored (without sparging) in a waterbath for three hours. The tubes were then sparged with H_2 and the assay was run as described in Section 3.1, with the exception that the check valve was not used for venting. The three assays run immediately showed twice the activity of the assays that were stored with DTT for three hours (Figure 3-4 and Table 3-8). From this it is concluded that a 12.5 mM concentration of DTT does offer some protection from oxidation at assay conditions (described in Section 3.1), but that this protection diminishes over time.

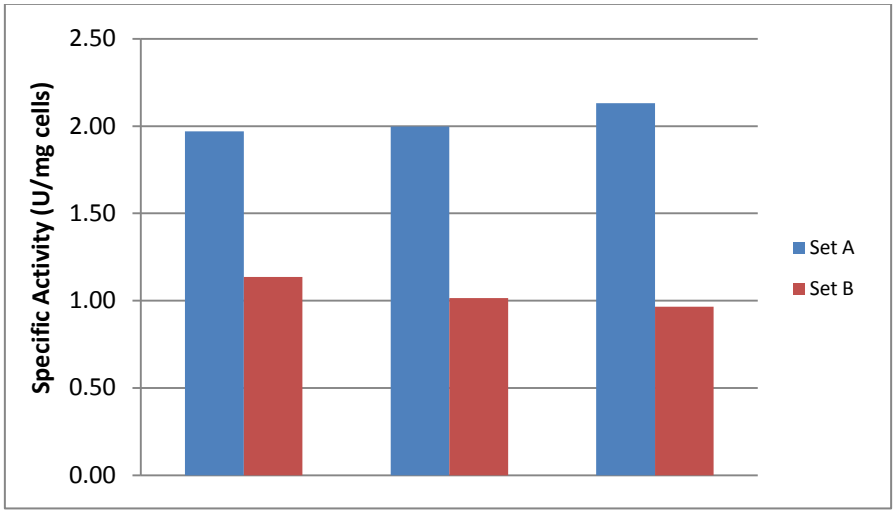

Figure 3-4: Specific activity of 3 assays prepared and run immediately (Set A) compared to samples where the cell mixture and electron mixtures were left unpurged in the water bath (w/ DTT) for 3 hours (Set B).

Table 3-8: Specific activity of 3 assays prepared and run immediately (Set A) compared to samples where the cell mixture and electron mixtures were left unpurged in the water bath (w/ DTT) for 3 hours (Set B)

	Set A	Set B
	1.97	1.14
	2.00	1.01
	2.13	0.97
Average	2.03	1.04
St. Dev.	0.09	0.09

It is hypothesized that O_2 slowly enters the assay system through the imperfect cap/septa/tube seal. This slow O_2 leak eventually overwhelms the DTT and inhibits the hydrogenase, making it necessary to perform the assay immediately, even if DTT is in the reaction mixture. It is thus necessary in the performance of hydrogenase assays to minimize the amount of time that cell mixtures electron acceptor mixtures are exposed to the environment, even when those mixtures are sealed.

3.3 Gas Solubility and Diffusion Modeling

An important aspect of maximizing hydrogenase activity in P11 is ensuring that sufficient H_2 is available to the enzyme. Since H_2 is supplied in the gas phase, its availability is dependent on the solubility of the gas. Perry's Chemical Engineering Handbook (Perry, 1997) gives a Henry's Law coefficient for H_2 of 74,600 atm at 37°C (linearly interpolated from data at 35°C and 40°C), which corresponds to a liquid mole fraction value of only 1.34×10^{-5} for an aqueous solution under 1 atmosphere of H_2. Since pure water has a concentration of approximately 55 M, this translates to a H_2 concentration of approximately 0.74 mM. This value is significantly smaller than the concentration of the electron acceptor and suggests (as is the premise of this

research) that improving H_2 pressure in the syngas could greatly improve enzyme activities and thus ethanol production. This is elaborated further in Chapter 4.

A related question to the solubility of H_2 is whether or not H_2 can be replenished by the gas in the headspace during the timeframe of an assay. Measuring activity with a known H_2 concentration (even if just during an initial time period) is important when trying to develop a model for hydrogenase activity. Additionally, some assays rely on analysis at a given point in the solution that may be far away from the gas-liquid interface (such as in a cuvette). Thus, it's important to assess the amount of H_2 exposure to hydrogenase at each point of the assay. The replenishment question is a diffusion effect and the following analysis was conducted to determine if H_2 in the headspace can replenish the dissolved H_2 during an assay.

3.3.1 H_2 Diffusion Modeling

The assay procedure described in Section 3.1 results in an initially saturated H_2 solution. Additionally, the liquid solution is stagnant, but the hydrogenase reaction is consuming H_2 in the bulk liquid of the cuvette during the assay. It is assumed that hydrogenase is equally distributed throughout the solution. The equation of continuity describes the competing effects of H_2 replenishment from the headspace via diffusion and the consumption of H_2 in the bulk by hydrogenase

$$\frac{\partial C(z,t)}{\partial t} = D_{AB}\frac{\partial^2 C(z,t)}{\partial z^2} + R \tag{3.18}$$

where $C(z,t)$ represents the concentration of H_2 dissolved in the liquid, D_{AB} is the binary diffusion coefficient of H_2 in water, z is the vertical distance above the bottom of the assay cuvette, and R is the molar consumption rate of H_2 per unit volume. For this analysis, the

concentration at the gas-liquid interface is assumed to be the concentration in equilibrium with the gas headspace, C_{sat}, as defined previously by Henry's Law. This gives two boundary conditions and an initial condition of

$$C(b,t) = C_{sat} \tag{3.19}$$

$$\left.\frac{\partial C(z,t)}{\partial z}\right|_{z=0} = 0 \tag{3.20}$$

$$\text{and } C(z,0) = C_{sat} \tag{3.21}$$

where b is the height of the liquid in the cuvette.

To solve Eqn 3.18, a solution of the form

$$C(z,t) = Rt + F(z,t) \tag{3.22}$$

is assumed, where F(z,t) is an unknown function. This solution satisfies Eqn 3.18 when

$$\frac{\partial F(z,t)}{\partial t} = D_{AB}\frac{\partial^2 F(z,t)}{\partial z^2} \tag{3.23}$$

$$F(b,t) = C_{sat} - Rt \tag{3.24}$$

$$\left.\frac{\partial F(z,t)}{\partial z}\right|_{z=0} = 0 \tag{3.25}$$

$$F(z,0) = C_{sat} \tag{3.26}$$

and R is constant. The solution to Eqn 3.23 subject to Eqns 3.24 – 3.26 and substitution back into Eqn 3.22 gives the following solution (Carslaw, 1959):

$$C(z,t) = Rt + \frac{2}{b}\sum_{n=0}^{\infty} e^{-D_{AB}(2n+1)^2\pi^2 t/(4b^2)}\cos\frac{(2n+1)\pi z}{2b}$$

$$\left\{\frac{(2n+1)\pi D_{AB}(-1)^n}{2b}\int_0^t e^{D_{AB}(2n+1)^2\pi^2 t/(4b^2)}\left(C_{sat} - Rt\right)dt + \int_0^b C_{sat}\cos\frac{(2n+1)\pi z}{2b}\,dz\right\}. \tag{3.27}$$

When solving the model using units of seconds for the time and units of mM for the H_2 concentration, the value of R must be in units of mM/s. Equation 3.27 was evaluated at several values of R, namely 10%, 25%, 50%, and 100% of the theoretical maximum H_2 consumption rate (-36.5 μmol/min/mg- see Section 4.2.6). Since 0.67 ml of the cell mixture (of which 10% is cell inoculum at 586 mg cells/L) is mixed with 2 ml of the electron mixture, the resulting cell concentration in the assay is 14.7 mg/L. Thus, the corresponding values of R (in mM/s) used in the model were -8.9×10^{-4}, -2.2×10^{-3}, -4.5×10^{-3}, and -8.9×10^{-3}, respectively. With C_{sat} of 0.74 mM (see first paragraph of this section), b equal to 2.67 cm (2.67 mL divided by 1 cm^2), and D_{AB} for H_2 in water as 7.81×10^{-5} cm^2/s (Green, 2008), the H_2 concentration profiles with time were calculated.

The profiles are shown in Figure 3-5 for z = 1 cm (1.67 cm below the surface- the approximate location of the spectrophotometer beam) and z = 2.5 cm (0.17 cm below the surface). By comparing the dashed and solid lines, virtually no difference exists between the H_2 profiles for the highest reaction rate evaluated, V_{max}. This suggests that diffusion is too slow compared to the reaction such that the concentration disappears uniformly throughout the cuvette with no appreciable H_2 diffusing into the cuvette. Only when the reaction rate drops to 50%, 25%, and 10% of V_{max} (values more typical of experiments) do the effects of diffusion from the headspace begin to be observed. This is manifest when the profiles at the two different heights start to differ at later times, with the height closer to the surface maintaining a higher H_2 concentration as a result of diffusion. The straight-line nature of the solid traces indicates that H_2 is not diffusing to this height in the cuvette.

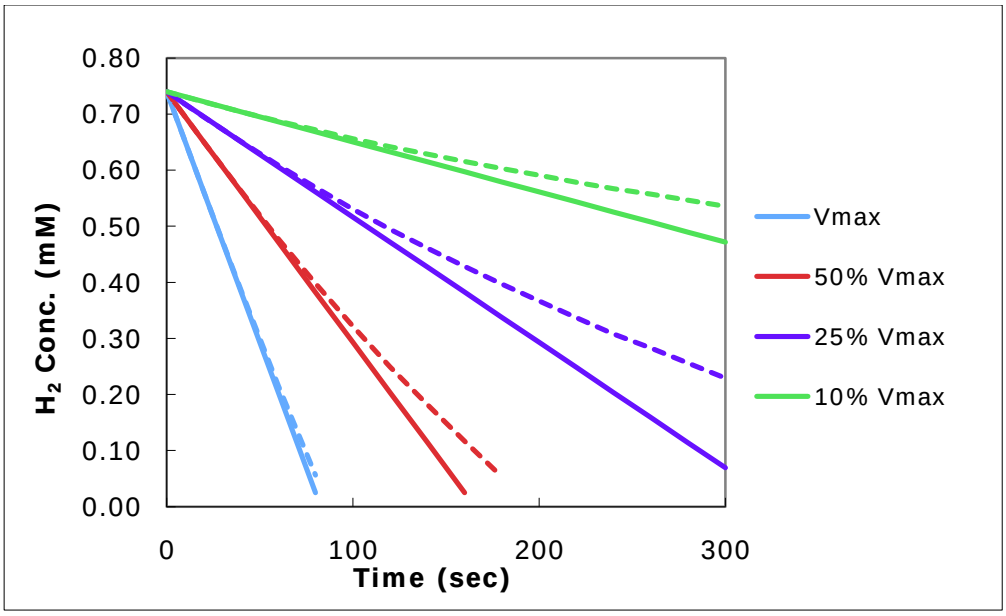

Figure 3-5: H_2 concentration profile at z = 1 cm (solid line) and z = 2.5 cm (dashed line)

From this analysis it is clear that though H_2 replenishment from the headspace does bolster H_2 concentrations near the surface, the rate of diffusion is still slow compared to the rate at which H_2 is consumed by hydrogenase. Additionally, at the location of the spectrophotometer beam, diffusion will have even less effect than near the surface. As shown, the H_2 concentration changes rather quickly with time. Since the parameter analysis for the rate law required a known H_2 concentration, and this work assumed a value of the initial H_2 concentration, it is evident that only initial slope data should be used for kinetic calculations.

To assess the error that could result from a rapidly changing H_2 concentration, a worst-case scenario is examined. When using the assay procedure described in Section 3.1 the H_2 concentration at t = 0 is assumed to be the H_2 concentration throughout the experiment. However, Figure 3-1 shows that approximately 10 seconds is required for mixing before BV reduction can be observed and suggests that initial slope measurements should be taken from this point. By subtracting the difference in H_2 concentrations between t = 10 seconds and t = 0

seconds and dividing by the H_2 concentration at t = 0 seconds, a percentage error of the initial H_2 concentration can be obtained. When this approach is applied for the 100% V_{max} model shown in Figure 3-5 (which is recreated at higher temporal resolution in Figure 3-6), a percentage error of ~12% is obtained. Actual errors for the assays performed in this work are expected to be much smaller (3-5%), because mixing is required for the reaction to begin and because the reaction rates tested were rarely above 50% V_{max}.

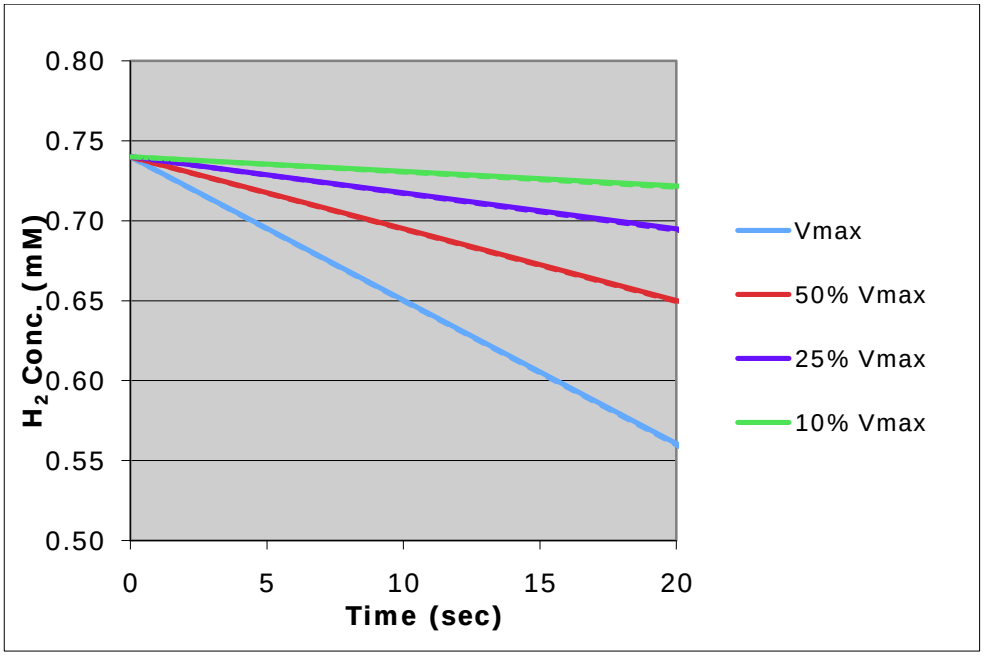

Figure 3-6: H_2 concentration profiles (first 20 seconds)

3.3.2 CO_2 Solubility and pH Effects

An additional complication regarding gas solubility occurs when one considers the entire syngas fermentation process. When syngas is mixed with aqueous solutions, the CO and CO_2

dissolve in the water as well. The complications to hydrogenase associated with CO will be discussed in Section 3.4, but the complications associated with CO_2 are discussed here.

When CO_2 dissolves in water it forms an equilibrium that alters the pH of the reaction system. Specifically, dissolved CO_2 {CO_2 (aq)}, can form carbonic acid, H_2CO_3, bicarbonate, HCO_3^-, and carbonate, CO_3^{2-}. Blanch and Clark (1997) gives the following equilibrium relationships between the dissolved species

$$\frac{[H^+][HCO_3]}{[CO_2]+[H_2CO_3]} = K_1 = 5.01x10^{-7}\,M \tag{3.28}$$

$$\frac{\left[H^+\right]\left[CO_3^{-2}\right]}{\left[HCO_3^-\right]} = K_2 = 5.62x10^{-11}\,M\ . \tag{3.29}$$

The overall effect of CO_2 dissolving in water is an acidification of the system.

An experiment in which CO_2 was purged through an aqueous buffered system (0.1 M potassium phosphate) at increasing partial pressures (i.e. individual tubes were purged with a specific CO_2 pressure until the pH reading stabilized) resulted in a steadily decreasing pH as shown in Figure 3-7. The primary ramification of this experiment for hydrogenase assays is to show that when assays are performed with mixtures of gases instead of pure H_2 (as is done in Chapter 4), the researcher should use nitrogen (or other inert, low-solubility gas) instead of CO_2, because the CO_2 can alter the pH of the system (even a buffered system). The resulting differences in enzyme activity due to pH may confound the activity differences observed with different substrate partial pressures.

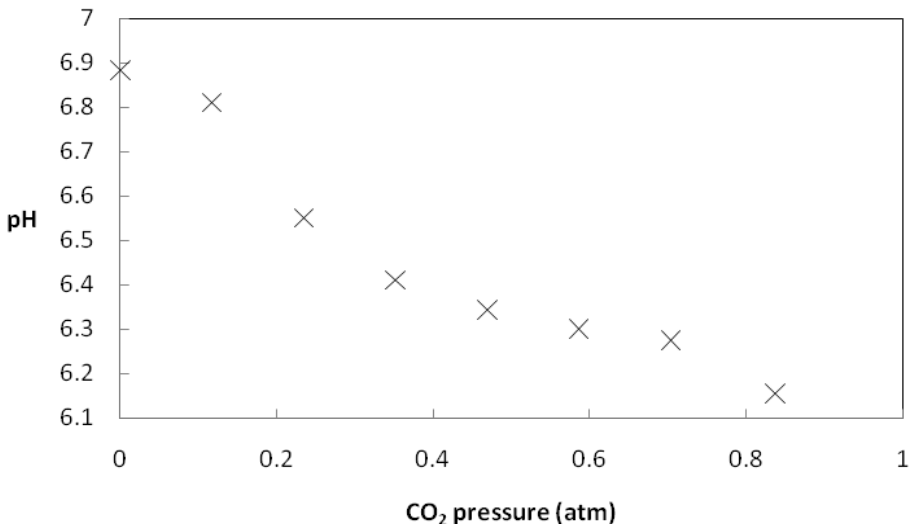

Figure 3-7: Increasing CO_2 partial pressures results in lower pH environments, even in a buffered system

3.4 Enzyme Inhibition

An apparent paradox exists for hydrogenase activity during syngas fermentation: many people have reported that CO strongly inhibits hydrogenase and yet hydrogenase is still active during syngas fermentation. This occurs despite the fact that syngas is primarily CO. In order to test the sensitivity of P11's hydrogenase to CO inhibition the following experiment was performed.

Six assay mixtures were prepared essentially as described in Section 3.1. Three of the mixtures were purged with 90% H_2 and 10% N_2 (the controls), while the other three were purged with 90% H_2 and 10% CO. The three assays without CO in the headspace had specific activities approximately 10x higher than the three assays with CO in the headspace (Table 3-3). This is equivalent to 90% inhibition of H_2 uptake by only 0.084 atm CO pressure (10% of the prevailing

0.84 atm ambient pressure in Provo, UT). The magnitude of this inhibition can be readily visualized in Figure 3-8.

Table 3-9: Effects of 10% CO on hydrogenase specific activity (U/mg cells)

	90% H_2, 10% N_2	90% H_2, 10% CO
	5.636	0.776
	5.682	0.422
	3.884	0.394
Average	5.068	0.531
St. Dev.	1.025	0.213

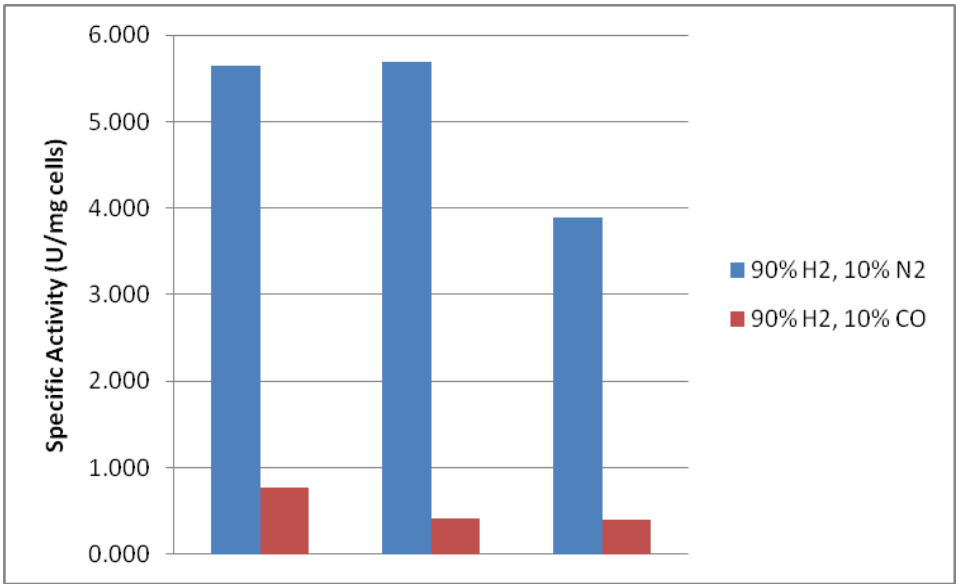

Figure 3-8: Effects of 10% CO on hydrogenase activity

The data confirms that CO is a potent inhibitor of hydrogenase in P11. However, hydrogenase remains active during syngas fermentation despite the fact that P11 is routinely exposed to CO partial pressures as high as 0.9 atm (See Chapter 5). The findings of Hurst (2005) show that Clostridial strain P7 cells grown on 0.9 atm CO have virtually no hydrogenase activity,

even when assayed with pure H_2. These phenomena can be reconciled by considering differences in the experimental techniques.

In Chapter 5 of this work, batch cultures of P11 were charged with syngas (to ~0.9 atm CO partial pressure) at the conclusion of each experimental day, but hydrogenase data was not collected again until the following day (~20 hours later). It is likely that much of the CO in the reactor was consumed during this time. The one exception to this procedure occurred on Day 0 of the 2nd intracellular pH experiment (Section 5.3.2) where the hydrogenase activity data was collected within a few hours of syngas charging. The specific activity on this day was extremely low when compared to data collected by the standard technique. In contrast to the technique used in this work, Hurst (2005) exposed P7 cells to constant CO pressures via a continuous gas system. Additionally, the gas headspace supplied by Hurst contained no H_2. In both the work presented in Chapter 5 and in the work of Hurst, hydrogenase assays were performed with 100% H_2.

From the work of Hurst (2005), it is apparent that growth under 0.9 atm CO partial pressure in the absence of H_2 severely limits hydrogenase production and expression. Thus, even when assayed under pure H_2, P7 cells showed limited activity. Similarly, the high partial pressure of CO after reactor gas-recharge in the work presented in Chapter 5, likely caused a significant inhibition of hydrogenase growth and expression. However, after much of this CO was consumed, the H_2 in the headspace likely facilitated the production and expression of hydrogenase, resulting in the hydrogenase specific activity profiles reported in Chapter 5. Further analysis needs to be done to assess the above hypothesis.

3.5 Whole Cell vs Purified Enzyme Assays

Hydrogenase can be assayed in several different ways. Hydrogenase activity can be estimated without disturbing the cells by measuring the uptake of H_2 gas from the headspace, but this method is faulty due to diffusion effects and other H_2 producing/consuming reactions (i.e. the water gas shift reaction). Additionally, hydrogenase can be assayed by permeabilizing the cell membrane just before performance of the assay, or by running assays after extensive hydrogenase purification procedures. Each method has its advantages and disadvantages. One advantage of performing assays on whole cells is that the hydrogenase enzyme remains in its physiological environment for longer and the enzymes do not need to be re-activated after a purification procedure. The major disadvantage of whole cell assays is that the measurement of activity is less direct and there is more opportunity for interference from other molecules in the solution. Unfortunately, large electron accepting molecules such as benzyl viologen, which are used to obtain a direct measurement of hydrogenase activity, do not fit through the cellular membrane without assistance. Consequently, a detergent is used to permeabilize the cell membrane and allow the electron accepting dye to interact with the enzyme. Though necessary for this purpose, the detergent introduces another variable and may have a negative effect on enzyme activity. To determine if exposure to Triton X-100 (a commonly used detergent) has negative effects on hydrogenase activity, the following experiment was performed.

Nine sets of cell mixtures and BV electron acceptor mixtures were prepared in an anaerobic glovebox as described in Section 3.1. Three of the sets (Set 1) were assayed immediately with the standard procedure (check valve excepted in all instances), three of the sets (Set 2) waited unmixed in the glovebox for three hours and were then assayed with the standard procedure (which includes the addition of Triton X-100 during the sparging of the cell mixture),

while the final three sets (Set 3) had Triton added to the cell mixture in the glovebox at the beginning of the experiment but were not run until four hours later (waiting unmixed in the glovebox during that time). The activity of the three samples run immediately and the activity of the three samples that waited unmixed and Triton free for three hours before being assayed with the standard procedure were relatively similar. However, the samples that were exposed to Triton for four hours before assaying had significantly lower activity (Figure 3-9 and Table 3-10). Set 1 is the standard protocol and serves as the reference point. Set 2 serves as a control to demonstrate that cellular activity did not change significantly during the experiment. Set 3 is the experimental variable and demonstrates clearly that prolonged exposure to Triton-X100 diminished the activity of the hydrogenase enzyme in P11.

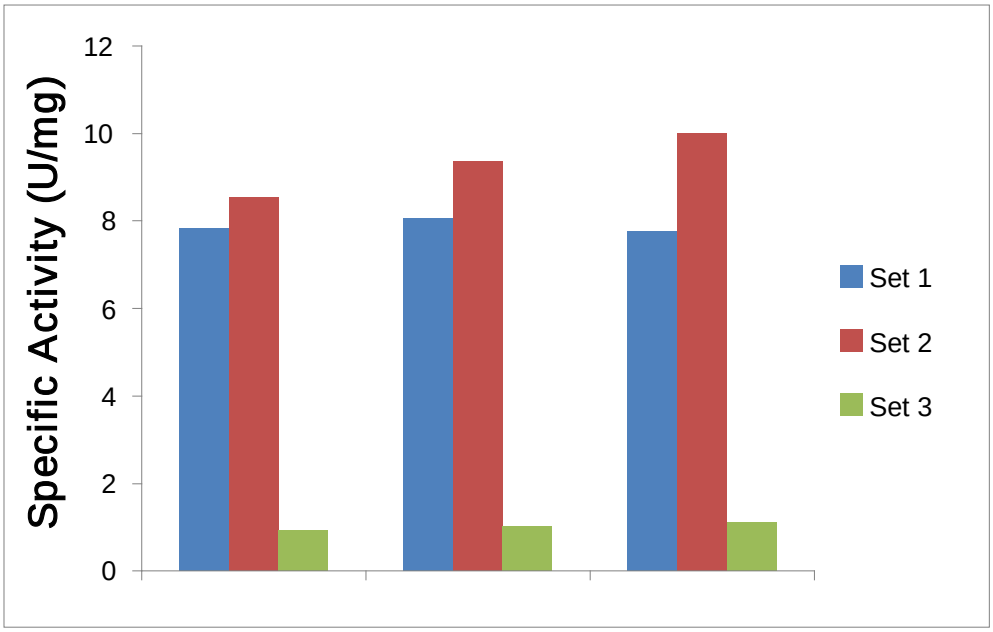

Figure 3-9: Hydrogenase specific activity as a function of various Triton treatments

Table 3-10: Hydrogenase specific activity as a function of various Triton treatments

	Hydrogenase Activities (U/mg cell)			Average Activity (U/mg)	St. Dev.
Set 1	7.82	8.06	7.76	7.88	0.16
Set 2	8.54	9.34	10.01	9.30	0.74
Set 3	0.92	1.03	1.12	1.02	0.10

From this experiment it is apparent that prolonged exposure to Triton X-100 dramatically affects the activity of the hydrogenase enzyme. Because of this effect, it is important to perform assays as soon as possible after permeabilizing the cell membrane with detergents. For this reason the suggested assay procedure contained in Section 3.1 instructs that Triton is to be added to the cells only during the final minute of gas purging. One additional item of interest from this experiment is that the Triton-free sets which were stored in the glovebox for three hours demonstrated slightly higher activity than the sets run immediately. Sitting in a solution with DTT for three hours (with no O_2 to scavenge) likely caused the hydrogenase enzymes inside P11 to enter a more reduced state, similar to how purified hydrogenase is activated before testing. In order to keep the cells in as natural a state as possible, the procedure outlined in Section 3.1 doesn't allow for cells to sit in DTT for any longer than 30 minutes. However, further study is needed on DTT reduction of hydrogenase before this effect can be fully understood.

3.6 Rate Discrepancies with Different Electron Acceptors

It has been regularly observed in the literature that the use of different electron acceptors results in different rates of hydrogenase activity being observed. Though explained more thoroughly in Chapter 4 in connection with calculations of kinetic constants, the results of an experiment in which different rates were observed for benzyl viologen and methyl viologen with

P11 are presented briefly. In this experiment, assays were performed in accordance with the procedure presented in Section 3.1 with the following exceptions: 1) the 0.3 psi check valve was not used during venting because we had not yet discovered its importance, and 2) the electron acceptor concentrations were varied according to Table 3-11. The activity of the assays run with benzyl viologen are clearly higher than the activity of the samples run with methyl viologen, despite the higher concentrations of methyl viologen that were used. This experiment confirms that measured activities depend not only on H_2 pressure, but also on electron acceptor identity and concentration. It sets the context for the discussion in Chapter 4 of how detailed analysis of kinetic rate laws overcame this apparent limitation and a recommendation on H_2 operating pressure was still able to be made and recommended.

Table 3-11: Experimental design for testing varying concentrations of electron acceptors

H_2 Press (atm)	BV Conc (mM)	MV Conc (mM)	Ave Spec Act (U/mgcells)
0.84	2	-	3.53
0.84	8	-	9.53
0.84	-	10	1.70
0.84	-	40	4.41
0.42	4	-	4.38
0.42	-	20	2.23
0.084	2	-	1.28
0.084	8	-	2.91
0.084	-	10	0.62
0.084	-	40	1.30

3.7 H_2 Pressure Effects

The assay procedure describe in Section 3.1 includes a step where the pressure in the cuvette is vented using a needle with a 0.3 psi check valve. This step was discovered after all of

the data in this Chapter was already obtained, but is used for one of the key experiments in Chapter 4. Before the check valve was used, a venting procedure was used where a needle without a check valve was inserted to relieve the excess pressure. This latter approach (without the check valve) involved trying to ensure that the needle was left in the cuvette long enough to relieve the excess pressure, but not long enough to allow O_2 contamination from the surrounding air. The inaccuracy of this approach lead to greater than necessary data scatter, which caused difficulty regressing the desired kinetic parameters.

Quantification of this improvement was accomplished by analyzing the precision of measurements taken during key experiments presented in this thesis. The experiments are the model fitting experiment (Section 4.2), the BV parameter-determining experiment (Section 4.3), the MV parameter-determining experiment (Section 4.3), and the 2nd intracellular pH experiment (Section 5.3.2). Of these four experiments only the model fitting experiment employed the 0.3 psi check valve during venting.

Quantification of the precision of the measurements for each experiment was accomplished as follows: 1) the standard deviation of the specific activity measurements for each design condition (particular H_2 pressure and electron acceptor concentration) was calculated, 2) the standard deviation at each design condition was normalized for the magnitude of the measurement by dividing it by the mean specific activity at that condition (reported as % of mean specific activity), and 3) the normalized standard deviations were averaged for each experiment. This procedure showed that for the four experiments, the model fitting experiment had the lowest average normalized standard deviation (Table 3-12), indicating that its measurements were the most precise of the four experiments.

Table 3-12: Average normalized standard deviations (ANSD)

Experiment	ANSD
BV parameter determining	14.15%
MV parameter determining	9.54%
2nd intracellular pH	9.36%
Model fitting	9.13%

Though the difference is small, this analysis shows that using a 0.3 psi check valve during venting when performing hydrogenase assays may result in greater precision of measurements, and consequently, in more accurate fitting of kinetic models. This is due to less variability in the pressure of the H_2 headspace.

3.8 Chapter 3 Conclusions

The analysis and experiments presented in this chapter enabled the development of a reliable and consistent assay for P11's hydrogenase. The following was learned as a result of the work in this chapter:

- Less than 4 minutes of sparging with 50 sccm H_2 is required to reduce O_2 levels to below 1 ppm in a 3 mL aqueous solution.
- Less than 1 minute of H_2 purging is required to fill a 3.5 mL cuvette to 99.9999% H_2.
- Including 12.5 mM DTT in the reaction mixture at pH 6 helps to scavenge O_2 and eliminate assay failures. This protection is insufficient to protect Hungate tubes that are left exposed to the air for several hours. DTT included in assays at pH 7.7 and 8.3 interferes with the assay due to direct reduction of the electron acceptor by DTT.

- Limited H_2 solubility and its slow diffusion through the stagnant aqueous reaction medium minimizes replenishment in the solution from the headspace. This necessitates the use of initial slopes when performing kinetic analysis.
- Dissolved CO_2 changes the pH of the assaying medium and assays should be performed with pure H_2 or H_2-N_2 mixtures whenever possible.
- 0.084 atm CO causes 90% inhibition of hydrogenase in permeabilized P11 cells.
- Prolonged exposure to Triton X-100 (used to permeabilize the cell membrane during assays) causes diminished hydrogenase activity.
- Use of different electron acceptors (and different concentrations of the same electron acceptor) results in different measured activities.
- Even small pressure variations between assays can make a difference on the precision of hydrogenase activity measurements.

The items learned during the development of an assay for P11 hydrogenase made possible the kinetic experiments (Chapter 4) that allowed calculation of the H_2 pressure required to maximize hydrogenase activity in the ethanol producing cells P11.

4 KINETIC MODELING OF P11 HYDROGENASE

Rate laws of varying complexity and sophistication have been used to model hydrogenase activity. As explained in Chapter 2, these different rate laws are derived from different chemical mechanisms. Iron-iron hydrogenase and nickel-iron hydrogenase are believed to have different reaction mechanisms (See Chapter 2). Some species (*Methanococcus voltae* and *Escherichia coli*) have been reported to possess as many as 4 different hydrogenase systems (Cammack, 2001). Because P11 is a recently discovered bacterium, very little work has been done to characterize its properties. It is not known whether the hydrogenase in P11 has an iron-iron core or an iron-nickel core, or whether it has multiple types of hydrogenase. In Chapter 3 an assay was developed to facilitate the obtaining of kinetic reaction rate data for P11 hydrogenase. In this chapter, the kinetic data is presented and evaluated to select the rate law that most describes P11's hydrogenase. From this rate law, a recommendation of H_2 partial pressure needed to maximize hydrogenase activity in P11 during syngas fermentation is presented.

4.1 Rate Law Derivations

Each kinetic rate law is derived from a reaction mechanism. To reduce two molecules of an oxidized electron acceptor (e.g. oxidized benzyl viologen- BV_{ox}) with one H_2 molecule, several distinct steps are required:

- One molecule of H_2 must bind to hydrogenase

- Two molecules of electron acceptor must bind to hydrogenase
- Electrons must be transferred from H_2 to the electron acceptors (either directly or by donating them first to hydrogenase)
- Two protons must detach from hydrogenase
- Two reduced electron acceptor molecules (e.g. BV_{red}) must detach from hydrogenase

These steps can happen in many different sequences and can be grouped together in multiple ways. In Sections 4.1.1 through 4.1.6, various kinetic mechanisms for hydrogenase are described, along with a corresponding rate law. In some cases, both the mechanism and the rate law were provided by the authors of the various papers, while in others only the mechanism was provided and the rate laws were derived as noted using a Mathcad program adapted from Fromm (1999). When rate laws were derived, it was assumed that all hydrogenase-substrate complexes were at pseudo-steady state and that product formation steps were irreversible. The various rate laws were compared with experiments, as noted in Sections 4.2 and 4.3, to determine the most appropriate rate law.

4.1.1 Michaelis-Menten Model

The Michaelis-Menten model is a result of the following reaction mechanism:

$$E + H_2 \underset{k_2}{\overset{k_1}{\rightleftharpoons}} EH_2 \xrightarrow{k_3} E + 2H^+ \tag{4.1}$$

where E represents hydrogenase, the k values represent the reaction rate constants for the individual reaction steps, and k_3 is assumed to be the rate-determining step. In this model,

$$\frac{V_0}{V_{\max}} = \frac{1}{\frac{K_{H_2}}{P_{H_2}} + 1}, \tag{4.2}$$

the rate of H_2 oxidation, V_0, is a function of H_2 pressure, P_{H_2}, and two constants, V_{max} and K_{H_2}

$$V_{\max} = k_3 E_t \tag{4.3}$$

$$K_{H_2} = \frac{k_3 + k_2}{k_1} \tag{4.4}$$

where E_t is the total hydrogenase concentration, K_{H_2} is the Michaelis constant, and V_{max} represents the maximum possible reaction rate (Nelson, 2005).

V_{max} may be increased by increasing the amount of enzyme in the cell (via genetic engineering), but the only route by which V_0 may approach V_{max} is when $P_{H_2} \gg K_{H_2}$. Typically, this implies that P_{H_2} is approximately 10 times greater than K_{H_2}. For the purpose of syngas fermentation, increasing P_{H_2} such that V_0 approaches V_{max} provides the greatest hydrogenase efficiency.

4.1.2 Ikeda or PEPE Family of Models

In a model described by Ikeda (1996) and Tatsumi (2000) the following mechanism is assumed

$$E_{ox} + H_2 \underset{k_2}{\overset{k_1}{\rightleftharpoons}} EH_2 \xrightarrow{k_3} E_{red} + 2H^+ \tag{4.5}$$

$$E_{red} + M_{ox} \underset{k_5}{\overset{k_4}{\rightleftharpoons}} EM \xrightarrow{k_6} E_{ox} + M_{red} \tag{4.6}$$

where M_{ox} is a double electron accepting molecule such as a quinone. Equations 4.5 and 4.6 result in:

$$\frac{V_0}{V_{\max}} = \frac{1}{1 + \frac{K_{H_2}}{P_{H_2}} + \frac{K_M}{[M_{ox}]}} \tag{4.7}$$

where

$$V_{\max} = \frac{k_3 k_6}{k_3 + k_6} E_t \tag{4.8}$$

$$K_{H_2} = \frac{k_6}{k_3 + k_6} \frac{k_2 + k_3}{k_1} \tag{4.9}$$

$$K_M = \frac{k_3}{k_3 + k_6} \frac{k_5 + k_6}{k_4} \tag{4.10}$$

as provided by the authors and confirmed using the program from Fromm (1999). This rate law is very similar in form to the Michaelis-Menten model, but with an additional term to account for the effect of the electron acceptor concentration. However, it should apparent from Eqns 4.4 and 4.9 that though K_{H_2} performs the same function in both equations (regulating the effect of H_2 pressure), the two constants are defined differently for the two models.

The PEPE (Proton-Electron-Proton-Electron) model (Adams, 1981) is more detailed, accounting for each proton or electron release step individually. This model retains the typical assumption that two separate one-electron accepting molecules are used (M_{ox}) instead of the two-electron accepting molecules assumed in the Ikeda model. The reactions for the PEPE model are shown below with the additional irreversible product formation step simplification.

$$E + H_2 \underset{k_2}{\overset{k_1}{\rightleftarrows}} EH_2 \tag{4.11}$$

$$EH_2 \xrightarrow{k_3} EH^- + H^+ \tag{4.12}$$

$$EH^- + M_{ox} \underset{k_5}{\overset{k_4}{\rightleftarrows}} EH^- M_{ox} \tag{4.13}$$

$$EH^{-}M_{ox} \xrightarrow{k_6} EH + M_{red} \tag{4.14}$$

$$EH \xrightarrow{k_7} E^{-} + H^{+} \tag{4.15}$$

$$E^{-} + M_{ox} \underset{k_9}{\overset{k_8}{\rightleftharpoons}} E^{-}M_{ox} \tag{4.16}$$

$$E^{-}M_{ox} \xrightarrow{k_{10}} E + M_{red} \tag{4.17}$$

Using the program from Fromm (1999), the resulting rate law is functionally identical to the Ikeda model:

$$\frac{V_0}{V_{\max}} = \frac{1}{1 + \frac{K_{H_2}}{P_{H_2}} + \frac{K_M}{[M_{ox}]}} \tag{4.18}$$

though with significantly different definitions of the constants:

$$V_{\max} = \frac{E_t k_3 k_6 k_7 k_{10}}{\left[k_3 k_6 \left(k_7 + k_{10}\right) + k_7 k_{10} \left(k_3 + k_6\right) \right]} \tag{4.19}$$

$$K_{H_2} = \frac{k_6 k_7 k_{10} \left(k_2 + k_3\right)}{k_1 \left[k_3 k_6 \left(k_7 + k_{10}\right) + k_7 k_{10} \left(k_3 + k_6\right) \right]} \tag{4.20}$$

$$K_M = \frac{k_3 k_7 \left[k_4 k_6 \left(k_9 + k_{10}\right) + k_8 k_{10} \left(k_5 + k_6\right) \right]}{k_4 k_8 \left[k_3 k_6 \left(k_7 + k_{10}\right) + k_7 k_{10} \left(k_3 + k_6\right) \right]}. \tag{4.21}$$

In addition, when the order of the final three proton and electron release steps of the PEPE model are switched (resulting in either the PEEP or PPEE models) the same functional form of the rate law (Eqn 4.18) is conserved. For this reason, the Ikeda model and the PEPE family of rate laws (including PEEP and PPEE) will all be evaluated together in Section 4.2.2.

4.1.3 Osz Triangular and Autocatalytic Model

Osz et al. (2005) investigated the well accepted "triangular" model described in Section 2.3.1, where E_1 through E_4 represent different redox states of the same hydrogenase:

$$E_1 \xrightarrow{k_1} E_2 \tag{4.22}$$

$$E_2 \xrightarrow{k_2} E_3 \tag{4.23}$$

$$E_3 \xrightarrow{k_3} E_4 \tag{4.24}$$

$$E_4 + H_2 + 2M_{ox} \xrightarrow{k_4} E_2 + 2H^+ + 2M_{red} \tag{4.25}$$

as well as an autocatalytic version of the same model, where the presence of E_3 facilitates greater conversion of E_2 to E_3:

$$E_1 \xrightarrow{k_1} E_2 \tag{4.26}$$

$$E_2 + E_3 \xrightarrow{k_2} E_3 \tag{4.27}$$

$$E_3 \xrightarrow{k_3} E_4 \tag{4.28}$$

$$E_4 + H_2 + 2M_{ox} \xrightarrow{k_4} E_2 + 2H^+ + 2M_{red} \ . \tag{4.29}$$

These two mechanisms reduce to the same form of the rate law:

$$\frac{V_0}{V_{\max}} = \frac{1}{1 + \dfrac{K_{H_2M^2}}{P_{H_2}\left[M_{ox}\right]^2}} \tag{4.30}$$

where

$$V_{\max} = \frac{k_2 k_3}{k_2 + k_3} E_t \tag{4.31}$$

$$K_{H_2M^2} = \frac{k_2 k_3}{k_4\left(k_2 + k_3\right)} \tag{4.32}$$

for the triangular model and

$$V_{\max} = k_3\left(E_t - \frac{k_3}{k_2}\right) \tag{4.33}$$

$$K_{H_2M^2} = \frac{k_3}{k_4} \tag{4.34}$$

for the model with the additional autocatalytic step (Osz, 2005). The form of the triangular rate law and its corresponding constant definitions were confirmed using the program from Fromm (1999), but the form and corresponding constant definitions of the autocatalytic rate law could not be confirmed using the same program. Because these two models reduce to the same functional form (Eqn 4.30), it is impossible to distinguish between them using an experimental design where only reactant concentrations and rates are known.

4.1.4 De Lacey Triangular Model

The De Lacey triangular model describes the reaction of H_2 with oxidized methyl viologen (M_{ox}), a one-electron acceptor molecule, via the [Ni-Fe] hydrogenase from *Desulfovibrio gigas* according to the following mechanism:

$$E_S + H_2 \underset{k_2}{\overset{k_1}{\rightleftharpoons}} E_R \tag{4.35}$$

$$E_R + M_{ox} \underset{k_4}{\overset{k_3}{\rightleftharpoons}} E_C + M_{red} + H^+ \tag{4.36}$$

$$E_C + M_{ox} \underset{k_6}{\overset{k_5}{\rightleftharpoons}} E_S + M_{red} + H^+ \tag{4.37}$$

where E_S, E_R, and E_C represent different redox states of hydrogenase (De Lacey, 2000). When this mechanism is simplified by assuming Eqns 4.36 and 4.37 are irreversible (initial rate assumption) and converted to a rate law using the program adapted from Fromm (1999), the mechanism reduces to a rate law of the form:

$$\frac{V_0}{V_{\max}} = \frac{1}{\frac{K_{H_2}}{P_{H_2}} + \left(K_M + \frac{K_{H_2M}}{P_{H_2}} \right) \frac{1}{[M_{ox}]}} \tag{4.38}$$

where

$$V_{\max} = k_1 k_3 k_5 E_t \tag{4.39}$$

$$K_{H_2} = k_3 k_5 \tag{4.40}$$

$$K_M = k_1\left(k_3 + k_5\right) \tag{4.41}$$

$$K_{H_2M} = k_2 k_5 \tag{4.42}$$

This rate law contains an H_2 regulating term and an electron acceptor regulating term like the Ikeda and PEPE models as well as an additional term that governs the affect of the product of H_2 pressure and electron acceptor concentration. Notably missing from Eqn 4.38 is a 1 in the denominator, which implies that if P_{H_2} and $\left[M_{ox}\right]$ were made sufficiently large, V_0 could be made to be larger than V_{max}. This inconsistency may make the De Lacey triangular model insufficient for correctly modeling hydrogenase activity.

4.1.5 EPEP Family of Models

The EPEP family of mechanisms (Adams, 1981) is similar to the PEPE family of mechanisms except that the first product released from the enzyme is a proton instead of the electron acceptor. The EPEP mechanism (using the irreversible product formation step simplification):

$$E + H_2 \underset{k_2}{\overset{k_1}{\rightleftarrows}} EH_2 \tag{4.43}$$

$$EH_2 + M_{ox} \underset{k_4}{\overset{k_3}{\rightleftarrows}} EH_2M_{ox} \tag{4.44}$$

$$EH_2M_{ox} \xrightarrow{k_5} EH_2^+ + M_{red} \tag{4.45}$$

$$EH_2^+ \xrightarrow{k_6} EH + H^+ \tag{4.46}$$

$$EH + M_{ox} \underset{k_8}{\overset{k_7}{\rightleftarrows}} EHM_{ox} \tag{4.47}$$

$$EHM_{ox} \xrightarrow{k_9} EH^+ + M_{red} \tag{4.48}$$

$$EH^+ \xrightarrow{k_{10}} E + H^+ \tag{4.49}$$

as derived using the program of Fromm (1999) results in a rate law:

$$\frac{V_0}{V_{\max}} = \frac{1}{1 + \frac{K_{H_2}}{P_{H_2}} + \left(K_M + \frac{K_{H_2M}}{P_{H_2}} \right) \frac{1}{[M_{ox}]}} \tag{4.50}$$

where

$$V_{\max} = \frac{k_5 k_6 k_9 k_{10} E_t}{k_5 k_6 k_9 + k_5 k_6 k_{10} + k_5 k_9 k_{10} + k_6 k_9 k_{10}} \tag{4.51}$$

$$K_{H_2} = \frac{k_5 k_6 k_9 k_{10}}{k_1 \left(k_5 k_6 k_9 + k_5 k_6 k_{10} + k_5 k_9 k_{10} + k_6 k_9 k_{10} \right)} \tag{4.52}$$

$$K_M = \frac{k_6 k_{10} \left(k_3 k_5 k_8 + k_3 k_5 k_9 + k_4 k_7 k_9 + k_5 k_7 k_9 \right)}{k_3 k_7 \left(k_5 k_6 k_9 + k_5 k_6 k_{10} + k_5 k_9 k_{10} + k_6 k_9 k_{10} \right)} \tag{4.53}$$

$$K_{H_2M} = \frac{k_2 k_6 k_9 k_{10} \left(k_4 + k_5 \right)}{k_1 k_3 \left(k_5 k_6 k_9 + k_5 k_6 k_{10} + k_5 k_9 k_{10} + k_6 k_9 k_{10} \right)}. \tag{4.54}$$

Interestingly, Eqn 4.50 is similar to Eqn 4.38 with exception that Eqn 4.50 has the additional 1 term that makes it more theoretically tenable. Additionally, when the order of the final three proton and electron release steps of the EPEP model are switched (resulting in either the EPPE or EEPP models), the same functional form of the rate law is conserved. This form is different from the PEPE family of models in that the EPEP rate laws have a combined $P_{H_2}[M_{ox}]$ term and different definitions of the constants.

4.1.6 Okura Model

The Okura model assumes a mechanism where the H_2 and MV (M_{ox}) attach to hydrogenase rapidly and reversibly in random sequences and the reaction does not occur until the H_2 and both MV molecules are all attached to hydrogenase. This model:

$$E + H_2 \underset{k_2}{\overset{k_1}{\rightleftharpoons}} EH_2 \tag{4.55}$$

$$E + M_{ox} \underset{k_4}{\overset{k_3}{\rightleftharpoons}} EM_{ox} \tag{4.56}$$

$$EH_2 + M_{ox} \underset{k_6}{\overset{k_5}{\rightleftharpoons}} EH_2M_{ox} \tag{4.57}$$

$$EM_{ox} + H_2 \underset{k_8}{\overset{k_7}{\rightleftharpoons}} EH_2M_{ox} \tag{4.58}$$

$$EH_2M_{ox} + MV_{ox} \underset{k_{10}}{\overset{k_9}{\rightleftharpoons}} EH_2 2M_{ox} \tag{4.59}$$

$$EM_{ox} + M_{ox} \underset{k_{12}}{\overset{k_{11}}{\rightleftharpoons}} E2M_{ox} \tag{4.60}$$

$$E2M_{ox} + H_2 \underset{k_{14}}{\overset{k_{13}}{\rightleftharpoons}} EH_2 2M_{ox} \tag{4.61}$$

$$EH_2 2M_{ox} \xrightarrow{k_{15}} E + 2M_{red} + 2H^+ \tag{4.62}$$

results in the following rate law (given by the authors and confirmed using Fromm's (1999) method):

$$\frac{V_0}{V_{\max}} = \frac{1}{\left(1+\frac{K_{H_2}}{P_{H_2}}\right) + \left(1+\frac{K_{H_2}}{P_{H_2}}\right)\frac{2K_M}{[M_{ox}]} + \left(1+\frac{K_{H_2}}{P_{H_2}}\right)\left(\frac{K_M}{[M_{ox}]}\right)^2} \tag{4.63}$$

where

$$V_{\max} = k_{15}E_t \tag{4.64}$$

$$K_M = \frac{k_4}{k_3} = \frac{k_6}{k_5} = \frac{k_{10}}{k_9} = \frac{k_{12}}{k_{11}} \tag{4.65}$$

$$K_{H_2} = \frac{k_2}{k_1} = \frac{k_8}{k_7} = \frac{k_{14}}{k_{13}} \tag{4.66}$$

and Eqn 4.62 is the rate determining step (Okura, 1981). Though this rate law (Eqn 4.63) has many terms, it only has three constants and they are directly associated with the quantities that they regulate, making it an important option.

4.1.7 Generic Form of Rate Law

In general, rate laws describing enzyme kinetics, such as those described above, follow the form

$$\frac{V_0}{V_{\max}} = \frac{1}{A + \frac{B}{P_{H_2}} + \frac{C}{[M_{ox}]} + \frac{D}{[M_{ox}]^2}} \quad . \tag{4.67}$$

Table 4-1 shows the associated parameters of A, B, C, and D for each model described above. As previously shown, similarly named parameters for each model are represented by different combinations of rate constants. However, the general form provides some insights. For instance, only the Osz Triangular and Autocatalytic model results in a rate law in which there is not a P_{H_2} term that is independent of the M_{ox} term. Only the Osz models and the Okura model have a term that regulates the effect of $[M_{ox}]^2$. Because A = 0 for the De Lacey Triangular model, the efficiency reported when reactant concentrations are made very large approaches infinity, instead of unity, which is impossible.

Table 4-1: Definition of constants for generic model

	A	B	C	D
Michaelis-Menten	1	K_{H_2}	0	0
Ikeda or PEPE family	1	K_{H_2}	K_M	0
Osz Triangular/Autocatalytic	1	0	0	$\frac{K_{H_2M^2}}{P_{H_2}}$
De Lacey Triangular	0	K_{H_2}	$K_M + \frac{K_{H_2M}}{P_{H_2}}$	0

EPEP family	1	K_{H_2}	$K_M + \frac{K_{H_2M}}{P_{H_2}}$	0
Okura	1	K_{H_2}	$2K_M\left(1+\frac{K_{H_2}}{P_{H_2}}\right)$	$\left(1+\frac{K_{H_2}}{P_{H_2}}\right)K_M^2$

4.2 Selection of a Rate Law

An experiment was designed to determine the most appropriate rate law for P11 hydrogenase from those presented in Section 4.1. It was decided to emphasize the dependence of hydrogenase activity on H_2 partial pressure by testing four different values of H_2 partial pressures and two different values of BV concentration, as understanding H_2 partial pressure dependence has been the focus of this work. Assays were prepared as described in Section 3.1 with the exception that the H_2 partial pressure and BV concentrations were adjusted to the values shown in Table 4-2. The data is shown below in connection with each model.

Table 4-2: Experimental design for model fitting experiment

H_2 Pressure (atm)	BV Conc (mM)	# of assays
0.084	2	2
0.084	8	2
0.21	2	3
0.21	8	3
0.42	2	2
0.42	8	2
0.84	2	2
0.84	8	3

4.2.1 Michaelis-Menten Model

The Michaelis-Menten model (Eqn 4.2)

$$\frac{V_0}{V_{\max}} = \frac{1}{\frac{K_{H_2}}{P_{H_2}} + 1} \tag{4.68}$$

describes hydrogenase specific activity as a function of H_2 partial pressure and two regressed parameters, V_{max} and K_{H_2}. When the data are fit to the Michaelis-Menten equation it becomes apparent that hydrogenase specific activity depends not only on H_2 partial pressure, but also on electron acceptor concentration (Figure 4-1). Consequently, the Michaelis-Menten equation only describes hydrogenase activity dependence on P_{H_2} for a specified electron acceptor concentration. In this analysis the regression parameters were calculated separately for BV concentrations of 2 mM and 8 mM.

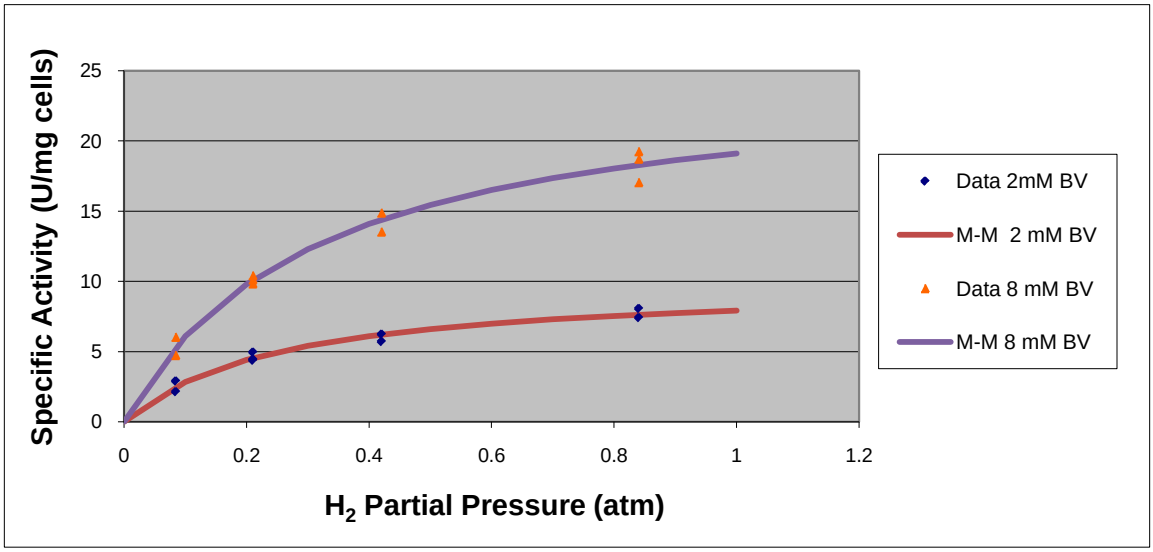

Figure 4-1: Michaelis-Menten regression at 2 mM and 8 mM BV

Least-squares regression of the data for the assays run with 2 mM BV yielded an R^2 value of 0.97 $(U/mg)^2$ and the R^2 value for the assays run with 8 mM BV was 0.98. From these values, Figure 4-1, and the randomly scattered residuals shown in Figure 4-2 it is clear that the Michaelis-Menten model very accurately fits the data when different BV concentrations are fit independently. The best-fit parameters obtained by least squares regression are shown with the R^2 values in Table 4-3.

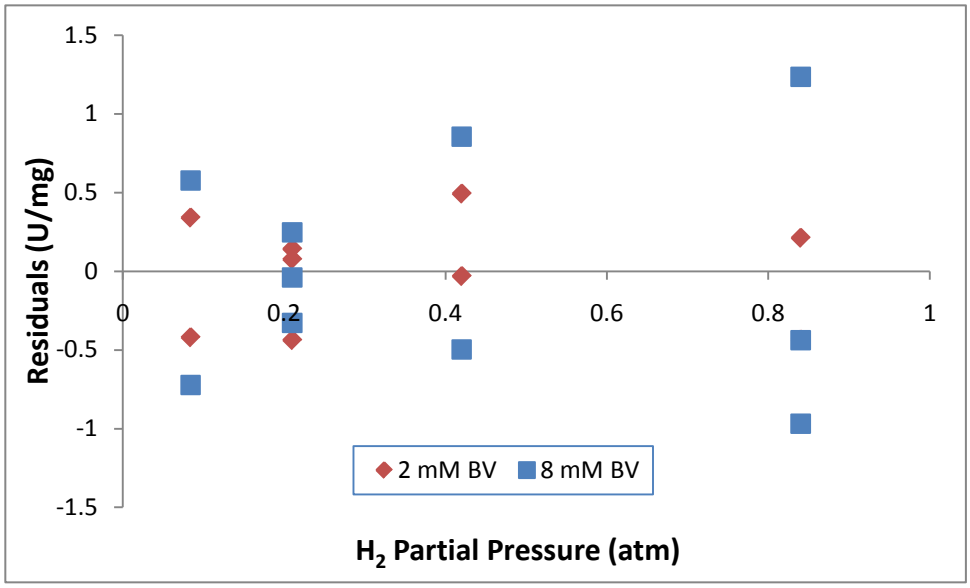

Figure 4-2: Residual plot for Michaelis-Menten regression

Table 4-3: Michaelis-Menten regression parameters

	2 mM BV	8 mM BV
V_{max} (U/mg)	9.89	25.09
K_{H2} (atm)	0.25	0.31
R^2	0.97	0.98

The difference in V_{max} between the 2 mM BV assays (9.89 U/mg) and the 8 mM BV assays (25.1 U/mg) clearly indicates the dependence of reaction rate on BV concentration. However, the K_{H_2} values for the two cases are relatively similar. An H_2 pressure of 10x the K_{H_2} value makes the K_{H_2} term relatively insignificant, causing the denominator to equal 1 such that $V_0 \approx V_{max}$. Thus, this model indicates that an H_2 pressure of 2.5-3.1 atm is needed to cause hydrogenase to operate near its theoretical maximum efficiency. This is valuable information that will be used later. However, the major weakness of this model is that its parameters depend on the concentration of BV used, because the concentration of electron acceptor in the physiological system is unknown.

4.2.2 Ikeda or PEPE Model

A model that is similar in form to the Michaelis-Menten model, but that accounts for the electron acceptor concentration, is the Ikeda or PEPE family of models described in Section 4.1.2.

$$\frac{V_0}{V_{max}} = \frac{1}{1 + \frac{K_{H_2}}{P_{H_2}} + \frac{K_M}{[M_{ox}]}} \tag{4.69}$$

The K_{H_2} term present in this model is different from the K_{H_2} term of the Michaelis-Menten Equation (See Eqns 4.4 and 4.9), but since they serve similar purposes (regulating the magnitude of the effect of H_2 pressure on V_0), the initial guess of K_{H_2} used for regression of the parameters of the Ikeda model was 0.3 atm as obtained from the Michaelis-Menten regression. The V_{max} initial guess value was also set close to that obtained by the Michaelis-Menten equation, 30 U/mg. Finally, an initial guess value of 4 mM was used for the K_M term because

this is between the values of BV concentration tested. Least squares regression gave the parameters listed in Table 4-4 and the fit shown in Figure 4-3. The resulting parameters are clearly different from those found by the Michaelis-Menten Equation and though the R^2 value is similar between the two, the downward trend in the 2 mM BV residuals of the Ikeda model show that the fit is not nearly as good (Figure 4-4).

Table 4-4: Regression parameters for Ikeda or PEPE-type models

V_{max} (U/mg)	125.84
K_{H2} (atm)	1.66
K_{BV}	30.80
R^2	0.98

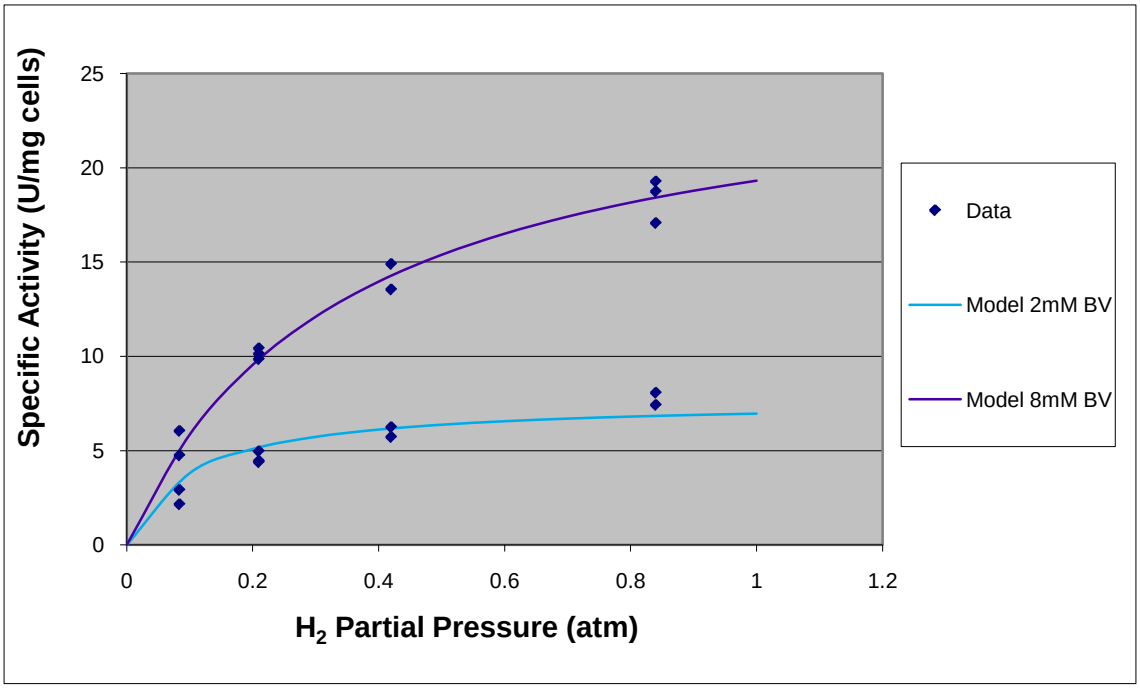

Figure 4-3: Regression of Ikeda/PEPE-type models

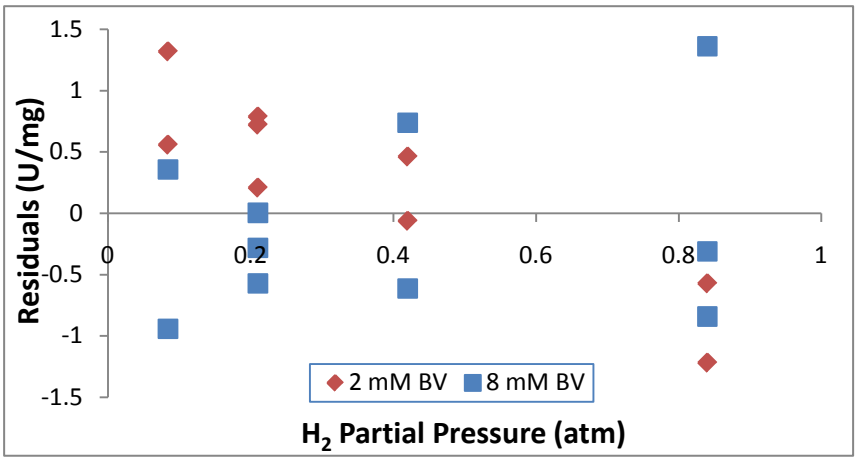

Figure 4-4: Residual plot for Ikeda/PEPE regression

4.2.3 Osz Triangular and Autocatalytic Model

The Triangular Model and Triangular Model with autocatalytic step described by Osz (2005) were discussed in Section 4.1.3. These models are derived from some of the current thinking about Ni-Fe hydrogenase mechanisms. It was shown that both the triangular model and the triangular model with autocatalytic step reduced to the same experimental form (Eqn 4.30):

$$\frac{V_0}{V_{\max}} = \frac{1}{1 + \frac{K_{H_2M^2}}{P_{H_2}\left[M_{ox}\right]^2}}. \tag{4.70}$$

The Osz models are essentially a combination of a power law model and the Michaelis-Menten equation. Since this equation only has two parameters, it is easy to fully specify. However, it is obvious from the R^2 parameter in Table 4-5, the fit shown in Figure 4-5, and the major trending of the residuals shown in Figure 4-6 that this model does not describe the data.

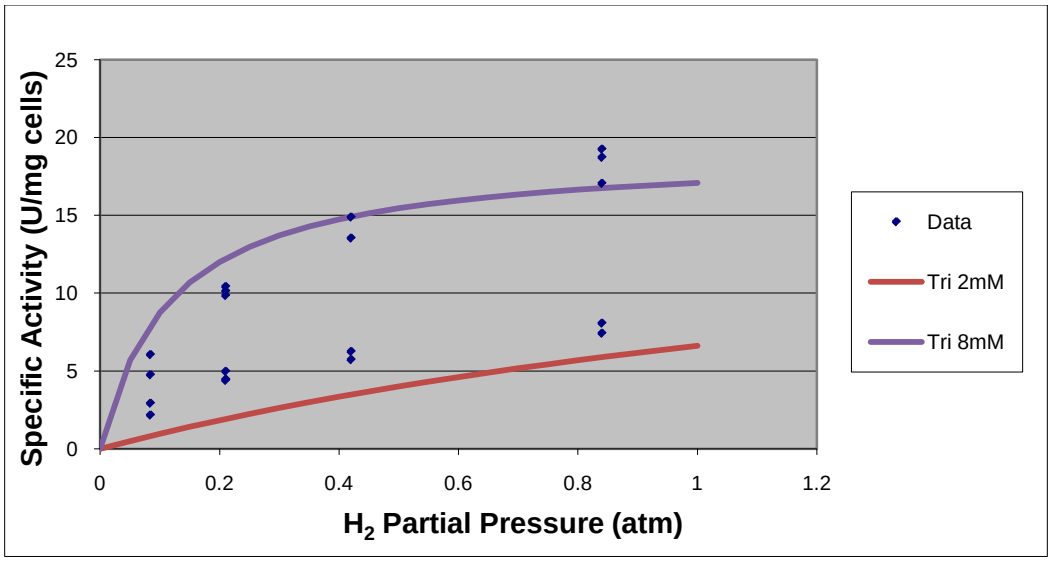

Figure 4-5: Regression of Osz models

Table 4-5: Regression parameters for the Osz triangular and autocatalytic models

$V_{max,ps}$ (U/mg)	19.10
$K_{M,ps}$ (atm*mM^2)	7.55
R^2	0.88

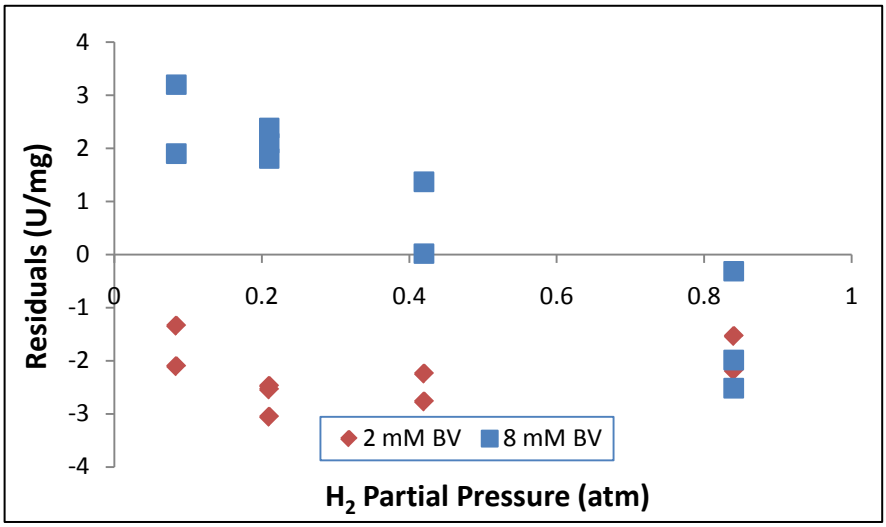

Figure 4-6: Residual plot for Osz models

4.2.4 DeLacey Triangular Model

The DeLacy triangular model (Eqn 4.38) was described in Section 4.1.4 to be a model for [Ni-Fe] hydrogenase that incorporates three different redox states of hydrogenase and results in the following rate law:

$$\frac{V_0}{V_{\max}} = \frac{1}{1 + \frac{K_{H_2}}{P_{H_2}} + \left(K_M + \frac{K_{H_2M}}{P_{H_2}} \right) \frac{1}{[M_{ox}]}} . \qquad (4.71)$$

When this model is fit to the data, using initial guess values of $V_{\max} = 30$ U/mg, $K_{H_2} = 0.3$ atm (close to the Michaelis-Menten parameters), $K_M = 0.4$ mM (between the two concentrations of BV tested), and $K_{H_2M} = 1.2$ (the product of the K_{H_2} and K_M guess values) the following parameters are obtained (Table 4-6).

Table 4-6: Regression parameters for De Lacey triangular model

V_{max} (U/mg)	29.91
K_{H2} (atm)	0.42
K_{BV} (mM)	8.69
K_{H2M} (mM*atm)	0.00
R^2	0.98

The V_{max} and K_{H_2} values obtained by this analysis are reasonable and appear consistent with the values obtained from the Michaelis-Menten equation. The K_M value also appears reasonable as it is very nearly in the range of BV concentrations tested…a mathematical necessity when the BV concentration visibly affects hydrogenase specific activity. The R^2 value is markedly better than the Osz models, and similar to that obtained for the Ikeda and PEPE

family of models as well as the Michaelis-Menten models. Additionally, it is clear from careful inspection of the 2 mM line of the model in Figure 4-7 and from the trending in the residuals shown in Figure 4-8 that the De Lacey triangular model still misses some of the true behavior.

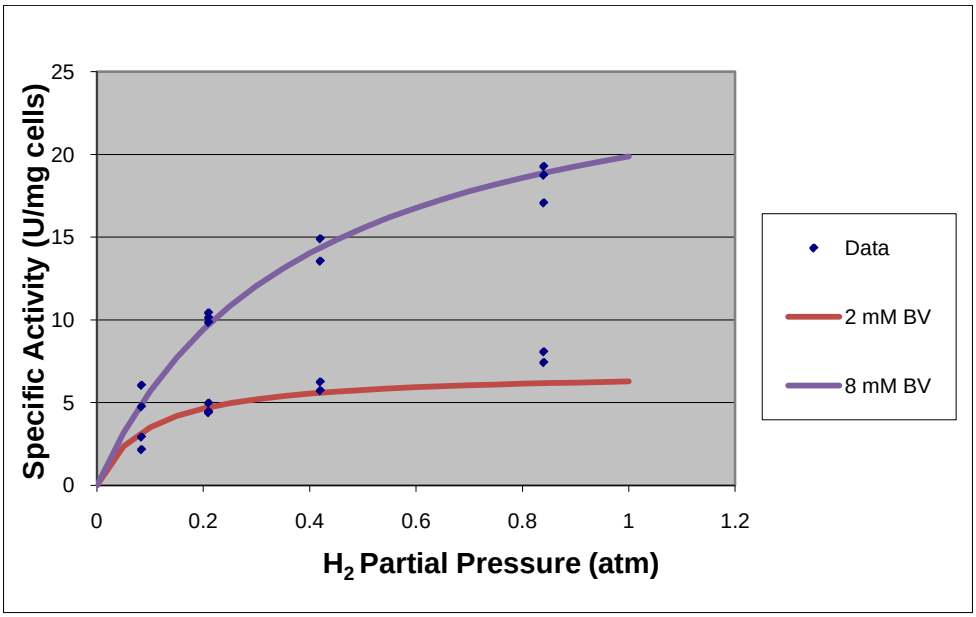

Figure 4-7: Regression with the De Lacey triangular model

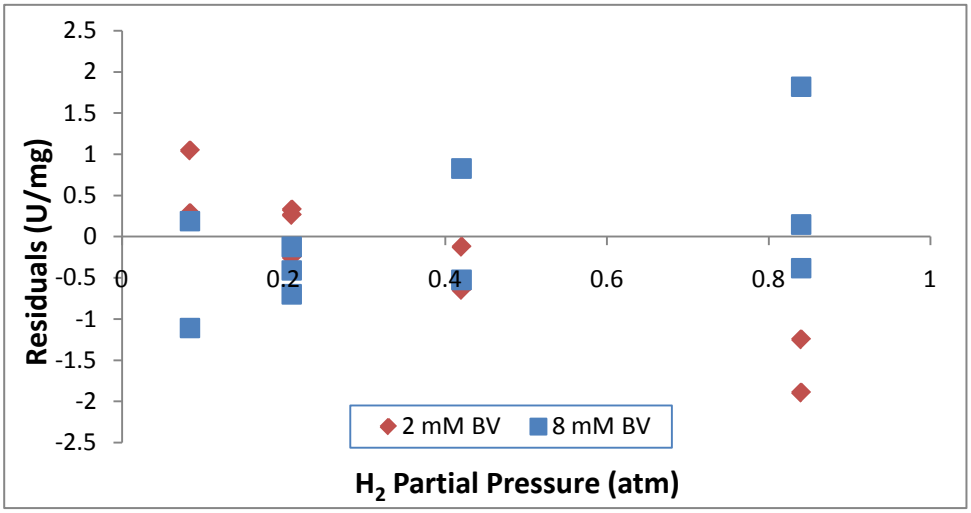

Figure 4-8: Residual plot for DeLacey model

4.2.5 EPEP Family of Models

The EPEP family of models (Eqn 4.50) was described in Section 4.1.5 and is shown below.

$$\frac{V_0}{V_{\max}} = \frac{1}{1 + \frac{K_{H_2}}{P_{H_2}} + \left(K_M + \frac{K_{H_2M}}{P_{H_2}} \right) \frac{1}{[M_{ox}]}} \tag{4.72}$$

In form, the EPEP model is very similar to the De Lacey triangular model just discussed (only a +1 term is added to the denominator), but they are derived from very different mechanisms. However, when this model is fit to the data (with the same initial guess values as used for the De Lacey model), it appears to describe the data very well (Figure 4-9). The values of the parameters obtained from this model are shown in Table 4-7. Additionally, the random nature of the residuals (Figure 4-10) demonstrates the fidelity of this model.

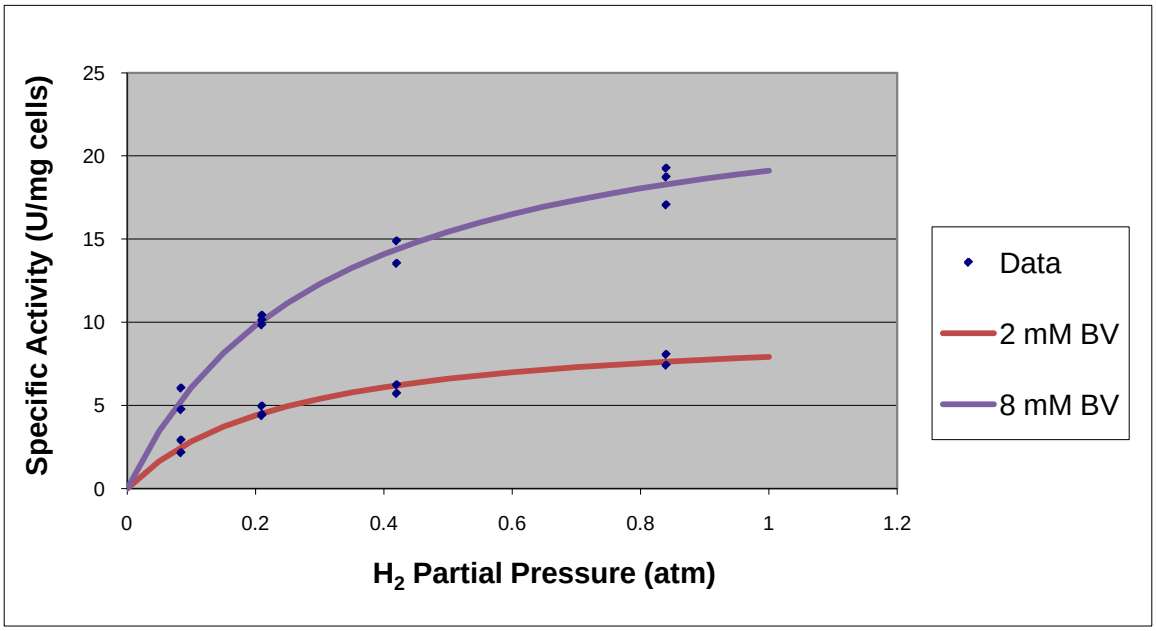

Figure 4-9: Regression of data with EPEP model

Table 4-7: Regression parameters for EPEP family of models

V_{max} (U/mg)	51.44
K_{H2} (atm)	0.42
K_{BV} (mM)	8.40
K_{H2M} (mM*atm)	1.74
R^2	0.99

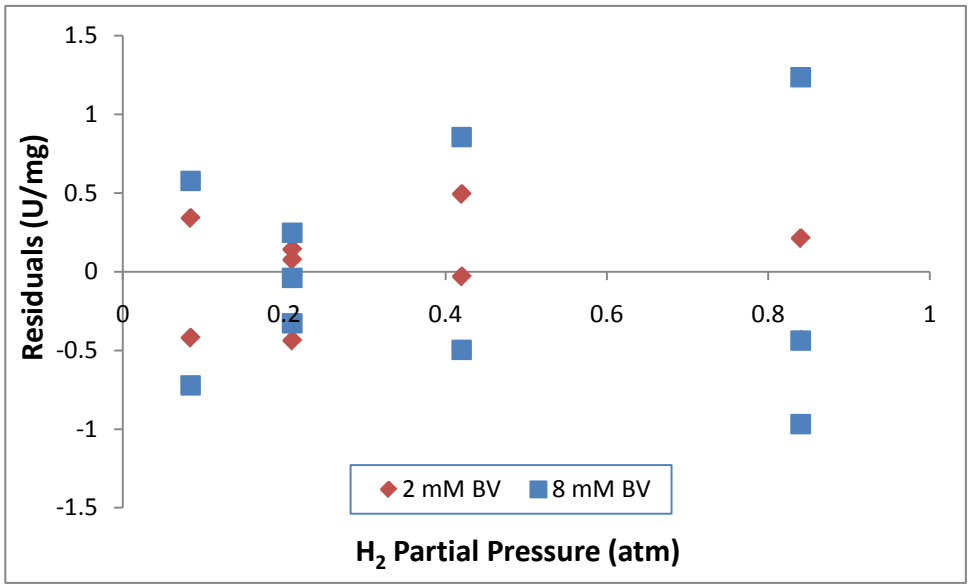

Figure 4-10: Residual plot for EPEP model

Several items are particularly noteworthy. First, the R^2 value for this fit is better than any of the other models we have evaluated. That the R^2 values and randomly scattered residuals are similar between the EPEP model and the Michaelis-Menten model implies that the two models describe P11 hydrogenase activity dependence on H_2 pressure with similar accuracy. However, unlike the Michaelis-Menten model, the EPEP model does this while also describing the dependence on the BV concentration. The fact that BV concentration affects reaction rates but is not explicitly included in the Michaelis-Menten model suggests that BV effects may confound

the parameters calculated for the Michaelis-Menten model, limiting their usefulness. The K_{H_2} term for the EPEP model is 0.42 atm, implying that approximately 4 atm of H_2 pressure is necessary to cause hydrogenase to operate near its maximum efficiency. The value of the K_M term (8.4 mM) is near the value obtained by the De Lacey triangular model and is believable because of its proximity to the concentrations of BV used for the experiment.

4.2.6 Okura Model

The Okura Model was described in Section 4.1.6 as a model where the H_2 and electron accepting molecules bind to hydrogenase in random and reversible order and the rate-determining step is the actual reaction and release of the products (Eqn 4.62). When the data was fit to the Okura model (Eqn 4.63)

$$\frac{V_0}{V_{\max}} = \frac{1}{\left(1+\frac{K_{H_2}}{P_{H_2}}\right)+\left(1+\frac{K_{H_2}}{P_{H_2}}\right)\frac{2K_M}{[M_{ox}]}+\left(1+\frac{K_{H_2}}{P_{H_2}}\right)\left(\frac{K_M}{[M_{ox}]}\right)^2} \tag{4.73}$$

the parameters shown in Table 4-8 were obtained. The Okura model gives a fit that has an identical R^2 value as the EPEP model, but does so using one fewer parameter in the model. This becomes important in Section 4.3. The graph of the model (Figure 4-11) is virtually indistinguishable from that of the Michaelis-Menten and EPEP models and the random nature of the residuals (Figure 4-12) shows that the Okura model provides a very good fit with the data. V_{max} and K_{H_2} are slightly lower in the Okura model than in the EPEP model but agree more closely with the values obtained from the Michaelis-Menten equations. K_M is about 5 times lower than the value obtained using the EPEP model.

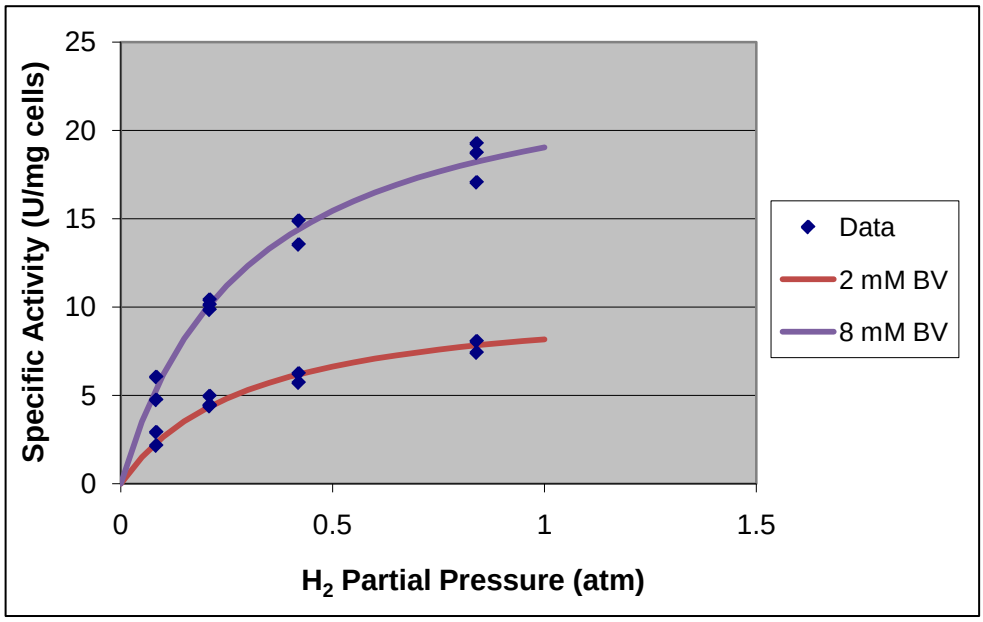

Figure 4-11: Data regression with the Okura model

Table 4-8: Regression parameters for the Okura model

V_{max} (U/mg)	36.45
K_{H2} (atm)	0.30
K_{BV} (mM)	1.70
R^2	0.99

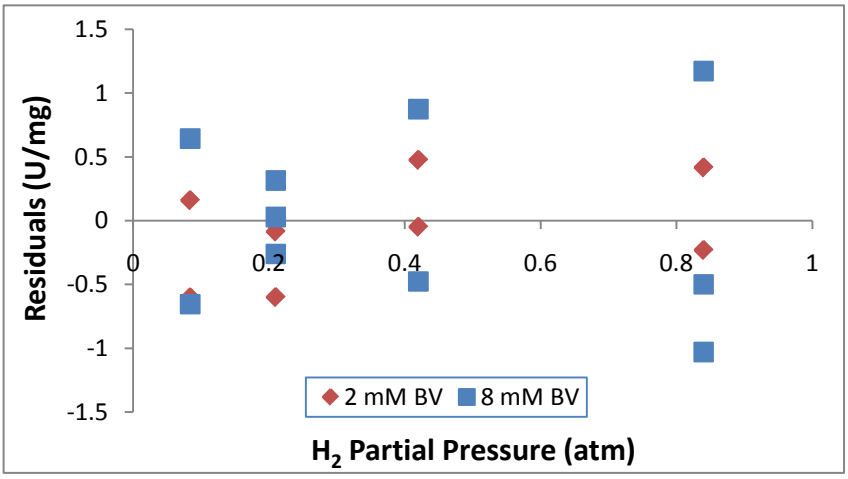

Figure 4-12: Residual plot for Okura regression

4.2.7 Selection of the Rate Law

Though the list of rate laws considered in the previous sections was not comprehensive, much can be gained by evaluating their data and models. The R^2 value from each of the models is displayed in Table 4-9. First, there are several models that clearly do not describe the data. The triangular model and rate law and the autocatalytic version of that mechanism and rate law described by Osz (2005) have the lowest R^2 value and strongly trended residuals (Figure 4-6) indicating that they definitely do not describe the data. The fits of the Ikeda or PEPE family of rate laws and the De Lacey triangular model are better, but the trending in their residuals (Figures 4-4 and 4-8) show that these models still miss describing the data. The Michaelis-Menten equation, the EPEP family of models, and the Okura model all have random residuals (Figures 4-2, 4-10, and 4-12) and high R^2 values, indicating that they describe the data accurately.

Table 4-9: R^2 values for regression models

Model	R^2 value
Michaelis-Menten	0.97 or 0.98
Ikeda or PEPE	0.98
Osz	0.88
De Lacey	0.98
EPEP	0.99
Okura	0.99

A major consideration when choosing which model to use is the number of experiments needed to fully specify the model. The Michaelis-Menten equation has only two parameters (V_{max} and K_{H2}) and can thus be specified with the smallest number of experiments. However,

because this model does not include the effects of the electron acceptor, it is likely that these effects confound the calculated parameters. This is demonstrated by the different K_{H2} and V_{max} values obtained using different concentrations of BV (Table 4-3). This confounding limits the usefulness of the Michaelis-Menten V_{max} parameter and the simplicity of the model does not provide a potentially useful K_{BV} parameter. Conversely, the EPEP model contains the most parameters of all three models (four parameters: V_{max}, K_{H2}, K_M, and an additional term regulating the effect of the product of P_{H2} and $[M_{ox}]$), making it difficult to perform enough experiments to cause its parameters to be fully specified. This is especially true when performing experiments with multiple electron acceptors. The Okura model, on the other hand, has a total of three parameters (V_{max}, K_{H2}, and K_M- one correlated with each of the three variables E_t, P_{H2}, and $[M_{ox}]$, respectively), and it is reasonable to perform the number of experiments necessary to fully specify this model. For this reason the Okura model is considered to be the best model with which to determine the kinetic parameters for P11 hydrogenase.

4.3 Determination of Kinetic Parameters

A second experiment provided the data necessary to assess the Okura model with multiple electron acceptors to provide a better estimate of model parameters. Additionally, it was important to assess whether the K_{H2} parameter is dependent or independent of the electron acceptor. It was shown in the previous section that the parameter is independent of the BV concentration (as seen by the good fit at two different BV concentrations) but the question arises as to whether the parameter varies with different electron acceptors. As noted in Section 4.1.6,

$$K_{H_2} = \frac{k_2}{k_1} = \frac{k_8}{k_7} = \frac{k_{14}}{k_{13}} \tag{4.74}$$

such that K_{H2} can be associated with rate constants related to enzyme- acceptor complexes. Since the identity and concentration of the physiological electron acceptor is unknown (though it is presumed to be ferredoxin), it was desirable to compare parameters across electron acceptors. Hydrogenase assays were performed according to the procedure described in Section 3.1, with the exception that the check valve was not yet used during venting. The experimental design is shown in Table 4-10.

Table 4-10: Experimental design for parameter calculating experiment

BV Conc (mM)	MV Conc (mM)	H_2 Press (atm)	Number of Runs
2	-	0.84	3
8	-	0.84	3
4	-	0.42	3
2	-	0.084	3
8	-	0.084	3
-	10	0.84	3
-	40	0.84	3
-	20	0.42	3
-	10	0.084	3
-	40	0.084	3

When the Okura parameters were calculated for the assays using BV, the following parameters were obtained.

Table 4-11: Okura parameters for BV experiment

V_{max} (U/mg)	21.92
K_{H2} (atm)	0.31
K_{BV} (mM)	2.42
R^2	0.89

Figure 4-13 is a 2-dimensional representation of what is really a 3-dimensional model surface. That V_{max} is different from V_{max} in the model fitting experiment is to be expected, because a different culture of cells is being used, which affects the total enzyme concentration. K_{H2}, however, should be similar to the model fitting experiment, and K_{BV} should be determined with greater precision as a result of testing three values of BV concentration instead of the two that were tested in the model fitting experiment. When Table 4-11 is compared with Table 4-8 (parameters from the model fitting experiment) it can be seen that the K_{H2} values are very similar between the experiments- thus confirming the correctness of this value. The K_{BV} value is slightly larger than in the model fitting experiment although the model fitting experiment had better repeatability as a result of using the check valve. The closeness of the K_{BV} values suggests that this value is ~ 2, with perhaps the model-fitting experimental value being more accurate due to the better repeatability. The residuals from the BV portion of the parameter determining experiment (Figure 4-14) show that precision of measurement decreased as reactant concentration increased. Consequently, a more exact K_{BV} value is difficult to determine without better repeatability in the multiple electron-acceptor experiment.

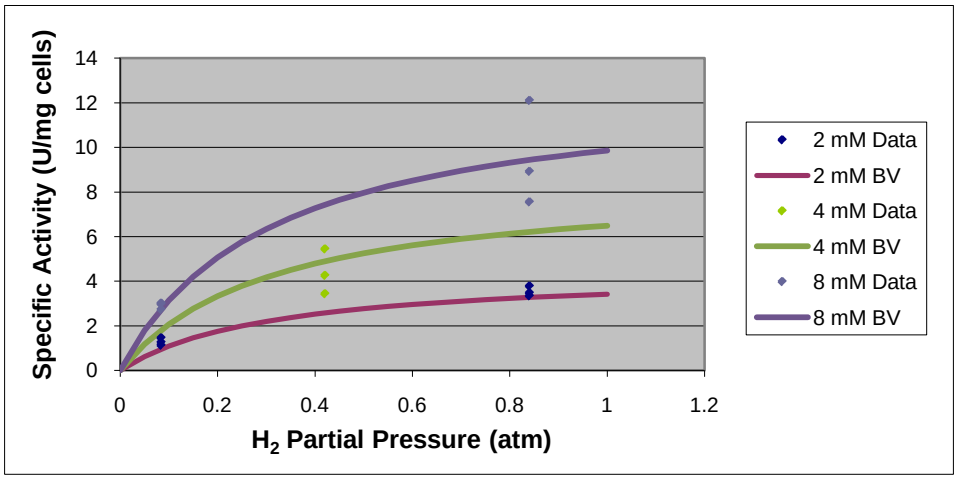

Figure 4-13: Okura model regression of parameter-determining experiment

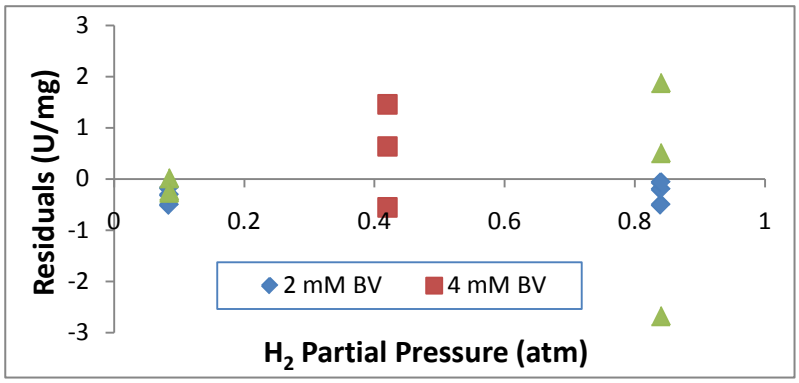

Figure 4-14: Residual plot for BV experiment

When the data from the MV assays was fit to the Okura model, the parameters shown in Table 4-12 were obtained. The fit is represented graphically in Figure 4-15 and the residuals are shown in Figure 4-16. The plots and R^2 value suggest that a reasonable fit to the data was obtained.

Table 4-12: Okura parameters for MV experiment

V_{max} (U/mg)	9.550
K_{H2} (atm)	0.308
K_{BV} (mM)	10.566
R^2	0.959

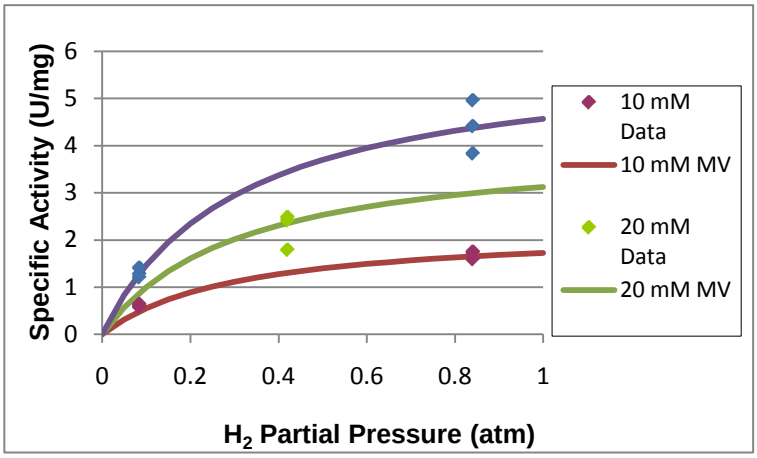

Figure 4-15: Okura model regression of parameter-determining experiment

The most important observation that arises from comparing Table 4-11 and Table 4-12 is that K_{H2} is the same for both experiments at a value of 0.31 atm. This demonstrates that this parameter is independent of the electron acceptor. This finding is critical since the physiological electron acceptor is different than BV or MV but the independence of K_{H2} on electron acceptor suggests that the regressed value can be used to provide guidance on hydrogenase efficiency during syngas fermentation.

The V_{max} values are different between the two tests, which is feasible since this parameter can be affected by the number of enzymes (due to cell assays on different days) and by the choice of electron acceptor. As for K_{MV} and K_{BV}, these parameters were expected to be different since they are electron-acceptor dependent. It should be noted that $K_{MV} > K_{BV}$, suggesting that at similar electron acceptor concentrations, hydrogenase efficiency is more sensitive to the MV concentration as compared to the BV concentration.

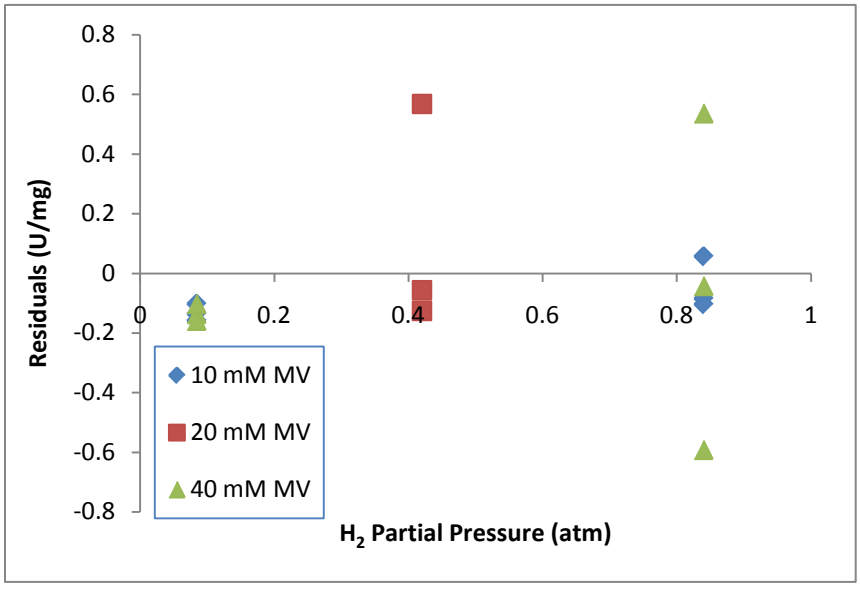

Figure 4-16: Residual plot for MV experiment

4.4 H_2 Partial Pressure Recommendation

In Section 4.3, it was determined that the K_{H_2} value in the Okura model of P11 hydrogenase has a value of 0.31 atm for assays run with both BV and MV. For the Okura model

$$\frac{V_0}{V_{\max}} = \frac{1}{\left(1+\frac{K_{H_2}}{P_{H_2}}\right)+\left(1+\frac{K_{H_2}}{P_{H_2}}\right)\frac{2K_M}{[M_{ox}]}+\left(1+\frac{K_{H_2}}{P_{H_2}}\right)\left(\frac{K_M}{[M_{ox}]}\right)^2} \tag{4.75}$$

it is apparent that V_0/V_{max} is greatest (i.e. the enzyme is most efficient) when P_{H_2} is » K_{H_2} and $[M_{ox}]$ is » K_M. When this occurs, the denominator approaches unity such that hydrogenase is operating at 100% of it theoretical maximum capacity.

Alteration of intracellular physiological electron acceptor concentrations $[M_{ox}]$ would require genetic engineering or culturing techniques beyond the scope of this project, but a variable that can be manipulated in a syngas fermentation system is the H_2 partial pressure, P_{H_2}. If P_{H_2} is ~3 atm (i.e. 10x K_{H_2}), then the $1+K_{H2}/P_{H2}$ terms in Equation 4.75 are 1.1 such that the efficiency of the enzyme is barely affected by P_{H_2}.

Based on the results above, H_2 sparging through the syngas fermentation system at 3 atm partial pressure will maximize hydrogenase efficiency, and consequently, maximize production of the electrons needed for ethanol creation. Unfortunately, it is unlikely that this partial pressure is realistic. However, it is important to recognize how P_{H_2} can affect the enzyme efficiency. For example, if P_{H_2} is 0.1 atm, 0.3 atm, 0.5 atm, or 3.0 atm, the $1+K_{H2}/P_{H2}$ terms would be 4.1, 2.0, 1.6, and 1.1, respectively. These first three partial pressures are more likely to occur in a syngas fermentation system such that the hydrogenase efficiency can be compromised

due to the partial pressure. Although the efficiency is compromised, the activity could be increased via the V_{max} parameter by increasing the number of enzymes.

4.5 Conclusions

In this chapter, several rate laws for hydrogenase activity were tested. It was determined that the Michaelis-Menten model, the EPEP model, and the Okura model all fit the data with good accuracy. However, the Michaelis-Menten equation does not account for the concentration of the electron acceptor and it is possible that electron acceptor effects confound the K_{H_2} parameter. Additionally, the EPEP model contains four parameters, which makes it difficult to perform enough experiments to fully specify the model. The Okura model has the ideal number of parameters: one that is a function of the enzyme/cell concentration, one that regulates the effect of H_2 pressure, and one that regulates the effect of electron acceptor concentration. Additionally, the number of assays needed to fully specify this model can easily be performed in one day. Thus, the Okura model was used for determining the kinetic parameters.

With the Okura model, the following parameters were determined:

Table 4-13: Kinetic parameters for P11 hydrogenase

K_{H2}	0.31 atm
K_{BV}	1.7-2.4 mM
K_{MV}	10.6 mM

These parameters should be good for any combination of H_2 pressures and BV or MV concentrations near which they were developed. They are, however, limited to use at the pH and

temperature at which they were generated (pH ~6 and Temp ~37°C). Effort was taken to develop these parameters at conditions similar to those employed by the commercial system, and the pH mentioned has been found to be approximately the intracellular pH at which hydrogenase functions (See Chapter 5). As noted previously, the best hydrogenase efficiency during syngas fermentation will occur when P_{H_2} is at least 3 atm.

5 PHYSIOLOGICAL ROLE OF HYDROGENASE

In Chapter 3, an assay was developed that gives reliable activity measurements for H_2 oxidation via hydrogenase. In Chapter 4 this assay was employed to find a kinetic model that accurately described P11's hydrogenase and to calculate a K_{H_2} value that reveals the H_2 partial pressure required to optimize hydrogenase activity in P11 during syngas fermentation. A major assumption motivating the work of Chapters 3 and 4 is that improving hydrogenase activity in P11 will increase ethanol production during syngas fermentation. The theoretical basis for that assertion was presented in Section 1.3, but may be summarized as follows: the electrons required to make ethanol must come from either CO or H_2, and obtaining electrons from H_2 leaves the carbon atom in CO available for incorporation into the ethanol molecule.

In this chapter, experimental evidence is presented to confirm a correlation between hydrogenase activity and ethanol production. Additionally, data is presented to show how hydrogenase activity varies as a function of pH. This includes a discussion and measurements of both intracellular and extracellular (media) pH, as wells as a discussion of how a pH differential across the cell membrane may assist the cell in maintaining hydrogenase activity in harsh environments.

5.1 Hydrogenase Activity Linked to Ethanol Production

An experiment was performed that provided evidence of a correlation between hydrogenase activity and ethanol production. In this experiment, three batch reactors (bottles) were monitored for cell mass (optical density or OD), media pH, ethanol concentration, acetic acid concentration and hydrogenase activity for approximately 20 days after inoculation. The results of this study showed a correlation between hydrogenase activity and ethanol production. The details are presented below.

5.1.1 Materials and Methods

Media for cell growth was prepared according to the recipes shown in Tables 3-1 through 3-6 with the exception that the Calcium Solution (Table 3-3) was combined with Mineral Solution (Table 3-2) and the cysteine-sulfide solution (Table 3-5) was added later (as described in this section). The pH of the cell growth medium was adjusted to 6.0 using a 5N potassium hydroxide solution. This was followed by placing 100 mL of the media in each of four experimental bottles and 50 mL in each of three passaging bottles, which were boiled with N_2 purging for about four minutes to remove any O_2 from the liquid. The bottles were sealed and given three repetitions of vacuuming of the headspace followed by pressurization with N_2, ending with venting of the excess N_2. 1 mL of cysteine-sulfide solution (40 g/L sodium sulfide and 40 g/L L-cysteine) was added to each experimental bottle and 0.5 mL of the cysteine-sulfide solution was added to each passaging bottle. All bottles were then autoclaved for 15 min at 121 ^{o}C. After cooling, the first passage bottle was inoculated with 7.5 mL of P11 bacteria culture.

Syngas (40% CO, 30% H_2, 30% CO_2) was then purged through the headspace of the first passage bottle for 1 min and the bottle was left pressurized to 1.5 atm gauge pressure. This bottle was then placed in a shaking incubator at 37 ^oC and 100 rpm to facilitate growth, while the remaining bottles were stored in a refrigerator until needed. When the culture was growing rapidly, about 5 mL of the solution was inoculated into the second passage bottle. When this second bottle reached an OD of 0.74, 4.5 mL of the solution was injected into the third passage bottle. When the cells reached 0.45 OD in the third passage bottle, 10 mL of the solution was inoculated into each of the 4 experimental bottles. After one day, three of the bottles had very similar optical densities while one bottle was different, so it was decided to exclude the dissimilar bottle from further experimentation. This pattern was confirmed on the second day, so all data collected and presented come from the three bottles that experienced similar growth during the first two days.

The optical density of the cell culture was measured at 660 nm using a Shimadzu PharmaSpec UV-1700 spectrophotometer by diluting a 0.5 mL sample with 0.5 mL of deioized water in an optical cuvette. pH measurements were taken by centrifuging a ~1 mL cell sample at 12,000 rpm for 14 minutes in a Labnet Spectrafuge and then measuring the pH with an Oakton pH meter. The supernatant was frozen for later ethanol and acetic acid concentration measurements with a Shimadzu gas chromatograph. Hydrogenase assays were performed as described in Section 3.1, with the following exceptions: the Triton was added in the glovebox instead of during purging, DTT solution was not used (the balance of the volume was made up with deionized water) and the samples were not intentionally vented before beginning the assay. Each sampling day was concluded by re-purging the syngas headspace for 1 minute and leaving the bottles pressurized to 22 psig with syngas while the cells grew in the shaking incubator.

5.1.2 Results

The results of this experiment can be seen in Figures 5-1 through 5-5. Figure 5-1 shows the OD measurement of cell samples taken during the experiment. It is clear from the data that the cells were inoculated while in their exponential growth phase as intended. Rapid growth continued until Day 4 and then the growth slowed until Day 8. On Day 8, a slow decline began, which continued until data collection ceased. Though the density of cells was decreasing during this time, it is apparent that the cells were still viable because inoculation into fresh media resulted in additional growth (data not shown).

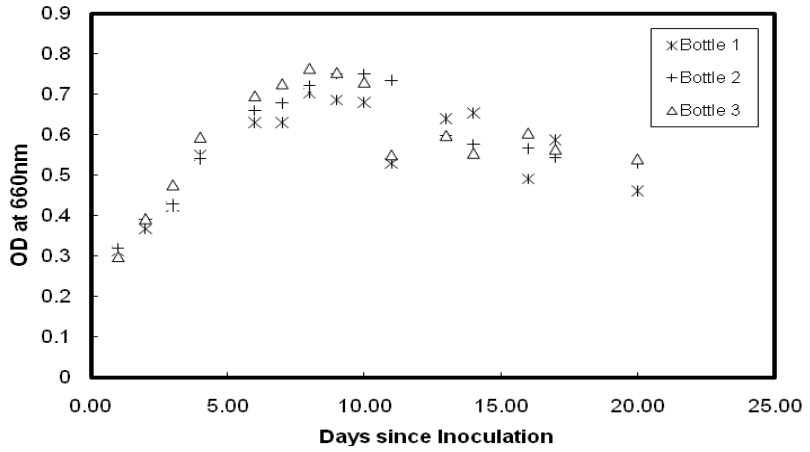

Figure 5-1: Optical density (OD) of cells in three independent batch reactors. The point shown for Bottle 2 on Day 11 is an average of two data points.

Figure 5-2 shows pH measurements taken from the supernatant of centrifuged cell samples. The data indicate a steady decline in pH for the first four days. This is followed by a slower decline from Days 4 to 9, at which point the pH stabilized at a value of about 4. It remained constant at this value for the remainder of the experiment.

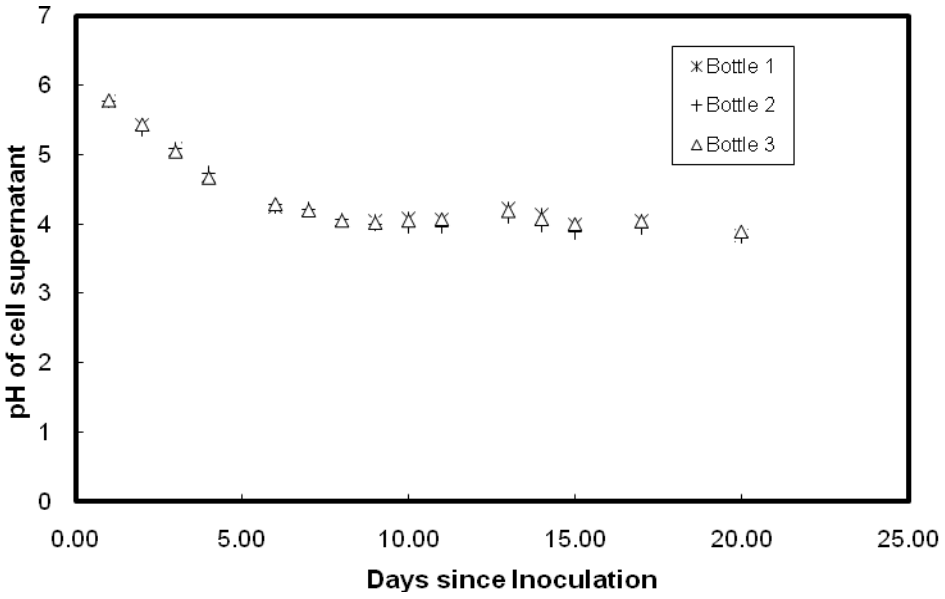

Figure 5-2: pH of cell supernatant for three independent bottle reactors

Figure 5-3 shows the acetic acid concentrations found in centrifuged samples during the experiment. The data indicate that acetic acid levels rose rapidly for the first six days of the experiment, rose more slowly from Day 6 to Day 9 and remained constant around 5 g/L for the remainder of the experiment. The data in Figure 5-4 indicate that ethanol concentration rose slowly for the first six days of the experiment, followed by a period of very rapid ethanol production from Day 6 to Day 11. After Day 11, the ethanol concentration remained virtually constant at just under 2 g/L. The low values on Days 9 and 17 are almost certainly a sampling error or a gas chromatograph (GC) error as they are conserved across both acetic acid and ethanol measurements and are inconsistent with the remainder of the data. Therefore, these data points were not considered in the analysis.

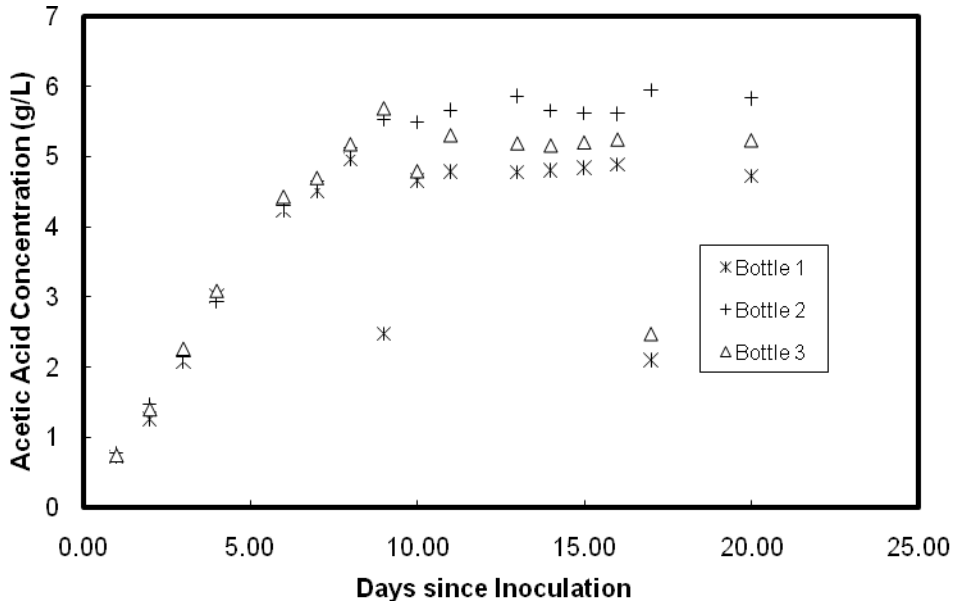

Figure 5-3: Acetic acid concentrations for 3 independent bottle reactors

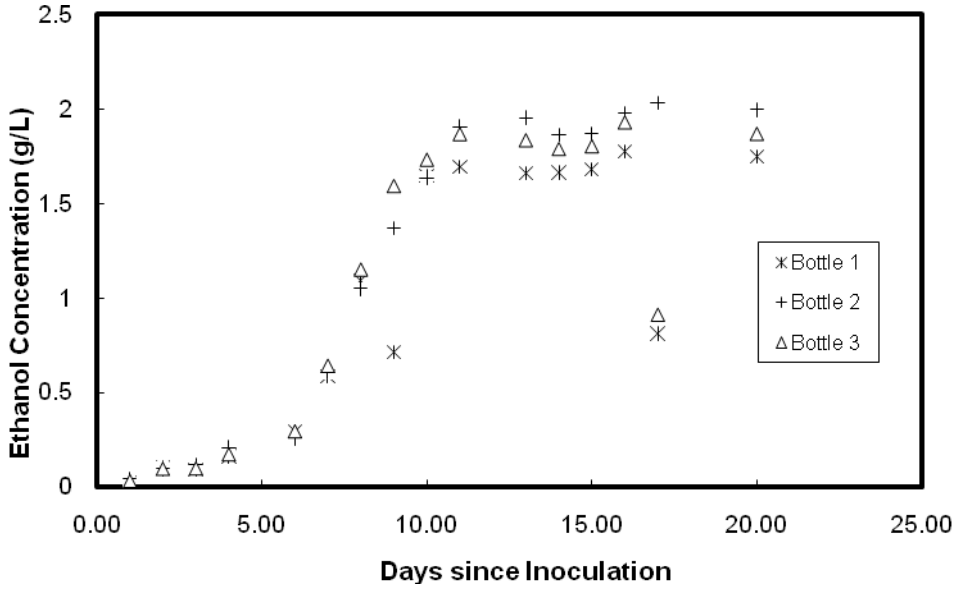

Figure 5-4: Ethanol concentrations for three independent bottle reactors

The data in Figure 5-5 show hydrogenase specific activity during the experiment. It is apparent that hydrogenase specific activity rose rapidly for the first four days of the experiment, reaching near-maximum levels on Day 4. This was followed by a period of consistently high activity from Day 4 to Day 9. On or about Day 9 or 10, hydrogenase activity suddenly ceased. When no activity was observed on Days 11, 13, and 14, it was decided that no further measurements needed to be taken. However, when these cells were later inoculated into fresh media, hydrogenase activity returned (data not shown).

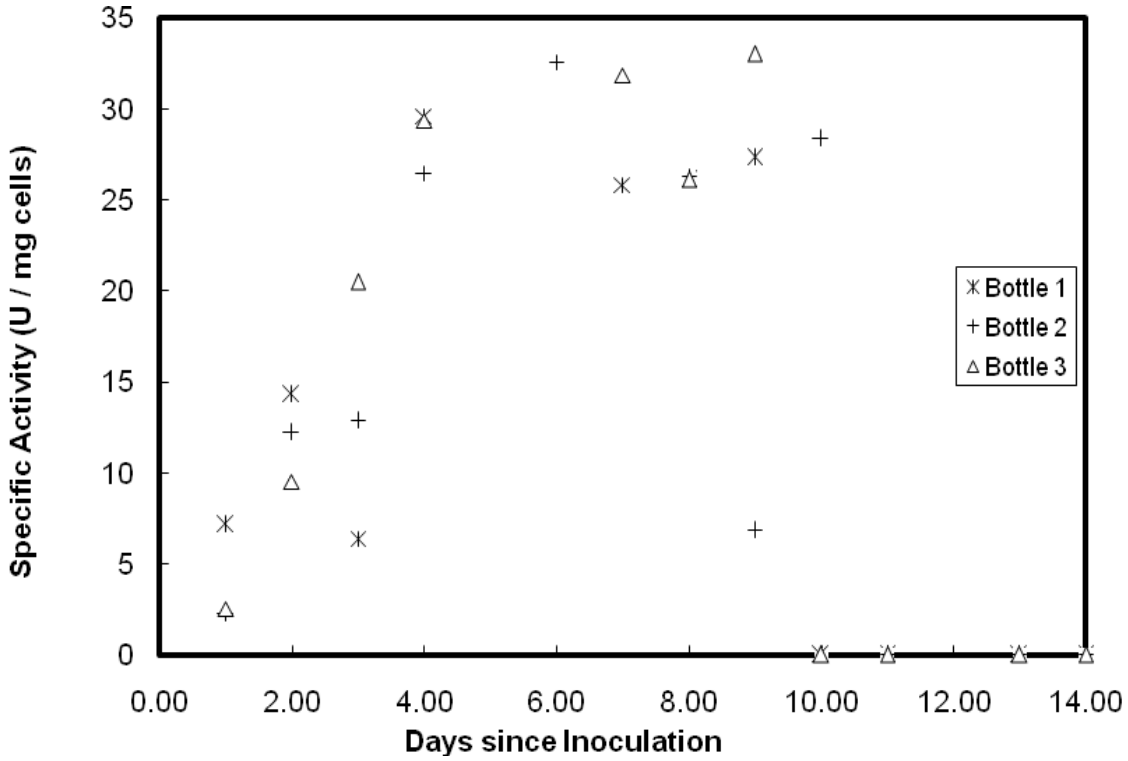

Figure 5-5: Time course of hydrogenase activity for three independent bottle reactors. Tests in which no reaction was observed were set to zero. The points for Bottle 2 on Days 1 and 2 and the point for Bottle 3 on Day 2 represent averages of two experimental runs.

5.1.3 Discussion

Many interesting trends can be observed in this data. First, from Figure 5-1, it is apparent that P11 cells follow the growth trends that are typical of bacteria in batch culture. Namely, they experience an exponential growth phase, followed by a transition to a stationary phase (White, 2000). The data in this experiment seems to indicate that the exponential growth phase lasted from inoculation to Day 4 or 5 and that the stationary phase occurred from Day 6 to day 11 or beyond. No explanation is given for the slow decline in cell mass observed from Day 8 onward, but it is known that this is typical of batch cultures of P11 (unpublished data). Additionally, it is known that the cells were still viable because inoculation into fresh media resulted in additional growth (data not shown).

The second interesting trend expands upon the first. By comparing Figures 5-1, 5-3, and 5-4, one can observe that acetic acid is produced primarily during the period of rapid cell growth and ethanol is produced once the cells have reached their stationary phase (Days 6 through 11). This is typical of acetogens (Grupe, 1992). In the acetyl-CoA pathway described in Section 1.3, it can be seen that both ethanol and acidic acid are produced from acetyl-CoA. Thus, it appears that the acetyl-CoA was directed primarily to produce cell mass and acetic acid during the first ~7 days of the experiment, and was directed primarily toward ethanol from Days 7-11.

It is particularly interesting to note that the period of highest hydrogenase activity begins two days before the period of most rapid ethanol production, Days 4 and 6 respectively. High hydrogenase activity (~30 U/mg) is then concurrent with rapid ethanol production from Days 6 to 10, after which hydrogenase activity suddenly ceases and ethanol production slows down (until Day 12). No hydrogenase activity is observed after Day 10, and no ethanol is produced after Day 12. One possible explanation of these phenomena is that hydrogenase is used to

created a reducing environment in the cell immediately prior to and concurrent with the period of most rapid ethanol production. Since ethanol is a more reduced product than acetic acid (by four electrons), it is feasible that the cell utilizes hydrogenase to generate the extra electrons (reducing power) needed to generate ethanol from acetyl-CoA instead of acetic acid. It is also feasible that both the change in hydrogenase activity and the change in rate of ethanol production are caused by some other factor (e.g. the transition to stationary phase). Hence, further research needs to be conducted if this assertion is to be made authoritatively.

That all observable metabolic processes seem to stop after about Day 12 is somewhat of a mystery. The cells are clearly still viable as seen by the growth and hydrogenase activity that begin again when the dormant cells are inoculated into fresh media. Hence, it appears that some environmental factor triggers the cessation of observable metabolic activity in the cells. Possible explanations include depletion of a vital nutrient from the media or toxic accumulations of excreted byproducts (White, 2000), such as ethanol. One additional possible factor that could affect both hydrogenase activity and product distribution is pH. Figure 5-2 shows that media pH changes dramatically over the first 8-9 days of the experiment. It is possible that this changing pH causes some of the observed changes in P11 behavior. The next two sections deal with the effects of pH on hydrogenase activity.

5.2 Hydrogenase Activity as a Function of pH

Virtually all enzymatic reaction rates are dependent on pH. This is primarily because different pH environments cause structural shift in enzymes, and the changing structure results in different reaction rates. However, hydrogenase has the potential to be especially dependent on

pH because protons are directly involved in the reaction. Consequently, an experiment was performed in which hydrogenase activity was measured as a function of pH.

5.2.1 Materials and Methods

Cells were prepared essentially as described in Section 5.1.1 and hydrogenase assays were performed essentially as described in Section 3.1, with the major exception being that the pH of the buffer used for the assays was set to various levels between 6 and 7.75 (in 0.25 pH increments). Additionally, the check valve was not yet used for venting when this experiment was performed. Duplicates were taken at each condition.

5.2.2 Results and Discussion

The data (shown in Figure 5-6, where each data point represents the average of a duplicate) shows a 400% increase in hydrogenase activity as the pH of the assay medium rises from 6 to 7.75. The trend is approximately linear. The observed behavior is consistent with intuition, for as the concentration of H^+ ions (the product of the hydrogenase H_2 oxidation reaction) rises (consistent with the pH decreasing) the activity of the hydrogenase H_2 oxidation reaction decreases. Additionally, this behavior is consistent with data for hydrogenase from other bacterial species as reported in the literature (Tsygankov, 2007).

One major implication of this study is that current procedures are testing hydrogenase activity at a pH far from which it is most active. Even more important, if syngas fermentation processes are run at a pH near 6, these results would imply that the reducing power of hydrogenase is severely under-utilized, and that additional reducing power may be able to be

obtained by increasing the pH of the culture medium. However, in the study reported in Section 5.1, increasing hydrogenase specific activity was found to be concurrent with decreasing media pH. Increasing hydrogenase activity can be due to either increased expression within the cell or changing environmental factors, so one possible explanation of these apparently conflicting phenomena is that hydrogenase *in vivo* is at a different pH than the external media, implying that a pH differential exists across the cell membrane. Another experiment was performed to investigate this phenomenon.

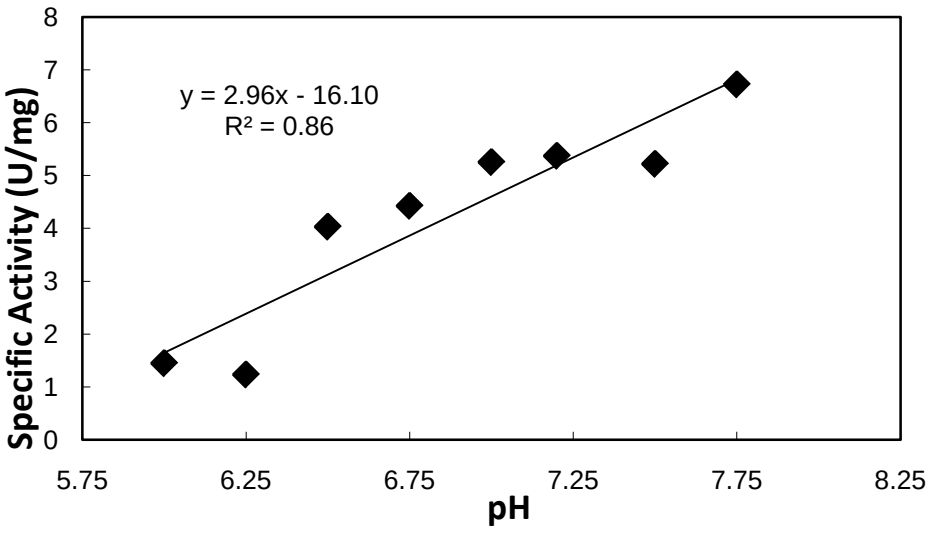

Figure 5-6: Hydrogenase activity as a function of pH. Each point is the average of a duplicate.

5.3 Intracellular pH and Generation of a Transmembrane pH Differential

An experiment was performed to investigate an explanation for a possible discrepancy in data presented in Sections 5.1 and 5.2. In Section 5.1, increasing hydrogenase specific activity was observed over the same time period that the media pH was rapidly decreasing, yet in Section

5.2, hydrogenase had significantly more activity at higher pH values. Possible explanations include that increasing hydrogenase activity is due to increased expression of hydrogenase within the cell (regardless of pH), or that P11's intracellular pH is different from the external media pH. Thus, an experiment was performed to measure the intracellular pH of a batch culture of P11 and to differentiate between these possible explanations.

5.3.1 Materials and Methods

Cells were prepared essentially as described in Section 5.1.1 and hydrogenase assays were performed as described in Section 3.1, with the exception that the check value was not yet used during venting of the assay cuvette. Data was obtained essentially as described in Section 5.1.1, with the additional intracellular pH procedure described below.

To determine intracellular pH, two extra 1 mL samples of cell broth (test sample and baseline sample) were collected inside the anaerobic chamber and centrifuged at 13,000 rpm for 5 minutes in a Labnet Spectrafuge. The supernatant was removed and the pellets were resuspended in a mixture of dipotassium phosphate (K_2HPO_4) and citric acid ($C_6H_8O_7$), known as McIlvaine buffer (McIlvaine, 1921), prepared to the previously determined media pH. Next, 50 µg of SNARF-4F fluorescent probe (Invitrogen, Product S-23291) was dissolved in 17 µL of dimethyl sulfoxide (DMSO) and this mixture was added to the resuspended cell mixture of the test sample. Nothing was added to the baseline sample. Both samples were then incubated at 37°C for at least 30 minutes.

During the incubation period the SNARF probe in the test sample penetrates the P11 cell membrane and its ester bond is cleaved by esterase enzymes native to most cells. The cleaved carboxylic acid product is impermeable to the cell membrane and remains trapped inside the cell

where its protonated and deprotonated forms partition according to the intracellular pH. After the incubation period, any uncleaved SNARF is removed from the sample by two repetitions of centrifuging, removing the supernatant, and resuspending the pellet in 1 mL of the McIlvaine buffer. The baseline sample is similarly washed to be consistent. The samples are then transferred to a fluorometer (PTI 814) where they are illuminated with 523 nm light.

A sample illuminated with 523 nm light fluoresces, and its emission is monitored over the range of wavelengths 550-700 nm. The emission count from the baseline sample is subtracted from that of the test sample and the resulting ratio of emission at 587 nm divided by the emission at 636 nm is used to determine the ratio of protonated to deprotonated SNARF-4F carboxylic acid. This ratio can be converted to an intracellular pH measurement via a calibration curve. (The calibration curve was generated via a saponification reaction in which the ester bond of the SNARF-4F probe was cleaved by a strong base before being suspended in different pH McIlvaine buffers. Each sample was evaluated in the fluorometer and a pH vs emission ratio curve was generated.) By this comparison the intracellular pH was determined for each day.

5.3.2 Results and Discussion

Calibration Curve

The calibration curve generated by the saponification reaction is shown in Figure 5-7. It was generated by calculating the emission ratio (587nm / 636 nm) for the saponified SNARF-4F carboxylic acid in McIlvaine buffers of pH 5.15, 5.4, 5.95, 6.45, 6.9, and 7.3. These values were fit by a 3rd order polynomial regression with high precision ($R^2 = 0.99997$).

$$Ratio = 0.269 \cdot pH^3 - 5.11 \cdot pH^2 + 30.74 \cdot pH - 55.82 \qquad (5.1)$$

Sample pH for the experimental tests was calculated from emission ratio using this calibration curve.

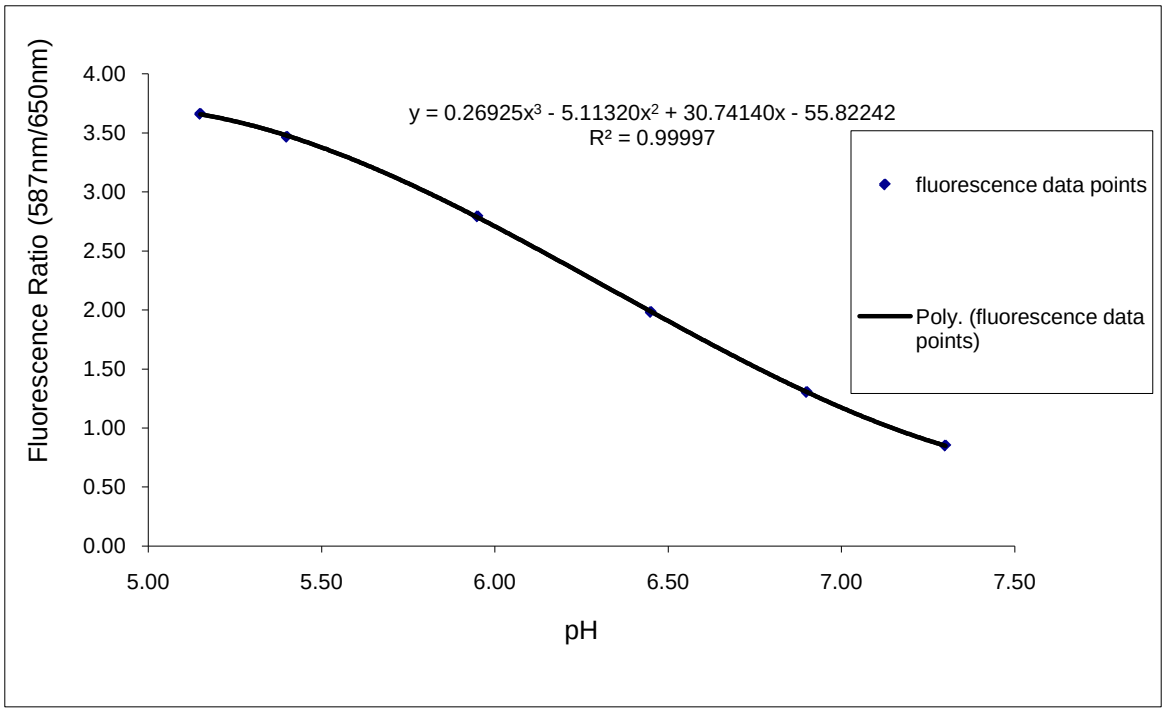

Figure 5-7: Calibration curve for determining pH from fluorescent emission ratio (587nm / 636nm)

Control Experiments

Several control experiments were conducted to ensure that the data was accurate. First, 5 different pH solutions (4.75, 4.98, 5.21, 5.52, and 5.77) of McIlvaine buffer were tested for fluorescence when no SNARF was present. At every pH, value the emission spectrum was identical (Figure 5-8), implying that the fluorescence of McIlvaine buffer is not pH dependent, which is the desired condition.

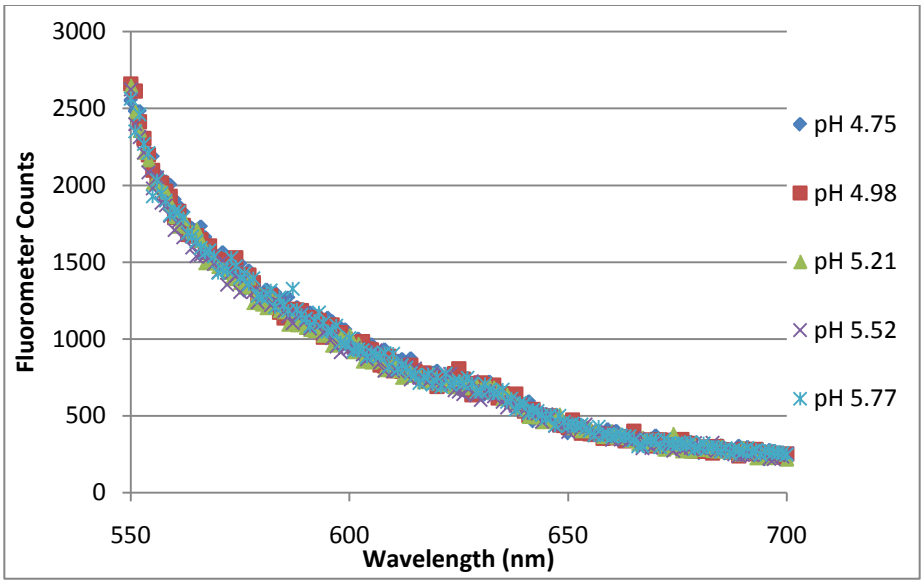

Figure 5-8: Fluorescence of McIlvaine buffer at different pH values

Second, an experimental sample that included cleaved SNARF-4F was re-tested for fluorescence 1.5 hours after its original test. This test was designed to show that any variation in time of preparation to time of fluorescence testing was inconsequential. Figure 5-9 shows the two fluorescence scans, with the large peak at ~590 nm due to the fluorescent indicator SNARF-4F. Though some difference does exit between the two samples, when the fluorescence count (FC) ratio at 587/636 nm was calculated for each test and converted to a pH measurement using the calibration curve, the difference between the measurements was 0.04 pH units.

$$Original: \frac{FC_{587}}{FC_{636}} = \frac{64876.4}{21040.4} = 0.269 \cdot pH^3 - 5.11 \cdot pH^2 + 30.74 \cdot pH - 55.82 \qquad (5.2)$$

$$pH = 5.73 \qquad (5.3)$$

$$1.5hrs: \frac{FC_{587}}{FC_{636}} = \frac{69434.9}{22101.7} = 0.269 \cdot pH^3 - 5.11 \cdot pH^2 + 30.74 \cdot pH - 55.82 \qquad (5.4)$$

$$pH = 5.69 \qquad (5.5)$$

This is sufficiently small that minor variations in the time sequence can be safely neglected.

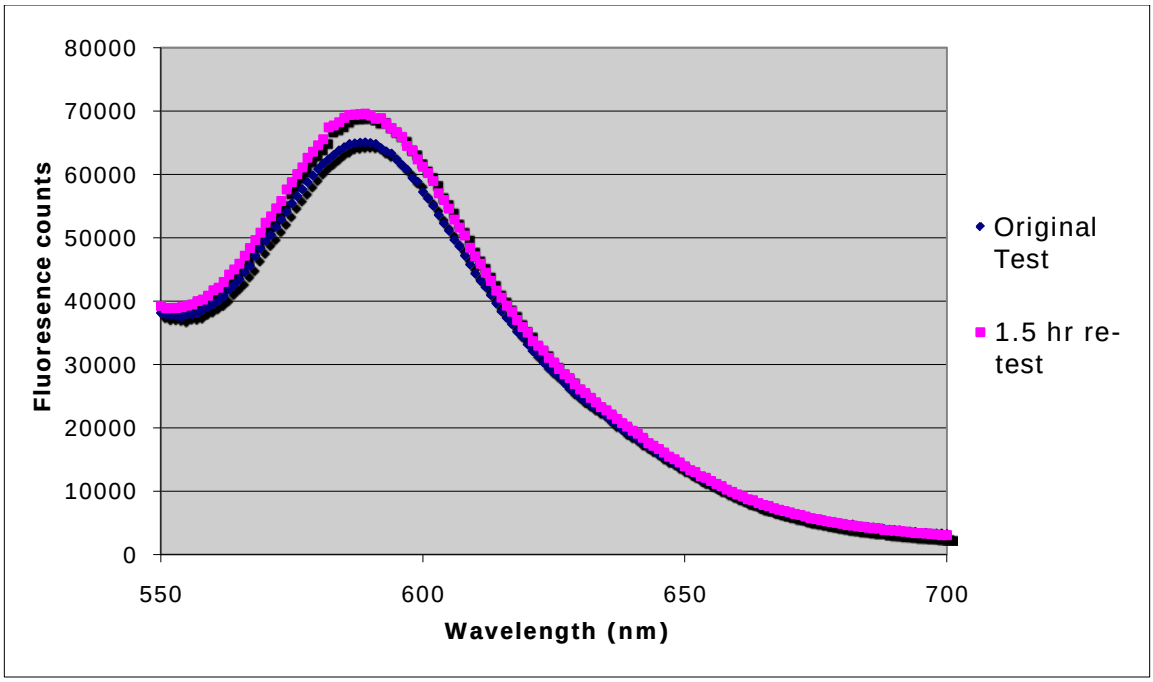

Figure 5-9: Fluorescence emission spectrum of an experimental sample tested at two different times

Finally, the fluorescence of uncleaved SNARF-4F (still in its acetate form) was tested at 4 different pH values. This test was designed to detect whether residual uncleaved SNARF-4F (left after the double washing procedure) could falsely account for the fluorescence behavior attributed to the carboxylic acid SNARF-4F. Ideally, the fluorescence of uncleaved SNARF-4F would be independent of pH because this would differentiate it from SNARF-4F in its carboxylic acid form.

To perform this test, uncleaved SNARF-4F was dissolved in DMSO and suspended in McIlvaine buffer at pH values of 4, 5, 6, and 7. The sample was illuminated with 523 nm light and the fluorescence spectrum between 550 nm and 700 nm was obtained (Figure 5-10). When the 587/636 nm ratio was calculated for each sample and used in Eqn 5-1, the calculated pH values shown in Table 5-1 resulted. Because these values are so different from the actual pH values, uncleaved SNARF-4F cannot be giving the signal attributed to carboxylic acid SNARF-

4F. The range of the calculated values (5.66 – 5.35 = 0.31) is 10% the range of the actual values (7 – 4 = 3), showing that uncleaved SNARF-4F is far less pH dependent than its cleaved (carboxylic acid) counterpart. Additionally, the double washing procedure described in the previous section should cause extracellular uncleaved SNARF-4F to be at a negligible concentration. The smaller pH sensitivity of uncleaved SNARF-4F (relative to carboxylic acid SNARF-4F) shows that it cannot be giving the signal attributed to SNARF-4F in the carboxylic acid form, and uncleaved SNARF's small concentration should minimize its effect on the overall fluorescence of an experimental sample.

Table 5-1: Calculated pH of uncleaved SNARF-4F in various pH solutions

Actual pH	Measured 587/636 nm ratio	Calculated pH
4	3.48	5.39
5	3.52	5.35
6	3.27	5.58
7	3.18	5.66

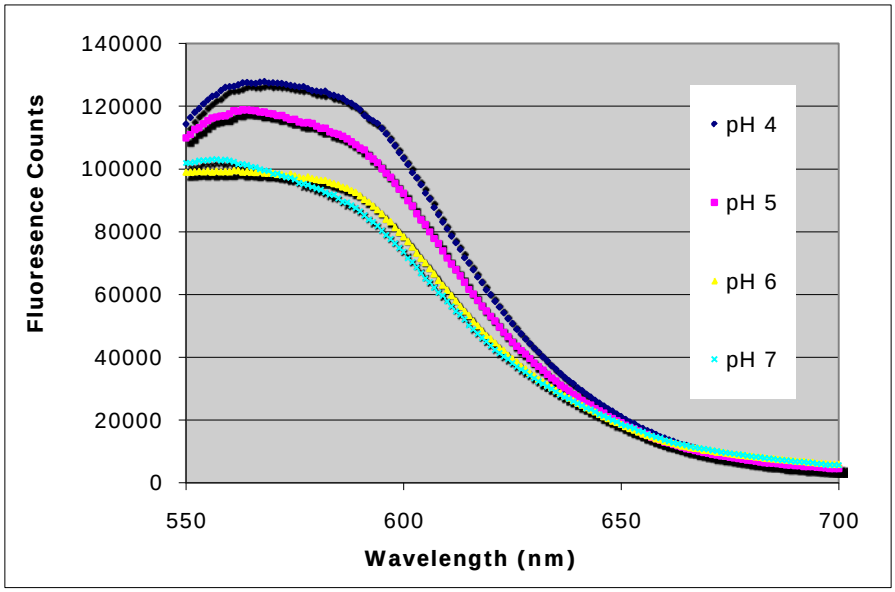

Figure 5-10: pH dependence of uncleaved (acetate form) SNARF-4F

Intracellular pH- Experiment 1

All of the same data was collected in this experiment as was collected in the experiment described in Section 5.1, with the additional intracellular pH information. The experiment was run twice. In the first experiment, media pH started at 6 and decreased steadily over the first four days to pH 4.5 where it remained for Days 4-9, acetic acid concentration rose steadily for ~six days to a value of 7 g/L and then decreased slightly on Days 8 and 9 to a value of 5.5 g/L, and the ethanol concentration rose from Days 2-6, remaining at value of ~3 g/L thereafter (Figures 5-11 and 5-12). All of these trends are the same as those described for the experiment in Section 5.1 with the exception that they occur earlier in time. This is likely due to a mature P11 inoculum when compared to the inoculum used for the experiment described in Section 5.1. Additionally, acetic acid concentration dipped slightly in the later days of the experiment (days 8-9) instead of remaining constant, a behavior more often observed with continuous-gas cultures of P11 (data not shown). This dip in acetic acid concentration may be due to re-incorporation of intracellular acetic acid into the metabolic pathway (Figure 1-2), especially because this dip is correlated with a sudden increase in intracellular pH (Figure 5-12).

The hydrogenase activity is also shown in Figure 5-11. This data has a much less pronounced run up phase than that seen in Section 5.1, but rises from < 4 U/mg to ~6 U/mg during the first four days of the experiment. Specific activity decreases slightly to 5.5 U/mg on Day 6, and then shows no activity on Days 8 and 9. The slightness of the run-up phase is probably a result of the time-shift due to a mature P11 cell inoculum, as described previously, while the high reading on Day 3 (9 U/mg) is possibly a result of imprecise venting techniques leaving extra H_2 pressure in the cuvette.

Internal pH measurements were stable around 5.5 (± 0.1) until Days 8 and 9 when they jumped to 5.8 and 5.7 respectively (Figure 5-12). This sudden change in intracellular pH happened concurrently with the cessation of hydrogenase activity and with the slight decline in acetic acid concentration, as mentioned previously. Intracellular pH measurements were not corrected for blank fluorescence during this initial experiment, but since this effect was later determined to be small for many of the days of the experiment, the data were included for comparison purposes. This inadequacy was better addressed in the 2nd iteration of this experiment.

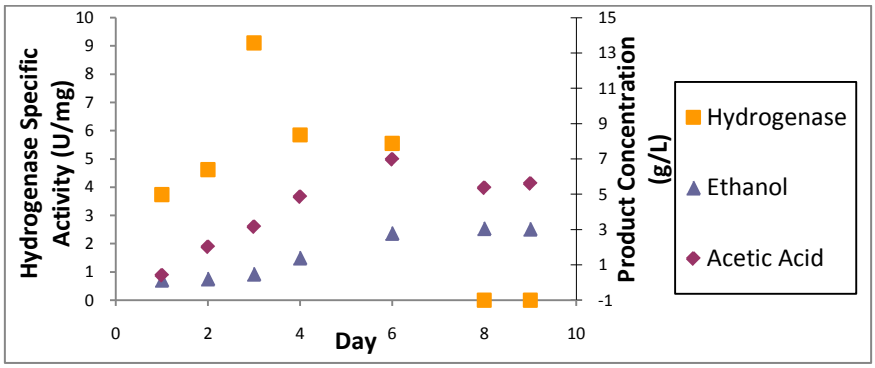

Figure 5-11: Hydrogenase specific activity and ethanol and acetic acid concentrations for first intracellular pH experiment

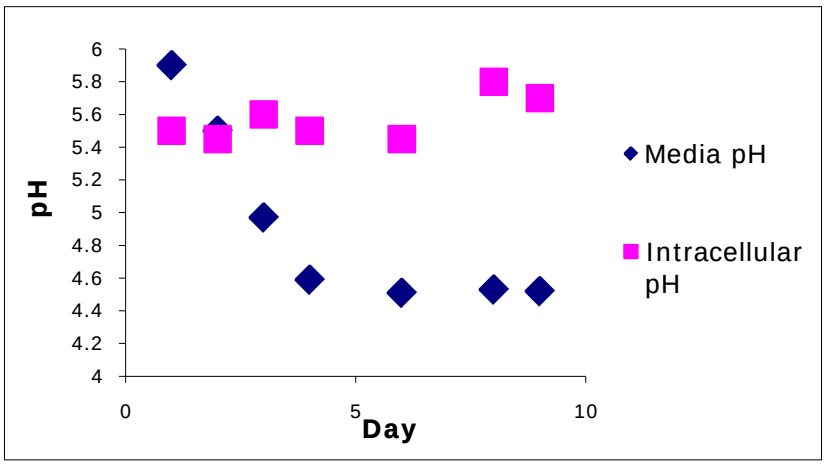

Figure 5-12: Media pH and intracellular pH for first intracellular pH experiment

Intracellular pH- Experiment 2

In the second iteration of the experiment just described, data was collected with the additional rigor of duplicated hydrogenase assays and correction to the internal pH measurements by subtracting out blank fluorescence. As shown in Figures 5-13 and 5-14, the media pH data and the ethanol and acetic acid concentration data are very similar between the two experiments. In both cases the media pH decreases and the ethanol and acetic acid concentrations increase, before leveling off and remaining relatively constant, with a slight dip occurring in the acetic acid concentration on days 8-9 as seen previously. The transition to stability occurs about the time the cell density (OD) reaches a maximum, which is different from the experiment described in Section 5.1 where ethanol concentration was still increasing rapidly when OD reached its maximum point (Figures 5-1 and 5-4).

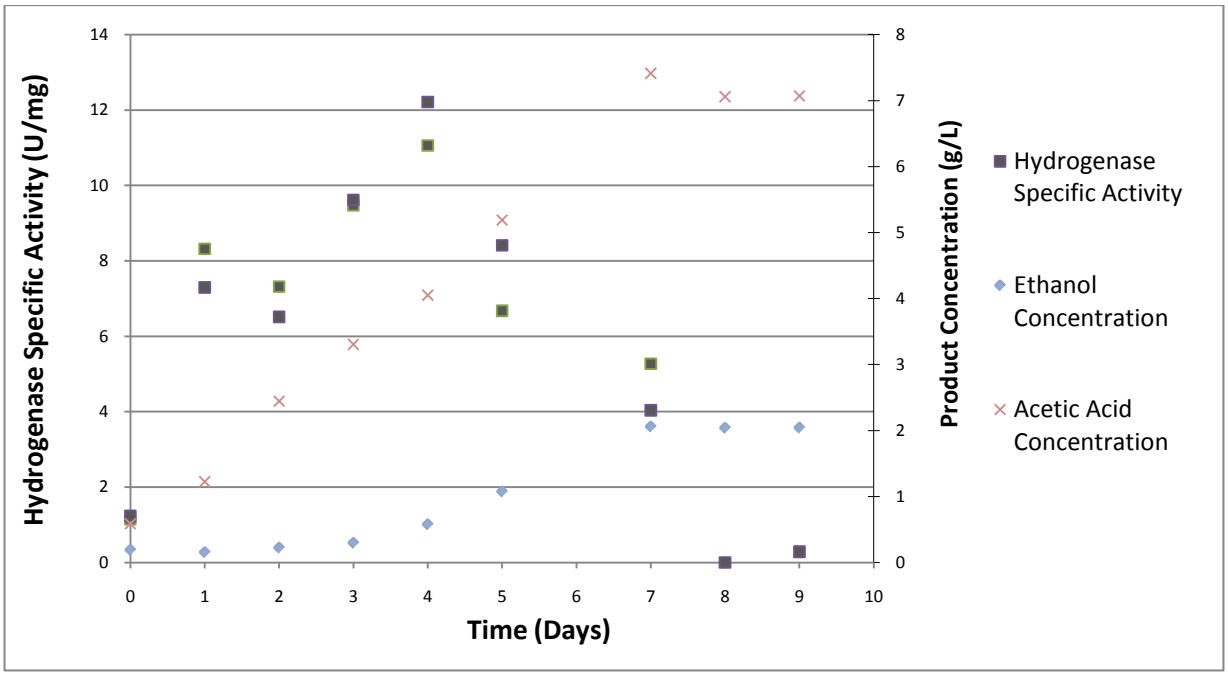

Figure 5-13: Data from second intracellular pH experiment

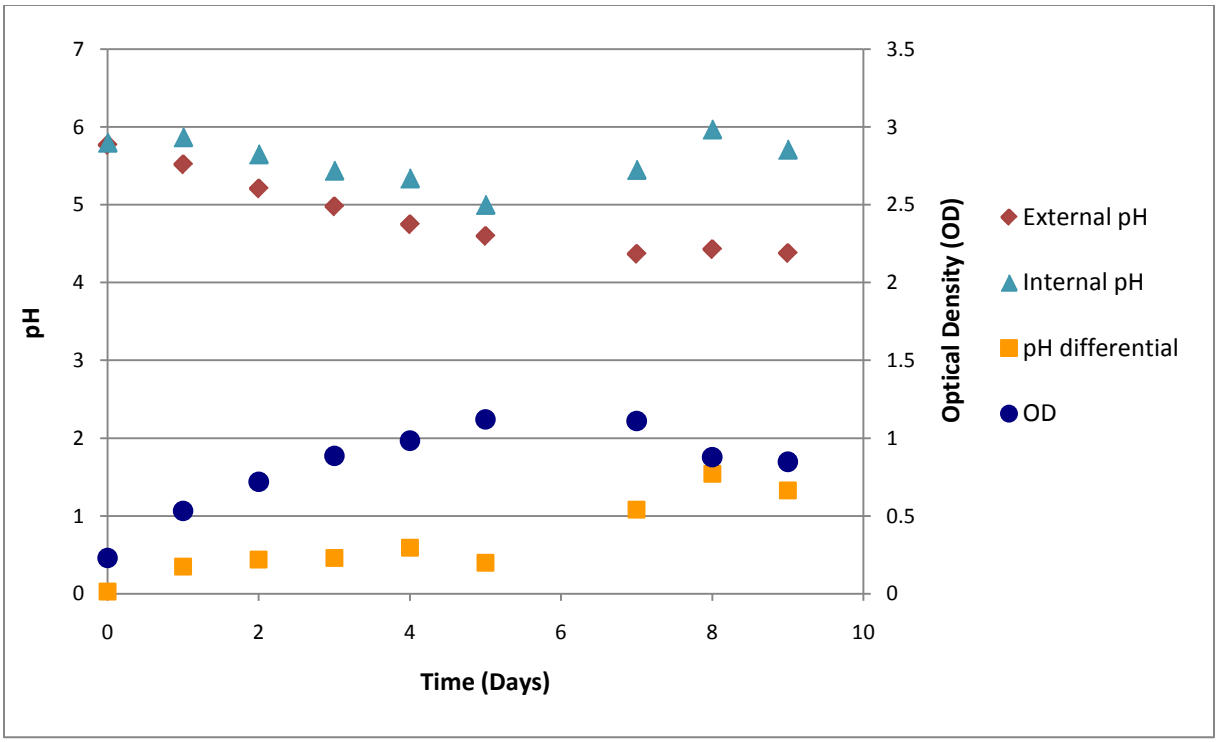

Figure 5-14: Data from second intracellular pH experiment

In the first intracellular pH experiment, it was determined that the cells' internal pH remained relatively constant around 5.5 for the first six days, before jumping to 5.8 and 5.7 on Days 8 and 9, respectively. In this experiment, the average intracellular pH was again approximately 5.5, but there was significantly more trending in the data (Figure 5-14). In this instance, intracellular pH dropped from a starting value of 5.8 to a minimum value of 5.0 on Day 5 before rising back to approximately its starting value on Days 8 and 9. The rise in intracellular pH from Day 7 to Days 8 & 9 is again associated with a slight decrease in acetic acid concentration and may be due to re-incorporation of intracellular acidic acid into the metabolic pathway, as shown in Figure 1-2. When intracellular pH is plotted as function of media pH, the diagram shown in Figure 5-15 results. This behavior is consistent with the behavior observed by Huang et al. (1985) in their studies with *Clostridium acetobutylicum*.

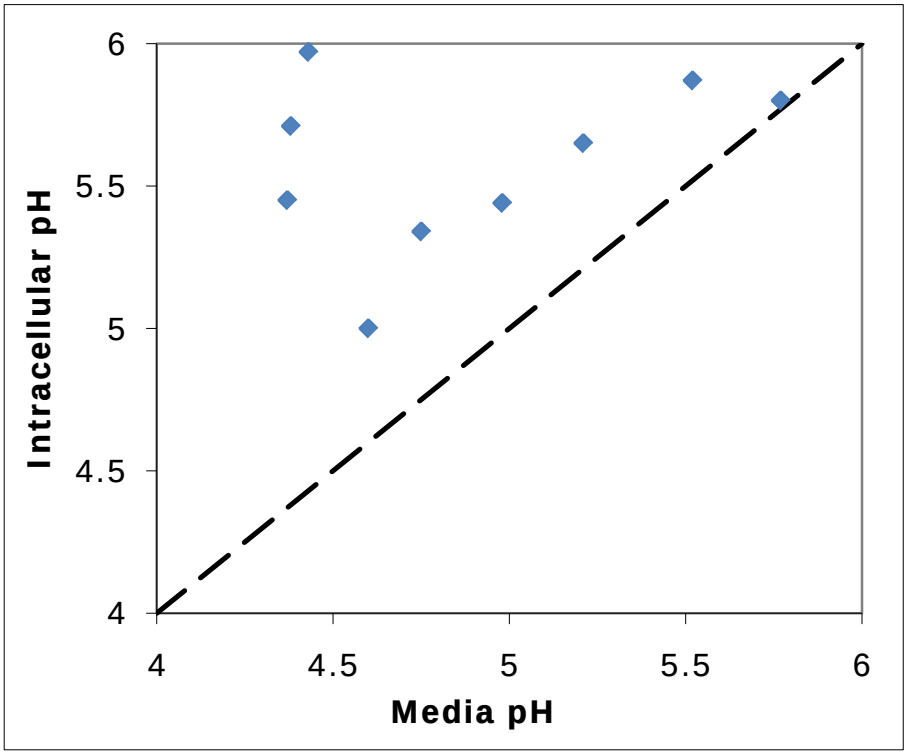

Figure 5-15: Intracellular pH as a function of media pH

It should be noted that the intracellular pH measurements reported for the 2nd intracellular pH experiment are more likely to be accurate than the values from the first experiment due to the subtracting of blank fluorescence described in Section 5.3.1. Blank values for Days 0 and 1 of the second experiment were determined *ex post facto* by subjecting a P11 solution with OD equal to that of the experimental day to the standard treatment for blanking samples and measuring the solution's fluorescence. This was not performed during the first experiment. This subtraction of black fluorescence created the dip in intracellular pH values seen for Days 4-7, but had little effect (±< 0.2 pH units) on the pH values measured for Days 0-3 and 7-9.

When hydrogenase specific activity trends are compared between the two iterations of the intracellular pH experiment, many similarities are observed. For Days 1 through 5 or 6 in both

experiments, P11 maintains a relatively-stable high level of hydrogenase activity, with a peak in that activity occurring on either Day 3 or 4 (Figure 5-11 and 5-13). On Day 7, the 2nd version of the experiment shows significantly lower hydrogenase activity, followed by no observable activity on Days 8 and 9. No data was collected on Day 7 during the 1st experiment, but this study also showed no activity on Days 8 and 9. One major difference is that no Day 0 point was collected during the 1st experiment, and the value measured for the 2nd experiment was very low relative the values measured for Days 1 through 5 or 6. Since the value on Day 0 was measured only a few hours after inoculation and charging with syngas, while all others samples were taken a day after the syngas recharge, it is possible that this low point was due to the high pressure of CO present in sample (Hurst, 2005, and Section 3.4 of this thesis). This could be true even though the sample was purged with H_2 prior to assaying it for hydrogenase activity.

The data from the 2nd iteration of the intracellular pH experiment clearly indicate that P11 is able to maintain an intracellular pH that is higher than the media pH surrounding the cells. However, intracellular pH does decrease during the period that hydrogenase activity is increasing. Because hydrogenase is more active at higher pH, the change in intracellular pH can not account for the increase in hydrogenase activity, and it must be concluded that increasing hydrogenase activity is due to increasing hydrogenase expression within the cell. Regardless, the maintenance of an intracellular pH that is above that of the surrounding media likely allows P11 to utilize the reducing power of hydrogenase for ethanol creation at a higher level than would be possible if hydrogenase were exposed to media pH.

5.4 Conclusions

Several important conclusions can be reached from the data presented in this Chapter. First, H_2 oxidation via hydrogenase appears correlated to ethanol production. In every case, high levels of hydrogenase activity precede the period of greatest ethanol production. Whether this is a causal factor (hydrogenase providing the reducing environment necessary for ethanol production) or whether both high hydrogenase activity and ethanol production are caused by some other cellular process (e.g. the transition from growth phase to stationary phase) should be the subject of future study.

Second, hydrogenase activity (oxidation) is clearly higher at basic pH than at acidic pH. Over the range tested (pH = 6-7.75), hydrogenase is approximately four times more active at the upper end of the range than at the lower end of the range. Since the reducing power of hydrogenase appears correlated with ethanol production, operation of syngas fermentation processes at higher pH may result in improved ethanol yields.

Third, intracellular pH for P11 cells was determined to be approximately 5.5. The more accurate test of intracellular pH shows that this parameter starts ~6, drops to ~5 and then returns to ~6 after the cessation of hydrogenase activity. Since hydrogeanse activity (always measured at pH 6) increases during the time that intracellular pH is decreasing, it must be concluded that increasing hydrogenase activity is due to an increase of hydrogenase expression within the cell. However, maintaining an intracellular pH above that of the surrounding media likely allows P11 hydrogeanse to function at a higher level than would be possible if it were fully exposed to media pH. Additionally, since the measured intracellular pH is still well below the optimal pH range for hydrogenase, it is possible that a higher pH environment would result in higher intracellular pH conditions, and subsequently higher hydrogenase activities.

6 CONCLUSIONS AND FUTURE WORK

Though much has been discovered as a result of the research presented in this thesis, more always remains to be accomplished. In this chapter, the conclusions of the current work are summarized, followed by recommendations for areas of future study. By understanding what has already been accomplished, future efforts can be directed along profitable paths, causing syngas fermentation studies to proceed along an efficient route. The conclusions and recommendations follow.

6.1 Conclusions

6.1.1 Hydrogenase Assay

An assay for efficiently and reliably assaying hydrogenase from P11 was developed. The full procedure is given in Section 3.1.1. Specific items of interest include:

- Less than 4 minutes of sparging with 50 sccm H_2 is required to reduce O_2 levels to below 1 ppm in a 3 mL aqueous solution.
- Less than 1 minute of H_2 purging is required to fill a 3.5 mL cuvette to 99.9999% H_2.
- Including 12.5 mM DTT in the reaction mixture at pH 6 helps to scavenge O_2 and eliminate assay failures. This protection is insufficient to protect Hungate tubes

that are left exposed to the air for several hours. DTT included in assays at pH 7.7 and 8.3 interferes with the assay due to direct reduction of the electron acceptor by DTT.

- Limited H_2 solubility and its slow diffusion through the stagnant aqueous reaction medium minimizes replenishment in the solution from the headspace. This necessitates the use of initial slopes when performing kinetic analysis.
- Dissolved CO_2 changes the pH of the assaying medium and assays should be performed with pure H_2 or H_2-N_2 mixtures whenever possible.
- 0.084 atm CO causes 90% inhibition of hydrogenase in permeabilized P11 cells.
- Prolonged exposure to Triton X-100 (used to permeabilize the cell membrane during assays) causes diminished hydrogenase activity.
- Use of different electron acceptors (and different concentrations of the same electron acceptor) results in different measured activities.
- Even small pressure differences between assays can make a large difference on measured hydrogenase activity.

By incorporating each of the above factors, the assay developed for P11's hydrogenase was made to give specific activity values with an average standard deviation of ~0.6 U/mg, well sufficient for performing kinetic studies.

6.1.2 Kinetic Experiments and Rate Laws

Several rate laws for modeling hydrogenase activity were tested, and it was determined that the Okura model was best suited for modeling H_2 oxidation via P11's hydrogenase.

$$\frac{V_0}{V_{\max}} = \frac{1}{\left(1+\frac{K_{H_2}}{P_{H_2}}\right)+\left(1+\frac{K_{H_2}}{P_{H_2}}\right)\frac{2K_M}{[M_{ox}]}+\left(1+\frac{K_{H_2}}{P_{H_2}}\right)\left(\frac{K_M}{[M_{ox}]}\right)^2} \quad (6.1)$$

The Okura model has an ideal number of parameters: one that is a function of the enzyme/cell concentration (V_{max}), one that regulates the effect of H_2 pressure (K_{H_2}), and one that regulates the effect of electron acceptor concentration (K_M). Since V_{max} will vary for each cell culture, a universal value could not be obtained, but the following values were determined for K_{H_2} and for K_M with both BV (K_{BV}), and MV (K_{MV}):

Table 6-1: Kinetic parameters for P11 hydrogenase

K_{H2}	0.31 atm
K_{BV}	1.7-2.4 mM
K_{MV}	10.6 mM

From these parameters and Eqn 6.1, it is apparent that if P_{H_2} is raised to ~3 atm all terms containing P_{H_2} in the denominator of Eqn 6.1 approach unity and the dependence of hydrogenase activity on H_2 pressure is effectively eliminated. Thus, the best hydrogenase efficiency during syngas fermentation will occur when P_{H_2} is at least 3 atm.

6.1.3 Physiological Role of Hydrogenase

The data presented in this thesis indicate that H_2 oxidation via hydrogenase is correlated to ethanol production in P11. In every instance, high levels of hydrogenase activity preceded the period of greatest ethanol production. Additionally, ethanol production always stopped within a

few days of the cessation of hydrogenase activity. Hydrogenase activity was found to be approximately 4x more active at pH 7.75 than at pH 6. Intracellular pH for P11 cells was determined to be between 5 and 6, even when media pH values were around 4.5. Because hydrogenase activity increases concurrently with a decrease in intracellular pH, the rise in hydrogenase activity is attributed to increasing cellular expression of hydrogenase instead of changing intracellular conditions. Regardless, maintaining an intracellular pH above that of the surrounding media likely causes P11 to maintain higher levels of hydrogenase activity than would be possible if hydrogenase were exposed to media pH. Since the reducing power of hydrogenase appears correlated with ethanol production, operation of syngas fermentation processes at higher pH may result in improved ethanol yields.

6.2 Future Work

The work presented in this thesis has exposed many new questions that can be profitably researched further. The sections below contain a few of these potentially valuable areas of research.

6.2.1 Hydrogenase Purification and Characterization

Though whole-cell studies of hydrogenase activity like those presented in this work retain the closest association with syngas fermentation via viable P11 cells, the cellular environment is admittedly a difficult environment in which to study enzyme properties. Significant insight could be gained by purifying hydrogenase from P11 and characterizing its properties.

First, this would allow conclusive determination of the structure of P11's particular hydrogenase. It would reveal whether the P11 hydrogeanse has an [Fe-Fe] core or an [Fe-Ni] core, and this would help improve further kinetic and mechanistic studies. Second, purified hydrogenase samples could be used for electrochemical assays like those described by Leger (2002) and De Lacey (2000), which are decoupled from the accompanying electron acceptor. This approach will explicitly give hydrogenase activity dependence on H_2 pressure, independent of the electron acceptor.

6.2.2 Ferredoxin Purification/Assay

The electron acceptor for the hydrogenase reaction in P11 has been assumed to be ferredoxin, because this is the electron acceptor reported for many Clostridia (Adams, 1981). This assertion could be verified by purifying ferredoxin from a P11 culture. Additionally, accretion of ferredoxin would be valuable for performing assays with the physiological electron acceptor. This would allow for the most physiologically accurate determination of hydrognease reaction kinetics, especially if the normal concentration of ferredoxin in viable P11 cells could be determined. If purification of ferrredoxin from P11 proves impractical, it can be purchased commercially and an assay similar to that described in Section 2.1.2 can be attempted.

6.2.3 Ni Supplementation

The experiment described in Section 5.1 showed a sudden cessation of hydrogenase activity after about 10 days of growth in a batch environment. However, cells in this condition transferred to fresh media resumed growth and hydrogenase activity. It is possible that this

cessation is due to depletion of a vital nutrient. One possibility is that nickel, a key nutrient for [Fe-Ni] hydrogenase creation, becomes depleted. A valuable experiment could be to perform batch studies where Ni is replenished to the media. If hydrogenase activity continues beyond the point where it fails in non-replenished samples, this would be evidence that changes are needed in the media to sustain long-term hydrogenase activity during syngas fermentation.

6.2.4 Sulfide Inhibition

The experiment described in Section 5.1 showed a steady increase in hydrogenase activity over the first four days after inoculation. This increase in activity has been attributed to increasing cellular expression of hydrogenase. However, an alternate explanation of these first four days that should be investigated is sulfide inhibition. Approximately 53 mg/L sulfide is included in the media during preparation, and preliminary research shows that significant amounts this sulfide are lost as gaseous hydrogen sulfide (H_2S) during each recharging of the gas headspace (occurring approximately once each day). Though no evidence exists that sulfide inhibits ferredoxin-linked hydrogenases (Chang, 2009), there have been reports of sulfide inhibition in NAD^+-linked hydrogenases (Aggag, 1974). Thus, it is possible that sulfide inhibits P11 hydrogenase and that the increase in observed hydrogenase activity is due to decreasing sulfide concentrations instead of increasing hydrogenase concentration. Measuring hydrogenase activity in the presence of different concentrations of sulfide would be one way of testing this hypothesis.

6.2.5 FDH and CODH Studies

Hydrogenase is one of only three gas substrate enzymes found on the acetyl-CoA syngas fermentation pathway. The other two are formate dehydrogenase (FDH) and carbon monoxide dehydrogenase (CODH). FDH reduces CO_2 to formate ($CHOO^-$) and CODH interconverts CO and CO_2 (Figure 1-2). Consequently, these two enzymes, as with hydrogenase, are directly affected by the partial pressures of the gases is the syngas feedstream.

Many of the concerns/techniques described in Chapter 3 of this work apply directly to the assay of FDH and CODH as well. Similarly, accurate assays of the activity of these other two gas substrate enzymes could yield valuable kinetic information that would allow further optimization of the partial pressures of the syngas feedstream.

6.2.6 Genetic Engineering

Effort in this thesis has been directed primarily at improving the efficiency of the hydrogenase enzyme during syngas fermentation. There is, however, a limit to improvements in efficiency. Once hydrogenase (and perhaps FDH and CODH) are caused to operate at maximum efficiency, no further improvements can be made by adjusting the pressures of the syngas feed stream. In this instance, further improvement can be made via genetic engineering studies designed to increase the number of hydrogenase (or FDH or CODH) enzymes present in the cell. In this way, both the efficiency of the enzymes and their total expression will be maximized.

6.3 Summary

Ethanol demand in the United States is increasing rapidly as it finds use as an alternative transportation fuel to petroleum-based gasoline. The bacterium *Clostridium P11* utilizes the acetyl-CoA pathway to convert synthesis gas (primarily CO, CO_2, and H_2) to ethanol, and this process is being explored commercially as an environmentally friendly way to produce ethanol. In the current work, the hydrogenase enzyme of P11 (one of two enzymes responsible for supplying electrons to the metabolic pathway) has been studied in considerable detail. In Chapter 3, an assay for determining P11 hydrogenase's H_2 oxidizing activity was developed and many of the difficulties of performing these assays were illuminated and addressed. In Chapter 4, the hydrogenase assay was used for kinetic studies and an appropriate rate law to describe hydrogenase activity dependence on H_2 partial pressure was selected. This rate law was used to determine that H_2 should be supplied at a pressure of ~3 atm partial pressure to maximize hydrogenase efficiency during syngas fermentation. In Chapter 5, a possible correlation between hydrogenase activity and ethanol production was revealed, and hydrogenase activity was measured as a function of pH. Additionally, the P11 intracellular pH was measured and it was proposed that pH control may bring additional efficiency improvements to syngas fermentation via P11. Much remains to be done, but this work improves the understanding and role of hydrogenase activity during syngas fermentation via P11.

REFERENCES

Adams, M. W. W. and L. E. Mortenson (1984). "The physical and catalytic properties of hydrogenase-II of *Clostridium pasteurianum*- A comparison with hydrogenase-I." Journal of Biological Chemistry **259**(11): 7045-7055.

Adams, M. W. W., L. E. Mortenson, et al. (1981). "Hydrogenase." Biochimica Et Biophysica Acta **594**(2-3): 105-176.

Aggag, M. and H. G. Schlegel (1974). "Studies on a gram-positive hydrogen bacterium, *Nocardia opaca 1 b*." Archives of Microbiology **100**: 25-29.

Ahmed, A. and R. S. Lewis (2007). "Fermentation of biomass-generated synthesis gas: Effects of nitric oxide." Biotechnology and Bioengineering **97**(5): 1080-1086.

Bagyinka, C., N. A. Zorin, et al. (1984). "Unconsidered factors affecting hydrogenase activity measurement." Analytical Biochemistry **142**(1): 7-15.

Blanch, H. W. and D. S. Clark (1997). Biochemical Engineering. New York, Marcel Dekker Inc.

Board of Regents for Oklahoma State University, Board of Reagents of the University of Oklahoma, et al. (2008). "Isolation and characterization of novel Clostridial species." US Patent Application 20080057554. Available from http://www.freepatentsonline.com/y2008/0057554. Internet, accessed 8 Feb 2010.

Cammack, R., M. Frey, et al. (2001). Hydrogen as a Fuel: Learning from Nature. London, Taylor & Francis Inc.

Carslaw, H. S. and J. C. Jaeger (1959). Conduction of Heat in Solids (2nd Edition). Glasgow, Oxford University Press.

Chang, A., M. Scheer et al. (2009). "BRENDA, AMENDA and FRENDA the enzyme information system: new content and tools in 2009." Nucleic Acids Res. **37**: Database issue, D588-D592.

Chen, J. S. and D. K. Blanchard (1979). "Simple hydrogenase-linked assay for ferredoxin and flavodoxin." Analytical Biochemistry **93**(1): 216-222.

Datar, R. P., R. M. Shenkman, et al. (2004). "Fermentation of biomass-generated producer gas to ethanol." Biotechnology and Bioengineering **86**(5): 587-594.

De Lacey, A. L., V. M. Fernandez, et al. (2007). "Activation and inactivation of hydrogenase function and the catalytic cycle: Spectroelectrochemical studies." Chemical Reviews **107**(10): 4304-4330.

De Lacey, A. L., J. Moiroux, et al. (2000). "Simple formal kinetics for the reversible uptake of molecular hydrogen by (Ni-Fe) hydrogenase from *Desulfovibrio gigas*." European Journal of Biochemistry **267**(22): 6560-6570.

de Luca, G., P. de Philip, et al. (1998). "The NADP-reducing hydrogenase of *Desulfovibrio fructosovorans*: Evidence for a native complex with hydrogen-dependent methyl-viologen-reducing activity." Biochemical and Biophysical Research Communications **248**(3): 591-596.

Demuez, M., L. Cournac, et al. (2007). "Complete activity profile of *Clostridium acetobutylicum* [FeFe]-hydrogenase and kinetic parameters for endogenous redox partners." Fems Microbiology Letters **275**(1): 113-121.

Dobrindt, U. and M. Blaut (1996). "Purification and characterization of a membrane-bound hydrogenase from *Sporomusa sphaeroides* involved in energy-transducing electron transport." Archives of Microbiology **165**(2): 141-147.

Energy Information Administration. "Official energy statistics from the U.S. government." Available from http://www.eia.doe.gov/. Internet; accessed 27 Aug 2009.

Fernandez, V. M. (1983). "An electrochemical cell for reduction of biochemicals: its application to the study of the effect of pH and redox potential on the activity of hydrogenases." Analytical Biochemistry **130**(1): 54-59.

Fisher, H. F., A. I. Krasna, et al. (1954). "The interaction of hydrogenase with oxygen." Journal of Biological Chemistry **209**: 569-78.

Fromm, S. J. and H. J. Fromm (1999). "A two-step computer assisted method for deriving steady-state rate equations." Biochemical and Biophysical Research Communications **265**(2): 448-452.

Gest, H. (1954). "Oxidation and evolution of molecular hydrogen by microorganisms." Microbiology and Molecular Biology Reviews **18**(1):43-73.

Green D. W. and R. H. Perry (2008). Perry's Chemical Engineers' Handbook (8th Edition). New York, McGraw-Hill.

Grupe, H. and G. Gottschalk (1992). "Physiological events in *Clostridium acetobutylicum* during the shift from acidogenesis to solventogenesis in continuous culture and presentation of a model for shift induction." Applied and Environmental Microbiology **52**(12): 3896-3902.

Guzmán, H. R., D. X. Nguyen, et al. (2001). "Ultrasound-mediated disruption of cell membranes. I. Quantification of molecular uptake and cell viability." Journal of the Acoustical Society of America **110**(1): 588-596.

Harrigan, P. R., M. J. Hope, et al. (1992). "Determination of the transmembrane pH gradients and membrane-potentials in liposomes." Biophysical Journal **63**(5): 1336-1345.

Heiskanen, H., I. Virkajarvi, et al. (2007). "The effect of syngas composition on the growth and product formation of *Butyribacterium methylotrophicum*." Enzyme and Microbial Technology **41**(3): 362-367.

Huang, L., L. N. Gibbins, et al. (1985). "Transmembrane pH gradient and membrane-potential in *Clostridium-acetobutylicum* during growth under acetogenic and solventogenic conditions." Applied and Environmental Microbiology **50**(4): 1043-1047.

Hurst, K. M. (2005). "Effects of carbon monoxide and yeast extract on growth, hydrogenase activity, and product formation of *Clostridium carboxidivorans* $P7^T$." M.S. thesis, Oklahoma State University.

Ikeda, T., T. Kurosaki, et al. (1996). "Measurements of oxidoreductase-like activity of intact bacterial cells by an amperometric method using a membrane-coated electrode." Analytical Chemistry **68**(1): 192-198.

Kellum, R. and H. L. Drake (1984). "Effects of cultivation gas-phase on hydrogenase of the acetogen *Clostridium-thermoaceticum*." Journal of Bacteriology **160**(1): 466-469.

Kim, B. H., P. Bellows, et al. (1984). "Control of carbon and electron flow in *Clostridium-acetobutylicum* fermentations - utilization of carbon-monoxide to inhibit hydrogen-production and to enhance butanol yields." Applied and Environmental Microbiology **48**(4): 764-770.

Klasson, K. T., M. D. Ackerson, et al. (1992). "Bioconversion of synthesis gas into liquid or gaseous fuels." Enzyme and Microbial Technology **14**(8): 602-608.

Lee, S. K., H. Chou, et al. (2008). "Metabolic engineering of microorganisms for biofuels production: from bugs to synthetic biology to fuels." Current Opinion in Biotechnology **19**(6): 556-563.

Lee, S. Y., J. H. Park, et al. (2008). "Fermentative butanol production by Clostridia." Biotechnology and Bioengineering **101**(2): 209-228.

Leger, C., A. K. Jones, et al. (2002). "Enzyme electrokinetics: Hydrogen evolution and oxidation by *Allochromatium vinosum* [NiFe]-hydrogenase." Biochemistry **41**(52): 15736-15746.

Leroux, F., S. Dementin, et al. (2008). "Experimental approaches to kinetics of gas diffusion in hydrogenase." Proceedings of the National Academy of Sciences of the United States of America **105**(32): 11188-11193.

Lewis, R. S., A. Frankman, et al. (2008). "Ethanol via biomass-generated syngas." International Sugar Journal **110**(1311): 150-+.

Maness, P. C. and P. F. Weaver (2001). "Evidence for three distinct hydrogenase activities in *Rhodospirillum rubrum*." Applied Microbiology and Biotechnology **57**(5-6): 751-756.

McIlvaine, T. C. (1921). "A buffer solution for colorimetric comparison." The Journal of Biological Chemistry **49**: 183-186.

Meyer, O. and H. G. Schlegel (1979). "Oxidation of carbon monoxide in cell extracts of *Pseudomonas carboxydovorans*." Journal of Bacteriology **137**(2): 811-17.

Meyer, O. and H. G. Schlegel (1980). "Carbon-monoxide - methylene-blue oxidoreductase from *Pseudomonas-carboxydovorans*." Journal of Bacteriology **141**(1): 74-80.

Mitchell, W. J. (1998). "Physiology of carbohydrate to solvent conversion by Clostridia." Advances in Microbial Physiology **39**: 31-130.

Nelson, D. L. and M. M. Cox (2005). Lehninger Principles of Biochemistry. New York, W. H. Freeman and Company.

Okura, I., K. Nakamura, et al. (1981). "Kinetics of methyl viologen reduction by hydrogen catalyzed by hydrogenase from *Desulfovibrio vulgaris.*" Journal of Inorganic Biochemistry **14**: 155-161.

Osz, J., G. Bodo, et al. (2005). "Theoretical calculations on hydrogenase kinetics: Explanation of the lag phase and the enzyme concentration dependence of the activity of hydrogenase uptake." Biophysical Journal **89**(3): 1957-1964.

Perry, R. H. and D. W. Green (1997). Perry's Chemical Engineers' Handbook (7^{th} Edition). New York, McGraw-Hill.

Pershad, H. R., J. L. C. Duff, et al. (1999). "Catalytic electron transport in *Chromatium Vinosum* [NiFe]-hydrogenase: application of voltammetry in detecting redox-active centers and establishing that hydrogen oxidation is very fast even at potentials close to the reversible H^+/H_2 value." Biochemistry **38**:8992-8999.

Ragsdale, S. W., J. E. Clark, et al. (1983). "Properties of purified carbon-monoxide dehydrogenase from *Clostridium-thermoaceticum*, a nickel, iron-sulfur protein." Journal of Biological Chemistry **258**(4): 2364-2369.

Ruschig, U., U. Muller, et al. (1976). "CO_2 reduction to formate by NADH catalyzed by formate dehydrogenase from *Pseudomonas-oxalaticus*." European Journal of Biochemistry **70**(2): 325-330.

Serebryakova, L. T., M. Medina, et al. (1996). "Reversible hydrogenase of *Anabaena variabilis* ATCC 29413: Catalytic properties and characterization of redox centres." Febs Letters **383**(1-2): 79-82.

Serebryakova, L. T. and M. E. Sheremetieva (2006). "Characterization of catalytic properties of hydrogenase isolated from the unicellular cyanobacterium *Gloeocapsa alpicola* CALU 743." Biochemistry (Moscow) **71**(12): 1370-1376.

Shenkman, R. M. (2003). "*C. carboxidovorans* culture advances and the effects of pH, temperature, and producer gas on key enzymes." M.S. thesis, Oklahoma State University.

Sun, Y. and J. Y. Cheng (2002). "Hydrolysis of lignocellulosic materials for ethanol production: a review." Bioresource Technology **83**(1): 1-11.

Tatsumi, H., K. Kano, et al. (2000). "Kinetic analysis of fast hydrogenase reaction of *Desulfovibrio vulgaris* cells in the presence of exogenous electron acceptors." Journal of Physical Chemistry B **104**(50): 12079-12083.

Tekle, E., R. D. Astumian, et al. (1994). "Selective and asymmetric molecular transport across electroporated cell membranes." Proceedings of the National Academy of Sciences **91**: 11512-11516.

Thauer, R. K. (1972). "Carbon dioxide reduction to formate by NADPH. Initial step in the total synthesis of acetate from carbon dioxide in *Clostridium thermoaceticum*." Febs Letters **27**(1): 111-15.

Thauer, R. K. (1973). "CO_2 reduction to formate in *Clostridium acidi-urici*." Journal of Bacteriology **114**(1): 443-4.

Thauer, R. K., B. Kaeufer, et al. (1975). "Active species of carbon dioxide utilized by reduced ferredoxin:carbon dioxide oxidoreductase from *Clostridium pasteurianum*." European Journal of Biochemistry **55**(1): 111-17.

Tibelius, K. H. and R. Knowles (1984). "Hydrogenase activity in *Azospirillum brasilense* is inhibitied by nitrite, nitric oxide, carbon monoxide and acetylene." Journal of Bacteriology **160**(1): 103-106.

Tsygankov, A. A., E. A. Minakov, et al. (2007). "Measuring the pH dependence of hydrogenase activities." Biochemistry (Moscow) **72**(9): 968-973.

United States Department of Energy. (2004). "Biomass feedstock composition and property database." Available from http://www.afdc.energy.gov/biomass/progs/search1.cgi. Internet; accessed 2 Sept 2009.

United States Department of Energy. (2007). "Biofuels in the U.S. transportation sector." Annual Energy Outlook 2007. Available from http://www.eia.doe.gov/oiaf/analysispaper/biomass.html. Internet; accessed 2 Feb 2010.

Valli, M., M. Sauer, et al. (2005). "Intracellular pH distribution in *Saccharomyces cerevisiae* cell populations, analyzed by flow cytometry." Applied and Environmental Microbiology **71**(3): 1515-1521.

Van Dijk, C., H. J. Grande, et al. (1980). "Properties of the hydrogenase of *Megasphaera-elsdenii*." European Journal of Biochemistry **107**(1): 251-261.

Van Dijk, C., S. G. Mayhew, et al. (1979). "Purification and properties of hydrogenase from *Megasphaera-elsdenii*." European Journal of Biochemistry **102**(2): 317-330.

von Abendroth, G., S. Stripp, et al. (2008). "Optimized over-expression of [FeFe] hydrogenases with high specific activity in *Clostridium acetobutylicum*." International Journal of Hydrogen Energy **33**(21): 6076-6081.

Wang, D. I. C., C. L. Cooney, et al. (1979). Fermentation and Enzyme Technology. New York, Wiley and Sons.

White, D. (2000). The Physiology and Biochemistry of Prokaryotes. New York, Oxford University Press.

Younesi, H., G. Najafpour, et al. (2005). "Ethanol and acetate production from synthesis gas via fermentation processes using anaerobic bacterium, *Clostridium ljungdahlii*." Biochemical Engineering Journal **27**(2): 110-119.